NILU report 28/2024

Monitoring of greenhouse gases and aerosols at Svalbard and Birkenes in 2023

Annual report

NILU report 28/2024

Monitoring of greenhouse gases and aerosols at Svalbard and Birkenes in 2023

Annual report

Stephen M. Platt, Tove Svendby, Ove Hermansen, Chris Lunder, Markus Fiebig, Ann Mari Fjæraa, Valentin Duflot, Norbert Schmidbauer, Cathrine Lund Myhre, Karl Espen Yttri, Sabine Eckhardt and Kerstin Stebel

nilu

ISBN 978-82-425-3177-3
ISSN 2464-3327

NILU report 28/2024

Norwegian Environment Agency M-2857 | 2024

Main office
NILU
P.O. Box 100
NO-2027 Kjeller,
Norway

Tromsø
NILU
Framsenteret
P.O. Box 6606
Stakkevollan
NO-9296 Tromsø,
Norway

Trondheim
NILU
Kjøpmannsgata 8
NO-7013 Trondheim,
Norway

Phone +47 63 89 80 00
nilu@nilu.no
www.nilu.com

Stiftelsen NILU
Org.no. 941 705 561

Certifications
NS-EN ISO 9001
NS-EN ISO 14001

Accreditation
NS-EN ISO/IEC 17025

Gothenburg
NILU Klimat- och
miljöinstitutet AB
Sven Hultins plats 5
SE-412 58 Göteborg
Sweden

Org.no. 559442-9580
www.nilu-research.se

Cover picture
Cathrine Lund Myhre,
NILU

Title
Monitoring of greenhouse gases and aerosols at Svalbard and Birkenes in 2023
Annual report

Norwegian title
Overvåkning av klimagasser og partikler på Svalbard og Birkenes i 2023
Årsrapport

Author(s)
Stephen M. Platt, Tove Svendby, Ove Hermansen, Chris Lunder, Markus Fiebig, Ann Mari Fjæraa, Valentin Duflot, Norbert Schmidbauer, Cathrine Lund Myhre, Karl Espen Yttri and Kerstin Stebel

Short summary (English)
This annual report for 2023 summarizes the activities and results of the greenhouse gas monitoring at the Zeppelin Observatory, situated on Svalbard, during the period 2001-2023, and the greenhouse gas monitoring and aerosol observations from Birkenes for 2009-2023.

Short summary (Norwegian)
Denne årsrapporten for 2023 presenterer aktiviteter og måleresultater fra klimagassovervåkingen ved Zeppelinobservatoriet på Svalbard for årene 2001-2023 og klimagassmålinger og klimarelevante partikkelmålinger fra Birkenes for 2009-2023.

Keywords
Greenhouse gases, Aerosols, Climate gases, Halocarbons
Drivhusgasser, Partikler, Klimagasser, Halokarboner

Number of pages
99

Classification
A-Open

Project leader
Wenche Aas

NILU project number
O-121002/O-113007

Client/Report prepared for
Norwegian Environment Agency
Postboks 5672 Sluppen, 7485 Trondheim

Contract reference
21087006/17078061

Signature of the responsible person
Aasmund Fahre Vik, Deputy CEO & CTO

Date
19.11.2024

Citation
Platt, S.M., Svendby, T., Hermansen, O., Lunder, C., Fiebig, M., Fjæraa, A.M., Duflot, V., Schmidbauer, N., Myhre, C.L., Yttri, K.E., Eckhardt, S., Stebel, K. (2024). Monitoring of greenhouse gases and aerosols at Svalbard and Birkenes in 2023. Annual report (NILU report 28/2024). Kjeller: NILU.

Contents

Summary

The monitoring program for greenhouse gases and aerosols tracks long-term changes in atmospheric composition at two sites: the Zeppelin Observatory, Ny Ålesund, Svalbard in the Arctic and the Birkenes Observatory in Aust Agder, Southern Norway. These observatories provide critical data on the levels of greenhouse gases and aerosols, providing insights into both regional and global atmospheric composition change and climate impacts. The monitoring programme for greenhouse gases and aerosols began in 1999 under a contract between the Norwegian Environment agency and NILU. NILU also operates a station at Trollhaugen, Dronning Maud land, which is not a part of the monitoring program, but which is included in this report for completeness and as a reference to the most clean, unpolluted air found on Earth.

In 2023, carbon dioxide (CO_2) concentrations continued to rise, with annual mean concentrations reaching 421.5 ppm at the Zeppelin Observatory (an increase of 1.8 ppm) and 426.0 ppm at Birkenes (an increase of 2.1 ppm), and a similar increase at Trollhaugen, which reached 416.4 ppm (an increase of 2.1 ppm). Methane (CH_4) annual mean concentrations also saw notable increases, with levels of 2007.6 ppb at Zeppelin (an increase of 8.0 ppb), 2016.2 ppb at Birkenes (an increase of 10.7 ppb), and 1871.1 ppb at Trollhaugen (an increase of 12.9 ppb). This increase in methane poses significant risks to climate targets. Nitrous oxide (N_2O) levels have also increased, reaching an annual mean of 337.0 ppb at Zeppelin, reflecting its strong contribution to greenhouse gas warming, with an increase of 1.18 ppb compared to the previous year. These rising levels across all sites indicate ongoing challenges in mitigating emissions of these key climate forcers.

Chlorofluorocarbons (CFCs) are potent greenhouse gases and ozone-depleting substances that have been heavily regulated under the Montreal Protocol. Measurements from the Zeppelin Observatory show that CFC concentrations, including CFC-11 (217.5 ppt) and CFC-12 (488.9 ppt), have been steadily declining, reflecting the success of the protocol in reducing their emissions. However, CFC-115 has shown a slight increase since 2017, reaching 8.9 ppt in 2023, which may be related to its use in the production of the first generation, hydrofluorocarbon (HFCs), replacement compounds. This upward trend highlights the importance of continued monitoring to ensure compliance with global agreements and to prevent any setbacks in protecting the ozone layer and mitigating climate change.

Perfluorinated compounds, such as PFC-14 (89.93 ppt) and PFC-116 (5.30 ppt), are extremely potent greenhouse gases with long atmospheric lifetimes, some up to 50,000 years. Although their concentrations remain low, all are steadily increasing, and their high global warming potentials make them crucial targets for long-term monitoring to mitigate their impact on climate change.

The aerosol scattering coefficient, which quantifies aerosols' ability to scatter sunlight and produce a cooling effect, has been decreasing at Birkenes by approximately 9% per year. This reduction in scattering, linked to the Gothenburg Protocol's success in reducing sulfate and other pollutants, implies a weakening of the cooling effect at Birkenes, potentially contributing to warming in this region. Conversely, at Trollhaugen in Antarctica, the aerosol scattering coefficient has been increasing by around 4% per year, possibly due to enhanced biological activity, thereby strengthening the cooling effect in this remote location. Aerosol absorption, which measures the warming effect and serves as an indicator of black carbon, continues to decline at all sites by 10 to 15% per year, reflecting the impact of air quality measures aimed at reducing black carbon emissions. This decline implies a reduced warming effect from aerosols. The single scattering albedo (SSA), which represents the balance between scattering (cooling) and absorption (warming), has been increasing at both Birkenes and Trollhaugen by approximately 1% per decade. This increase in SSA suggests a stronger relative cooling effect, although the net impact on climate will ultimately depend on the total aerosol concentration.

Sammendrag

Gjennom overvåkingsprogrammet for klimagasser og aerosoler måles langsiktige endringer i den atmosfæriske sammensetningen to steder i Norge: Zeppelinobservatoriet i Ny-Ålesund (Svalbard) i Arktis og Birkenesobservatoriet i Aust-Agder i Sør-Norge. Data fra disse observatoriene gir viktig informasjon om nivåene av klimagasser og aerosoler, og de gir innsikt i både regionale og globale endringer i atmosfærisk sammensetning og klimapåvirkning. Overvåkingsprogrammet for klimagasser og aerosoler startet i 1999, via en kontrakt mellom Miljødirektoratet og NILU. NILU er også vitenskapelig ansvarlig for en stasjon på Trollhaugen i Dronning Mauds Land, Antarktis. Data og analyser fra denne stasjonen er ikke en del av overvåkingsprogrammet, men er inkludert i denne rapporten for å gi et mer helhetlig bilde av den globale situasjonen, og som en referanse til den reneste og minst forurensede luften på jorden.

I 2023 fortsatte konsentrasjonen av karbondioksid (CO_2) å stige, og de årlige middelverdiene var 421.5 ppm på Zeppelin (en økning på 1.8 ppm), 426.0 ppm på Birkenes (en økning på 2.1 ppm) og 416.4 ppm på Trollhaugen (en økning på 2.1 ppm). Konsentrasjonene av metan (CH_4) økte også merkbart i 2023, med årlige middelverdier på 2007.6 ppb på Zeppelin (en økning på 8.0 ppb), 2016.2 ppb på Birkenes (en økning på 10.7 ppb) og 1871.1 ppb på Trollhaugen (en økning på 12.9 ppb). Denne økningen i metan er en utfordring med tanke på å nå klimamålene. Nivået av lystgass (N_2O) har også økt og nådde i 2023 et årsmiddel på 337.0 ppb på Zeppelin, noe som gir et betydelig bidrag til oppvarmingen fra klimagasser. Dette var en økning på 1.18 ppb fra året før. Økte nivåer ved alle stasjonene vitner om pågående utfordringer med å redusere utslippene fra disse viktige klimapådriverne.

Klorfluorkarboner (KFKer) er kraftige klimagasser og ozonnedbrytende stoffer som har blitt strengt regulert under Montrealprotokollen. Målinger fra Zeppelinobservatoriet viser at konsentrasjonen av KFKer, inkludert KFK-11 (217.5 ppt) og KFK-12 (488.9 ppt), har vært jevnt avtagende, noe som reflekterer protokollens suksess i å redusere utslippene. KFK-115 har imidlertid vist en liten økning siden 2017 og nådde 8.9 ppt i 2023, trolig forårsaket av bruken av denne gassen i produksjon av hydrofluorkarboner (HFKer), erstatningsstoffer for KFKer. Denne oppadgående trenden understreker viktigheten av fortsatt overvåking for å sikre etterlevelse av globale avtaler, for å forhindre tilbakeslag i beskyttelsen av ozonlaget og i arbeidet med å redusere klimaendringer.

Perfluorerte forbindelser, som PFK-14 (89.93 ppt) og PFK-116 (5.30 ppt), er ekstremt potente klimagasser med lang atmosfærisk levetid, noen opptil 50 000 år. Selv om konsentrasjonene fortsatt er svært lave, øker de jevnt, og gassenes høye globale oppvarmingspotensial (GWP) gjør dem til viktige mål for langsiktig overvåkning for å redusere deres påvirkning på klimaendringer.

Aerosol spredningskoeffisient, som angir aerosolenes evne til å spre sollys og som har en avkjølende effekt, har avtatt på Birkenes med ca. 9 % per år. Denne reduksjonen i spredning, knyttet til en vellykket implementering av Gøteborgprotokollen for å redusere sulfat og annen forurensning, innebærer en reduksjon av den avkjølende effekten av aerosoler på Birkenes og vil potensielt bidra til en oppvarming i denne regionen. Aerosol spredningskoeffisientene har derimot økt på Trollhaugen i Antarktis (~4 % per år), trolig forårsaket av økt biologisk aktivitet, og har dermed forsterket avkjølingen i denne regionen. Aerosol absorpsjonskoeffisient, som måler aerosolenes oppvarmingseffekt og som også er en indikator på svart karbon (sot), fortsetter å avta (-10 til 15 % per år) på alle målestasjonene, noe som gjenspeiler en vellykket implementering av luftkvalitetstiltak for å begrense utslipp av svart karbon. Denne nedgangen innebærer redusert oppvarming fra aerosoler. Enkeltspredningsalbedo (SSA), som viser forholdet mellom spredning (avkjøling) og absorpsjon (oppvarming), øker på både Birkenes og Trollhaugen (~1 % per tiår). Denne økningen av SSA indikerer en sterkere relativ avkjølende effekt av aerosoler, selv om den totale aerosoleffekten avhenger av den samlede konsentrasjonen av aerosoler.

Monitoring of greenhouse gases and aerosols at Svalbard and Birkenes in 2023

Annual report

1 Aerosol measurements in the monitoring programme

This year NILU has significantly updated the reporting of aerosol physical and optical properties in the monitoring program for greenhouse gases and aerosols at Svalbard and Birkenes. With several years' worth of data, it has now been possible to determine statistically significant trends for many of NILUs aerosol measurements. Furthermore, the way NILU performs many of NILU's measurements is also changing. In 2023 NILU began implementing Aerosol, Clouds and Trace Gases Research Infrastructure (ACTRIS) routines for harmonized measurements and data quality control as part of the ACTRIS labelling process. These updates are timely, since there has been considerable focus on aerosol uncertainties, and how changes in aerosols might be related to record global average temperatures seen in 2023, as well as the impact of numerous wildfires. With these updates, the monitoring equipped to understand long term developments in aerosols and contribute to more informed policy decisions regarding air quality and climate change mitigation.

1.1 Aerosols and climate

An aerosol is a suspension of liquid or solid particles in the air. Aerosols can have numerous sources, both natural and man-made, ranging from pollen or sea spray to black carbon (soot) and tire wear. They can also be secondary, produced from precursor gases by chemical processes in the atmosphere involving volatile organic compound (VOC) precursors and sunlight.

Aerosols are currently the largest uncertainty in understanding of climate change. They directly affect the climate via their impact on incoming solar radiation, either scattering light which cools the planet or absorbing light causing warming Overall, the direct aerosol radiation effect causes cooling by around 0.1°C (dark blue in Figure 1.1, from the intergovernmental panel on climate change, IPCC, 6th Assessment Report, Masson-Delmotte et al., 2021). However, the largest effect of aerosols is due to their impact on cloud

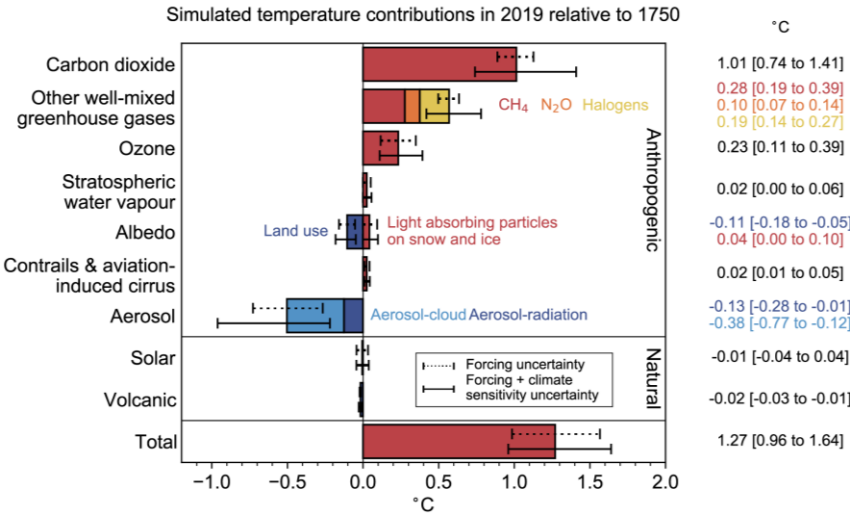

Figure 1.1: Effective radiative forcing (ERF) from key climate drivers, highlighting the uncertainty in aerosol forcing compared to other contributors. Aerosols, particularly through their interactions with clouds, remain the largest source of uncertainty in climate projections, from the IPCC 6th Assessment Report (Masson-Delmotte et al., 2021).

formation. Clouds cannot form Earth's atmosphere without aerosol particles providing a surface for condensation. Since clouds reflect sunlight into space-i.e., they modify Earth's albedo- it follows that aerosol particles have a major impact on climate. This aerosol cloud effect is thought to cause around 0.4°C of cooling (light blue in Figure 1.1). If aerosol cooling is at the lower end of the uncertainty range (more cooling), it means aerosols are masking more of the warming from greenhouse gases than previously thought. If aerosol emissions decrease, the hidden warming could be revealed, potentially leading to faster climate warming.

1.2 How changing Aerosols concentrations might be linked to recent warming

Recent NILU data reveal that long-term trends in aerosol scattering and absorption show significant changes, particularly at the Birkenes site, where a decrease in aerosol scattering has been observed. Aerosols, especially sulfate, play a vital role in cooling the atmosphere by reflecting sunlight. However, the observed decrease in aerosol scattering at Birkenes—estimated at roughly 9% per year—is closely linked to reductions in sulfate aerosols due to successful air quality initiatives, such as the Gothenburg Protocol. While this decline benefits human health and reduces acid rain, it also decreases the cooling effect of aerosols, thereby contributing to an increased warming influence on the climate.

This reduction in sulfate aerosols and corresponding decrease in NILU's aerosol optical depth (AOD) measurements, which quantify the amount of solar radiation scattered or blocked by aerosols, represents a positive shift in climate forcing. Similar global trends show that lower aerosol concentrations may lead to an 'unmasking' of warming previously mitigated by these particles. For instance, a recent study likened stricter sulfur emissions controls over the ocean to 'inadvertent geoengineering,' predicting a warming effect of 0.16°C from 2020 to 2027 as a result (Yuan et al., 2024). Importantly, if the true cooling effect of aerosols is at the lower end of current estimates (more negative in Figure 1.1), this unmasking effect could be even more profound, leading to greater warming than currently projected. However, it should be noted that the Yuan study omits deep ocean heat uptake, a factor in global heat distribution, which may influence the accuracy of its warming projections.

Moreover, evolving aerosol emissions and their complex impacts are highlighted in research by Persad et al. (2023), which underscores that models that omit aerosol properties may underpredict temperatures, particularly at regional levels. Regional climate models not accounting for aerosols may show lower temperature estimates than global models, potentially underestimating climate risks in specific areas. Understanding these dynamics is essential for accurate climate projections and for assessing regional vulnerabilities. NILU's long-term aerosol monitoring thus provides critical data that can refine climate models, enhancing accuracy in predicting aerosol impacts on both global and regional scales.

By offering real-world observations of both scattering and absorbing aerosols, NILU's data bridge the gaps identified in recent studies and support more precise climate risk assessments. This work underscores the importance of maintaining aerosol monitoring to understand and address the potential acceleration of climate warming as aerosol concentrations decrease.

1.3 Possible increased contribution of biomass burning to aerosol concentrations

In 2023 NILU implemented calculations of 'equivalent black carbon' (eBC) and its optical properties for Zeppelin, Birkenes, and Trollhaugen observatories, providing important insights into changes in black carbon (BC) levels and its sources such as from biomass burning vs fossil fuel burning. Black carbon

absorbs light, causing warming, and, when deposited on snow, reduces surface reflectivity and further accelerates warming. Additionally, BC impacts cloud formation. The combined effect is generally warming. BC is also strongly associated with significant negative health effects.

eBC is a calculation of BC based on measurements of highly light absorbing aerosol particles (since these are almost exclusively made of BC). A notable trend observed by NILU is the increase in an optical property of eBC called the 'absorption Ångstrøm exponent' (AAE), which has been rising by 3 to 4% per decade. A higher AAE suggests a greater contribution of BC from solid fuel burning, such as BC from wood combustion, which absorbs light differently across wavelengths than BC from fossil fuels. At the same time, overall eBC levels have decreased by 10 to 16% per decade, suggesting reductions in fossil fuel sources of BC—likely driven by stricter regulations on vehicle emissions and the switch to electric vehicles.

Further evidence of increasing biomass burning contributions comes from filter-based measurements of BC ('elemental carbon,' EC) and the tracer compound Levoglucosan, which is only released when wood is burned. The companion report on *Monitoring of Long-Range Transported Air Pollutants in Norway* (Aas et al., 2024) shows that Levoglucosan concentrations are rising relative to EC (Figure 1.2), indicating a larger share of BC from biomass burning.

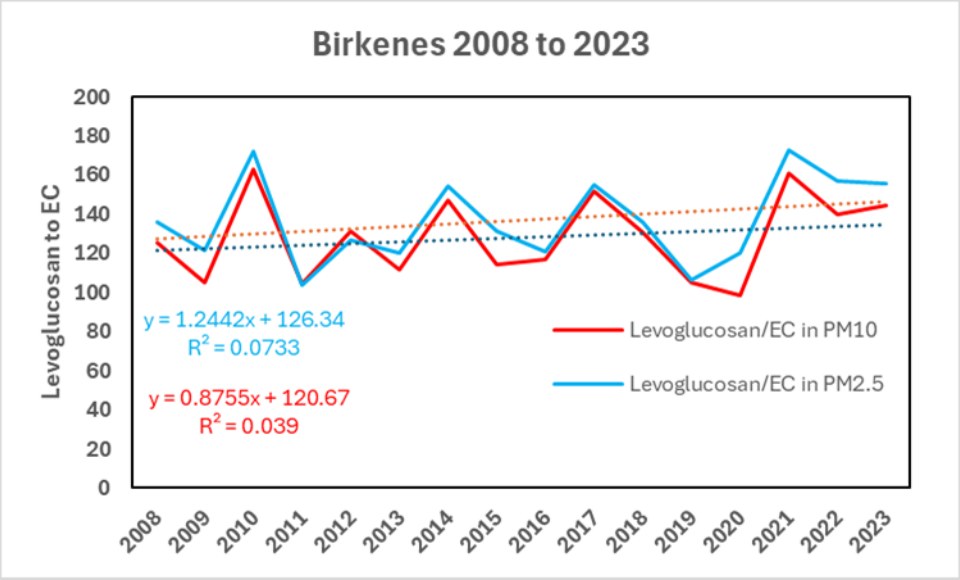

Figure 1.2: Increased relative levels of the biomass burning aeroosl tracer 'Levoglucosan' are oberved in both fine (PM2.5, blue) and coarse (PM10, red) aerosol fractions between 2008 and 2023 at the Birkenes Observatory.

Wildfires are another important contributor to BC from biomass burning and recent studies highlight that wildfire activity has intensified in forested and tundra regions, notably in Alaska, Canada, Siberia, and Scandinavia (Byrne et al., 2024; Cunningham et al., 2024). Some of the most intense fire seasons on record have been observed in these regions, closely correlating with record-high temperatures. For example, the 2020 Siberian Arctic fire season was among the most intense in the past 40 years, with nearly 44% of the total burned area since 1982 occurring in just 2019 and 2020 alone (Bondur et al., 2020). NILU's own measurements coupled to modelled emissions and the transport model FLEXPART also show a clear influence of North Amercan wildfires on BC levels in 2023 (Figure 1.3).

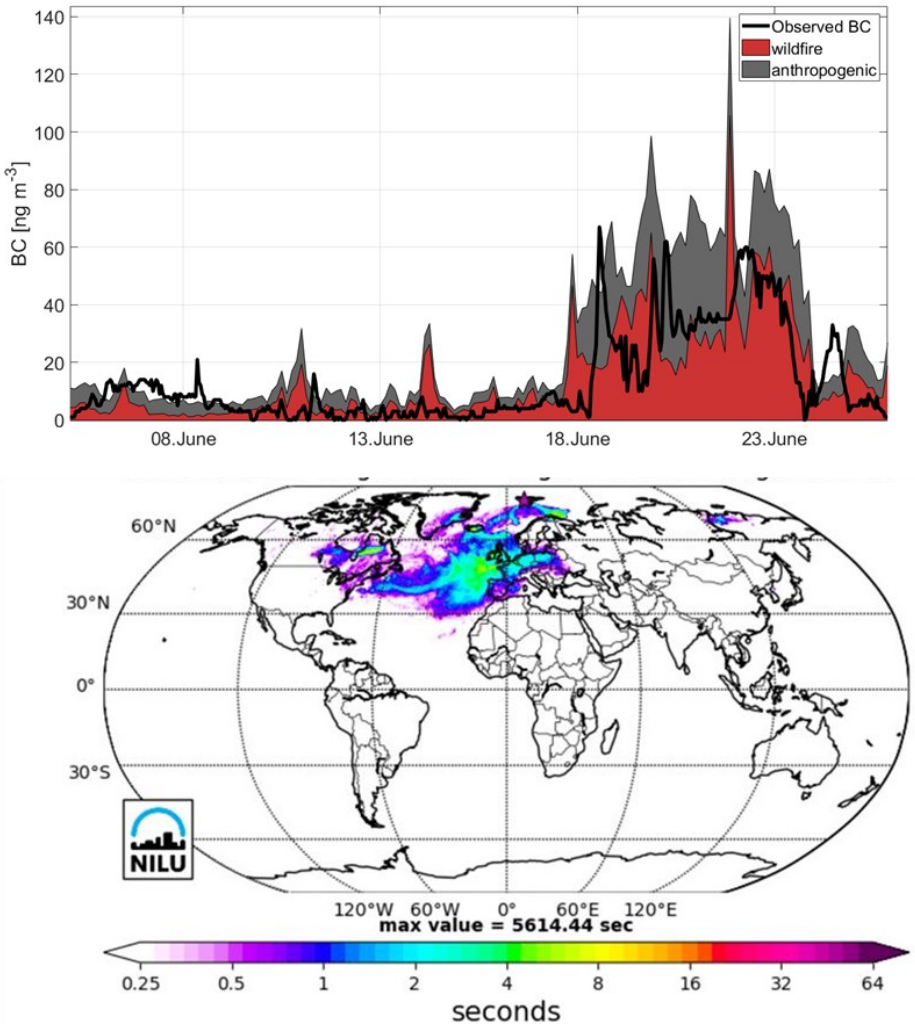

Figure 1.3: Top: oberved black carbon (BC) levels in June 2023 at the Zeppelin Observatory, Svalbard, (black line) and simulated wildfire (red) and anthropogenic emissions (grey). The simulated emissions are from the Copernicus Atmospheric Monitoring Service (CAMS) global biomass burning emissions based on fire radiative power (GFAS) dataset (https://ads.atmosphere.copernicus.eu/datasets/cams-global-fire-emissions-gfas?tab=overview). Bottom: The BC concentrations at Zeppelin were estimated using the FLEXPART model to determine the residence time in seconds of the air masses at the Earth's surface before reaching the observatory, the so called 'footprint'. Longer residence times indicate increased sensitivity to emissions, and NILU's simulations show that the foorptint of the Zeppelin Observatory extended over North America during the wildfires in that region in 2023.

Increased wildfire emissions contribute to BC levels and have two critical negative effects on climate: they release large amounts of carbon, as seen with the 2023 Canadian wildfires, which matched the annual fossil fuel emissions of large nations, and they reduce the resilience of forests as carbon sinks, damaging the ability of forests to absorb CO_2 from the atmosphere.

1.4 The new role of ACTRIS in the monitoring programme

The Aerosol, Clouds, and Trace Gases Research Infrastructure (ACTRIS) is a European initiative designed to harmonize and improve the quality of measurements related to short-lived atmospheric constituents, including aerosols, clouds, and trace gases. Implementation of the Norwegian membership of ACTRIS is supported by the Research Council of Norway's ACTRIS Norway project, which began in 2022. Bringing together numerous observation stations across Europe, ACTRIS provides a unified framework for measuring many of the aerosol parameters in the monitoring programme, as well as the VOCs, ensuring that the data collected is consistent and comparable. This is vital for understanding how these particles and gases affect climate and air quality, for example by streamlining the process of model evaluation, removing the need to account for differences which would normally exist in a large dataset.

2 Monitoring of greenhouse gases and aerosols at Svalbard and Birkenes in 2023

Monitoring of greenhouse gases and aerosols at Svalbard and Birkenes in 2024 is one of three annual reports on the state of the atmosphere in Norway, Svalbard, and Antarctica. The other two are *Monitoring of long-range transported air pollutants in Norway* (Aas et al., 2024), and *Monitoring of the atmospheric ozone layer and natural ultraviolet radiation* (Svendby et al., 2024).

Under this programme, NILU measures the long-term developments of the main greenhouse gases, climate-relevant trace gases, and aerosol optical and physical properties (Table 1), at two Norwegian sites: Zeppelin and Birkenes (Figure 2.1). Additional measurements are performed by NILU at Trollhaugen, Antarctica, which are also included in the report for completeness, though they are not funded by the Norwegian Environment Agency.

Figure 2.1: NILU's atmospheric monitoring sites under the monitoring programme for greenhouse gases and aerosol at Zeppelin, Svalbard (78.90°N, 11.88°E, 472 m a.s.l.) and Birkenes in Southern Norway.

Within the monitoring programme, NILU has state-of-the-art in-situ measurements of all major climate forcers. These measurements include all climate parameters shown in Figure 2.2 from the Intergovernmental Panel on Climate Change (IPCC) Sixth Assessment Report (AR6, Masson-Delmotte et al., 2021). This figure highlights the contribution of key greenhouse gases, such as carbon dioxide (CO_2), methane (CH_4), and nitrous oxide (N_2O), to warming. It also depicts the cooling effects of aerosols, including sulfate (SO_2) and black carbon. Additionally, NILU performs total column measurements for aerosol. Many of NILU's measurements contribute to international research infrastructures, such as the Integrated Carbon Observation System (ICOS) and the Aerosol, Clouds, and Trace Gases Research Infrastructure (ACTRIS), ensuring data interoperability in support of global climate research, as also indicated in (Table 1). A full description of the methodology for NILU's measurements is presented in Annex B, with data coverage for the reporting year included in Table B 1.

NILU's measurements support national and international stakeholders, policy makers and the scientific community by contributing to an improved understanding of the drivers of climate change, the effect on atmospheric composition of natural and anthropogenic emissions, and the impacts of mitigation activities. The programme is set up to provide the knowledge needed to meet national and international obligations (Table 2), covering the major atmospheric components influencing global warming.

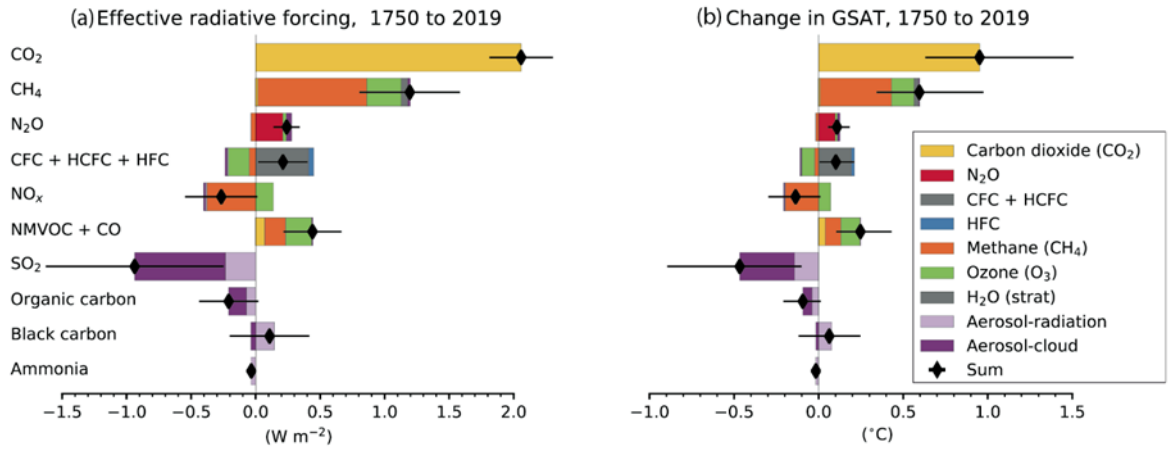

Figure 2.2: Changes in effective radiative forcing (a) and global surface air temperature (GSAT, b) from 1750 to 2019, driven by various atmospheric components, including carbon dioxide (CO_2), methane (CH_4), nitrous oxide (N_2O), chlorofluorocarbons (CFCs), hydrochlorofluorocarbons (HCFCs), hydrofluorocarbons (HFCs), nitrogen oxides (NO_x), non-methane volatile organic compounds (NMVOCs), sulfate aerosols (SO_2), organic carbon, black carbon, and ammonia. Source: IPCC AR6, 2021 (Masson-Delmotte et al., 2021).

Table 1: Summary of the measurement programme at Birkenes, Zeppelin, and Troll Observatories.

Component	Birkenes Start	Zeppelin Start	Troll Start	International network	Comment
Trace gases					
CO_2	2009	2012	2014	ICOS	Zeppelin: since 1990 by Univ. Stockholm, since 2012 by NILU. ICOS class 1 site since 2017. Birkenes: ICOS class 2 site since 2020. Trollhaugen is not in ICOS.
CH_4	2009	2001	2022	ICOS	ICOS labelling as above
N_2O	(-)	2009	(-)	ICOS	ICOS labelling and implementation in 2017
CO	(-)	2001	(-)	ICOS	ICOS labelling and implementation in 2017
CFCs					
CFC-11*, CFC-12*, CFC-113* CFC-115*	(-)	2001		AGAGE	* These components are not within the required precision of AGAGE, but a part of the AGAGE quality assurance programme. This is related to the measurements in the period 2001 to 2010, before the installation of the Medusa instrument. After 2010, the measurements are with the same precision as the rest of the measurements in the AGAGE network.
HCFCs					

Component	Birkenes Start	Zeppelin Start	Troll Start	International network	Comment
HCFC-22, HCFC-141b, HCFC-142b	(-)	2001		AGAGE	
HFCs					
HFC-125, HFC-134a, HFC-152a, **HFC-23**, **HFC-227ea**, **HFC-236fa**, **HFC-245fa**, **HFC-365mfc**, **HFC-32**, **HFC-4310mee**, **HFC-143a**	(-)	2001		AGAGE	Blue text indicates the extension and components added to the program in 2015.
PFCs					
PFC-14, PFC-116 , PFC-218, PFC-318	(-)	2001		AGAGE	Blue text indicates the extension and components added to the program in 2015.
Halons					
H-1211, H-1301 , **H-2402**	(-)	2001		AGAGE	Blue text indicates the extension and components added to the program in 2015.
Other chlorinated hydrocarbons					
CH_3Cl, CH_3Br, CH_2Cl_2, $CHCl_3$, **CCl_4**, CH_3CCl_3, $CHClCCl_2$*, CCl_2CCl_2*	(-)	2001		AGAGE	Blue text indicates the extension and components added to the program in 2015.
Other fluorinated compounds					
SF6 , **NF_3**	(-)	2001		AGAGE	Blue text indicates the extension and components added to the program in 2015.
SO_2F_2	(-)	2016		AGAGE	
VOCs					
C_2H_6 – ethane, C_3H_8 – propane, C_4H_{10} – butane, C_5H_{12} – pentane, C_6H_6 – benzene,	(-)	2010		ACTRIS, EMEP	VOCs were included in the national monitoring programme from 2015, but the measurements are harmonised back to 2010.

Component	Birkenes Start	Zeppelin Start	Troll Start	International network	Comment
$C_6H_5CH_3$ – toluene					
Aerosol properties					
Aerosol Optical depth	2009	2002	2014	ACTRIS	Zeppelin (in Ny-Ålesund) and Trollhaugen: spectral {368, 412, 500, 862 nm} in collaboration with PMOD/WRC; Birkenes spectral {spectral at 340, 380, 440, 500, 675, 870, 1020, 1640 nm} in collaboration with Univ. Valladolid, Spain.
Particle Number Size Distribution (PNSD)	2009	2020	2022	ACTRIS, EMEP	Zeppelin: fine and coarse mode (0.01 µm < Dp < 10 µm), coarse mode. Birkenes fine and coarse mode (0.01 µm < Dp < 10 µm), Trollhaugen: fine mode (0.01 µm < Dp < 0.8 µm)
Aerosol Scattering Coefficient	2019	2015	2014	ACTRIS	Birkenes: spectral {450,550,700 nm}; Zeppelin spectral {450, 550, 700 nm}, operated by Univ. Stockholm.
Aerosol Absorption Coefficient, equivalent black carbon	2017	2015	2020	ACTRIS	7-wavelength {370,470,520,590,660,880,950 nm}. Trollhaugen and Birkenes have has additional 3-wavelength {470,522,660 nm}. Equivalent black carbon is the absorption coefficient divided by the mass absorption cross section (MAC)

Table 2: National and international agreements supported by the Norwegian national monitoring of greenhouse gases and aerosols.

Agreement	Date Ratified	Parties	Summary of Obligation
Paris Agreement[1]	4th Nov 2016	194/198 Parties including Norway	Limit global warming to 2°C or preferably 1.5°C or below. Commit to emission reduction targets, e.g., EU aiming for 55% reduction by 2030.
Global Methane Pledge[2]	4th Nov 2021	100+ Parties including Norway	Voluntarily reduce global methane emissions by at least 30% from 2020 levels by 2030. Improve reporting transparency.
Montreal Protocol & Kigali Amendment[3]	16th September 1987 & 15th October 2016	197 Parties including Norway	Monreal: Reduce ozone-depleting substances. Kigali: Cut hydrofluorocarbons (HFCs) use by over 80% in the 21st century to combat global warming.
Klimaloven[4]	-	Norway	Cut greenhouse gas emissions by at least 50 to 55% by 2030 compared to 1990 levels.

[1] https://unfccc.int/process/the-paris-agreement/status-of-ratification

[2] https://www.globalmethanepledge.org/; [3] http://ec.europa.eu/clima/policies/strategies/2030/ and http://www.consilium.europa.eu/uedocs/cms_data/docs/pressdata/en/ec/145397.pdf

[4] https://lovdata.no/dokument/NL/lov/2017-06-16-60

2.1 Greenhouse gases

Greenhouse gases (GHGs) are atmospheric gases that trap heat in the Earth's atmosphere by absorbing outgoing thermal radiation, as part of the 'greenhouse effect'. The greenhouse effect is essential to life as without it the planet would be several degrees cooler. However, changes to the Earth's radiative balance, referred to as forcings result in changes to the Earth's climate. The sensitivity of climate to these forcers depends on various feedback mechanisms and interacting processes.

The most important climate forcers are carbon dioxide (CO_2), methane (CH_4), and nitrous oxide (N_2O), due to their abundance and their ability to absorb heat efficiently (Figure 2.2). CO_2, primarily released from fossil fuel combustion, is the largest contributor to global warming, while CH_4, from agriculture, waste, and fossil fuels, has a much higher global warming potential (GWP) than CO_2 but a shorter atmospheric lifetime. N_2O, released mainly from agricultural activities, is also a potent greenhouse gas with a long lifetime. Together, these gases drive climate change by enhancing the greenhouse effect and leading to increased global temperatures. Several of the other gases in this section, such as carbon monoxide do not directly cause warming, but are indirect greenhouse gases which modify atmospheric chemical processes, affecting the lifetimes of GHGs.

The Paris Agreement aims to limit global warming to well below 2°C, and preferably to 1.5°C above pre-industrial levels, to reduce the risks and impacts of climate change. However, current greenhouse gas emission trends make achieving these targets increasingly challenging. According to the IPCC Sixth Assessment Report (AR6, Masson-Delmotte et al., 2021), to limit warming to 1.5°C, global net CO_2 emissions must reach zero by around 2050, and substantial reductions in methane and other greenhouse

gases are also critical. The cumulative effects of CO_2, CH_4, and N_2O are driving the warming observed today, and immediate, deep emissions reductions are essential to mitigate further global temperature rise.

Table 3 summarises the main results from the monitoring programme for 2024 for GHGs and the trends over the period 2001 to 2024, including 2024 global annual mean values from the Bulletin of the American Meteorological Society (BAMS, Blunden et al., 2024). Note that BAMS does not provide global means for all compounds in this report, and NILU reports the global means in all instances where these are available. All peak concentrations of the measured gases are significantly lower at Zeppelin than at other sites at the Northern hemisphere, due to the station's remote location. Birkenes is closer to the main source areas and the regional vegetation is important for regulating the carbon cycle, resulting in much larger variability in the concentration level compared to the Arctic region. Most greenhouse gases and other climate gases have numerous sources, both anthropogenic and natural. Trends and future changes in concentrations are thus determined by the future balance of their sources and sinks. Mean annual concentrations for all greenhouse gases for all years are given in Table A 1, and the trends for all years in Table A 2.

Table 3: Greenhouse gases measured at Zeppelin, and Birkenes and Trollhaugen where stated; lifetimes in years, global warming potential (GWP) for 100 year horizon and annual mean concentrations for 2024, change from last year, and trends per year over the measurement period. Red is increasing and blue is decreasing trends. Global means for 2024, taken from Bulletin of the American Meteorological Society (Blunden et al., 2024) and WMO (2024), are included for comparison, wehere available. All concentrations are mixing ratios in ppt, except for methane, nitrous oxide and carbon monoxide (ppb) and carbon dioxide (ppm). The isotopic ratio is in per mille (‰). Trend calculations described in Appendix II.

Component	Chemical formula	Life-time	GWP	Global mean 2024	Annual mean 2024	Absolute change last year	Trend /yr
Carbon dioxide - Zeppelin	CO_2	**	1	420.0	421.5	1.8	2.5
Carbon dioxide - Birkenes					426.0	2.1	2.5
Carbon dioxide -Trollhaugen					416.4	2.1	2.3
Methane - Zeppelin	CH_4	11.8	28	1934	2007.6	8.0	7.3
Methane - Birkenes					2016.2	10.7	9.7
Methane- Trollhaguen					1871.1	12.9	-
Carbon monoxide	CO	few months	-	-	125.2	10.2	-0.6
Nitrous oxide	N_2O	109	273	336.9	337.0	1.18	1.04
Isotopes							
Methane isotopic ratio	$\delta^{13}C_{CH4}$	-	.	-	-47.96	-0.15	-0.037
Chlorofluorocarbons							
CFC-11	CCl_3F	52	5 560	217.1	217.5	-2.98	-1.78
CFC-12	CF_2Cl_2	102	11 200	485.4	488.9	-4.61	-2.79
CFC-113	CF2ClCFCl2	93	6 520	67.1	68.1	-0.46	-0.61
CFC-115	CF_3CF_2Cl	540	9 600	-	8.9	0.06	0.03
Hydrochlorofluorocarbons							
HCFC-22	$CHClF_2$	11.9	1 960	247.5	256.4	-2.07	4.95

Component	Chemical formula	Life-time	GWP	Global mean 2024	Annual mean 2024	Absolute change last year	Trend /yr
HCFC-141b	$C_2H_3FCl_2$	9.4	860	24.5	26.0	-0.14	0.44
HCFC-142b	CH_3CF_2Cl	18	2 300	21.0	22.4	-0.34	0.38
Hydrofluorocarbons							
HFC-125	CHF_2CF_3	30	3 740	38.8	47.6	4.12	2.03
HFC-134a	CH_2FCF_3	14	1 530	129.5	136.9	5.10	5.31
HFC-152a	CH_3CHF_2	1.6	164	7.4	10.8	0.03	0.34
HFC-23	CHF_3	228	14 600	36.8	37.4	0.88	1.08
HFC-365mfc	$CH_3CF_2CH_2CF_3$	8.9	914	1.07	1.32	-0.03	0.05
HFC-227ea	CF_3CHFCF_3	36	3 600	2.2	2.49	0.20	0.14
HFC-236fa	$CF_3CH_2CF_3$	213	8 690	-	0.26	0.02	0.01
HFC-245fa	$CHF_2CH_2CF_3$	7.7	858	-	4.07	0.11	0.20
HFC-32	CH_2F_2	5.4	771	28.3	42.7	5.02	2.83
HFC-4310mee	$C_5H_2F_{10}$	17	1 600	-	0.32	0.00	0.01
HFC-143a	CH_3CF_3	51	5 810	28.4	32.5	1.75	1.60
Perfluorinated compounds							
PFC-14	CF_4	50 000	7 380	89.4	89.93	0.93	0.91
PFC-116	C_2F_6	10 000	12 400	5.24	5.30	0.09	0.09
PFC-218	C_3F_8	2600	9 290	0.76	0.78	0.02	0.02
PFC-318	$c\text{-}C_4F_8$	3200	10 200	2.1	2.16	0.12	0.07
Sulphurhexafluoride	SF_6	3 200	25 200	11.4	11.63	0.37	0.31
Nitrogen trifluoride	NF_3	569	17 400	-	3.39	0.28	0.11
Sulphuryl fluoride	SO_2F_2	36	4 630	-	3.07	0.10	0.10
Halons							
H-1211	$CBrClF_2$	16	1 930	2.84	2.97	-0.10	-0.07
H-1301	$CBrF_3$	72	7 200	3.32	3.39	-0.009	0.02
H-2402	$CBrF_2CBrF_2$	28	2 170	0.396	0.39	-0.004	-0.01
Halogenated compounds							
Chloromethane	CH_3Cl	0.9	5.5	549.9	512.84	-1.45	-0.45
Bromomethane	CH_3Br	0.8	2.4	6.47	6.59	0.05	-0.13
Dichloromethane	CH_2Cl_2	0.49	11.2	-	73.24	1.16	2.06
Trichloromethane	$CHCl_3$	0.5	20.6	-	11.87	-0.60	0.16
Carbon tetrachloride	CCl_4	32	2200	73.8	74.07	-1.07	-0.93
Trichloroethane	CH_3CCl_3	5	161	0.98	1.05	-0.11	-1.42
Trichloroethene	$CHClCCl_2$	0.02	0.04	-	0.20	-0.03	-0.02
Tetrachloroethene	CCl_2CCl_2	0.3	6.3	-	1.91	-0.13	-0.10
Volatile Organic Compounds (VOC)							
Ethane	C_2H_6	Ca 78 days*	-	-	1559.77	43.15	0.30
Propane	C_3H_8	Ca 18 days*	-	-	476.75	-15.54	-9.35

Component	Chemical formula	Life-time	GWP	Global mean 2024	Annual mean 2024	Absolute change last year	Trend /yr
Butane	C_4H_{10}	Ca 8 days*	-	-	111.81	-8.94	-3.42
Pentane	C_5H_{12}	Ca 5 days*	-	-	24.92	-2.57	-0.83
Benzene	C_6H_6	Ca 17 days*	-	-	57.37	-1.50	-1.73
Toluene	$C_6H_5CH_3$	Ca 2 days*	-	-	23.06	3.70	-1.18

**The lifetimes of VOCs are strongly dependent on season, sunlight, other components etc. The estimates are global averages given in C. Nicholas Hewitt (ed.): Reactive Hydrocarbons in the Atmosphere, Academic Press, 1999, p. 313. The times series for these are short and the trend is very uncertain.*

2.1.1 Carbon dioxide (CO_2)

Key findings for CO_2: NILU's observations show a consistent global increase in CO_2, with no signs of slowing down. The annual peaks in CO_2 concentrations occur during the Northern Hemisphere winter, when emissions are higher and vegetation uptake is reduced. In contrast, troughs generally appear during the growing season, when vegetation absorbs more CO_2. Short-term fluctuations are also observed, often caused by long-range transport of polluted air from regions such as Central Europe, North America, and Russia. The mean concentrations for 2023 in ppm and increases compared to the previous year (in parentheses) were 421.5 (1), 426.0 (2.1), and 416.4 (2.1) at Zeppelin, Birkenes, and Trollhaugen, respectively, representing record high annual means at all sites.

CO_2 is the most important greenhouse gas driving climate change. Anthropogenic CO_2 emissions are primarily from fossil fuel burning and cement production. These are small compared to natural sources such as respiration and ocean release, but this is sufficient to exceed the natural sinks e.g. photosynthesis and ocean sedimentation, causing levels to rise. Global fossil CO_2 emissions have consistently increased over the past decades (Figure 2.3) except for a few years marked by international crises. NILU initiated CO_2 measurements at the Zeppelin Observatory in 2012, though the University of Stockholm, began measurements in 1990 (and even earlier, in 1988, in Ny Ålesund). Continuous CO_2 measurements have been conducted at Birkenes since May 2009. CO_2 measurements at Trollhaugen, which are not financed by the monitoring programme, are added here for comparison, and began in 2014. Birkenes exhibits larger CO_2 variations than Zeppelin due to its proximity to sources. Zeppelin experiences the greatest CO_2 variability during winter and spring, largely due to the polar dome phenomenon. In winter, the polar dome limits air exchange, keeping local emissions contained, while in spring, this barrier weakens, allowing polluted air from distant regions such as Europe and Asia to enter and cause variability. In contrast, Birkenes shows substantial CO_2 variations year-round because it's closer to populated and industrialized areas, with less seasonal isolation. Both sites experience episodes of elevated CO_2 due to long-range transport of pollution from regions like Central Europe, North America, or East Asia. The lowest CO_2 levels are seen at Trollhaugen, where levels are below the global mean. This reflects the remoteness of the Trollhaugen site in Antarctica. Generally, high levels occur when meteorological conditions lead to transport from Central Europe or the UK at Birkenes, and from Central Europe or Russia at Zeppelin. Annual increases compared to the global mean are shown in Figure 2.4.

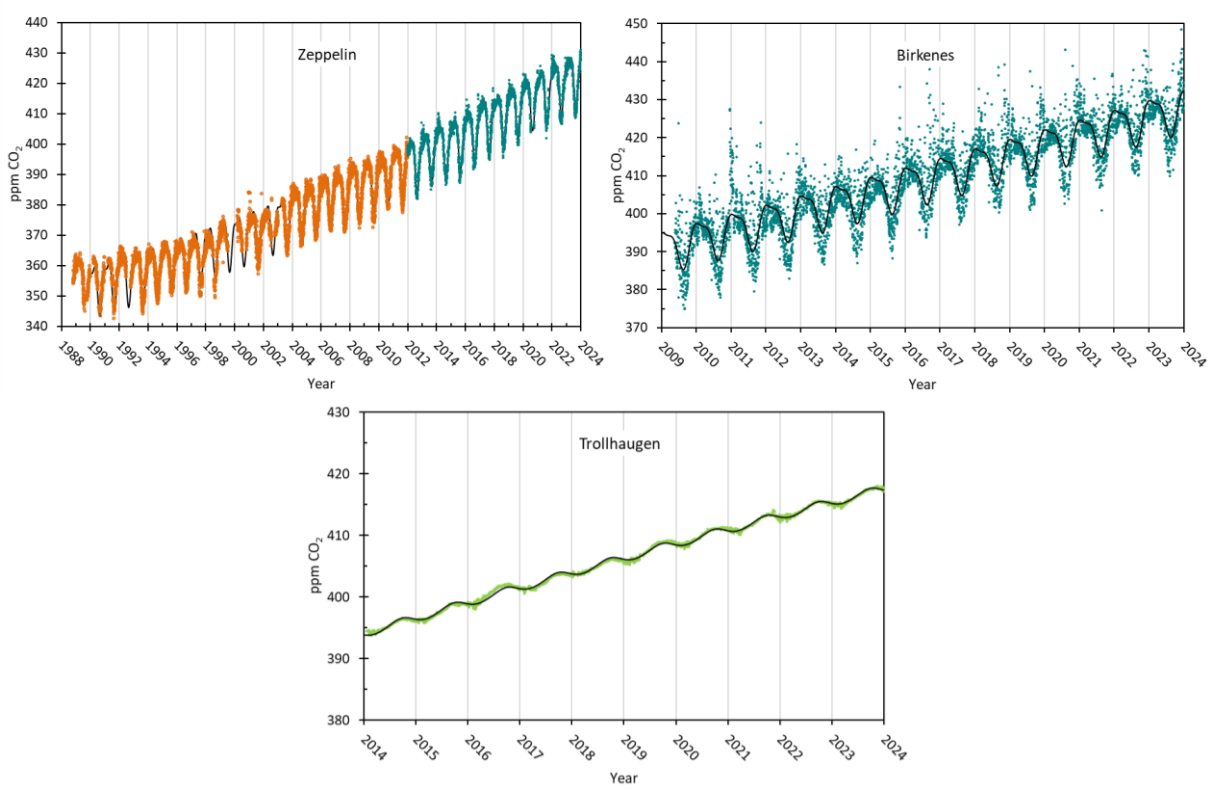

Figure 2.3: Top left: daily mean CO_2 concentrations at Ny Ålesund (1988 to 1990, not included in trend calculations or fitting) and the Zeppelin Observatory from 1990 to 2024. Prior to 2012, ITM University of Stockholm provided all data (orange) subsequent data from NILU are shown in green. Top right: daily mean CO_2 at Birkenes (green). Lower: daily mean CO_2 at Trollhaugen (light green). The black solid lines are the empirical, fitted, mixing ratio, with fit coefficients yielding the trend. This trend calculation is described in Appendix II.

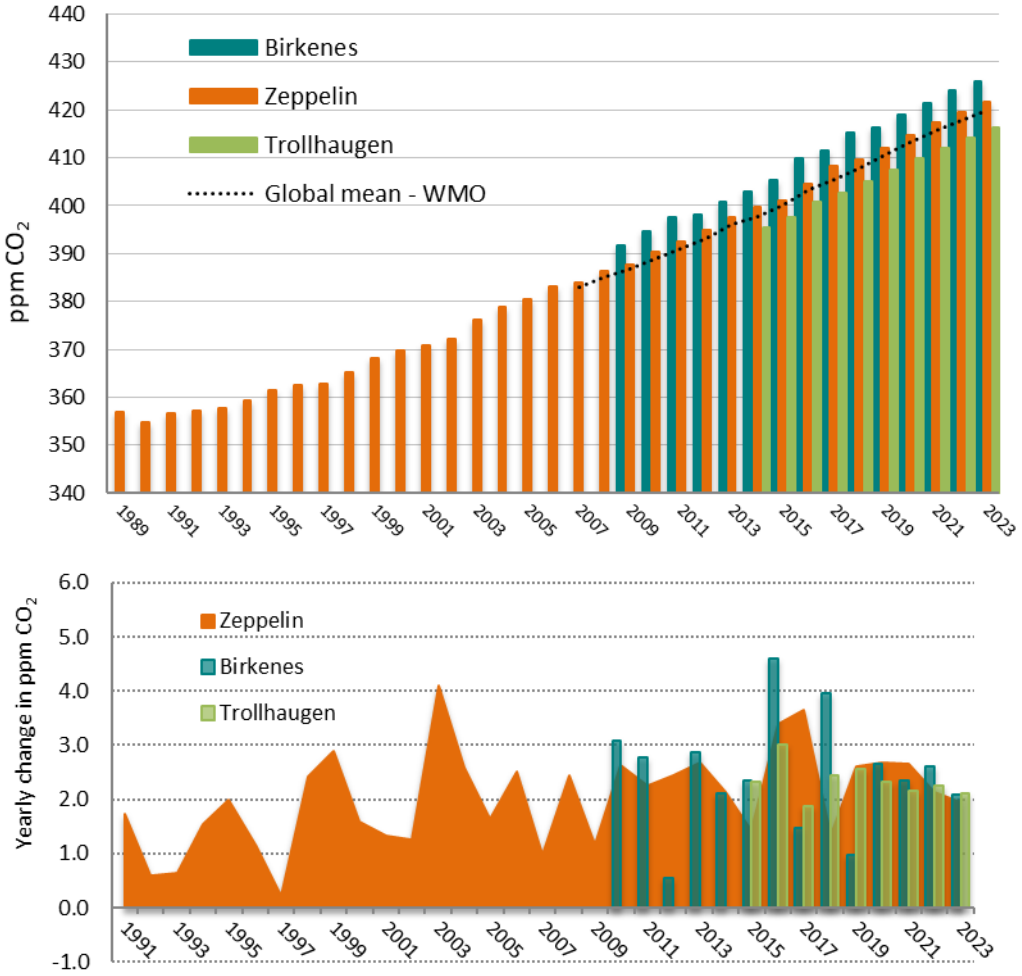

Figure 2.4: Upper panel: the annual mean concentrations of CO_2 measured at Zeppelin Observatory for the period 1989 to 2024 shown in orange. Prior to 2012, ITM University of Stockholm provides all data. The annual mean values from Birkenes are shown as green bars, and for Trollhaugen in light green. The global mean values as given by WMO (2008 to 2023) are included in the black dashed line. The yearly annual increases are shown in the lower panel, orange for Zeppelin, green for Birkenes, and light green for Trollhaugen.

2.1.2 Methane (CH_4)

Key findings for CH_4: Data from Birkenes and Zeppelin both show accelerating increases in CH4, threatening the Paris agreement goal of limiting warming to 2 or preferably 1.5°C. The seasonal pattern in the time series is a result of higher CH4 removal rates in Summer via the main sink, the OH radical, which is produced via reactions involving sunlight. As is the case for CO_2, long range transport from polluted regions causes episodes of high concentration. The mean methane concentrations in ppb for 2023 and increases compared to the previous year (in parentheses) were 2007.6 (8.0) at Zeppelin, 2016.2 (10.7) at Birkenes, and 1871.1 (12.9) at Trollhaugen, representing record high annual means at all sites.

CH_4 is the 2nd most important greenhouse gas, due to a high GWP of ~28, and plays a central role in atmospheric chemistry. The atmospheric lifetime[1] of methane is 11.8 years (Masson-Delmotte et al., 2021), when indirect effects (e.g., on OH radical levels) are included. Excluding indirect effects, the lifetime is ~9 to 10 years. CH_4 in the environment is formed when organic compounds are broken down in anoxic conditions. This is either by thermogenesis (mainly combustion) or biogenesis (mainly microbial), and is due to biogenic or anthropogenic activity, each accounting for around half of the global atmospheric methane burden (Table 4). The main cause of the ongoing methane increases since ~2006 (Figure 2.6 and Figure 2.7) is thought to be increased tropical wetland activity and extent, i.e., increased methanogenic bacterial activity[2]. The main sink is removal by free hydroxyl radicals (OH) to eventually produce water and CO_2. A small fraction is also removed by surface deposition and reaction with chloride radicals (Cl). Since methane reacts with OH, increased CH_4 emissions reduce OH levels, which in turn extends methane's lifetime in the atmosphere. This positive feedback leads to higher CH_4 concentrations over time, as well as increases in other compounds that rely on OH for removal, such as most VOCs (Isaksen and Hov, 1987; Prather et al., 2001). Of concern are other possible climate feedbacks involving CH_4 including thawing permafrost (which may release trapped CH_4 and widen wetland extent) and decomposing gas hydrates.

There has been an increase in the concentrations of CH_4 at Birkenes and Zeppelin over the last years (Figure 2.5), and in general the concentrations are higher at Birkenes than at Zeppelin and higher at Zeppelin than Trollhaugen (Figure 2.6). A seasonal variation is clearly visible, although stronger at Birkenes than Zeppelin and Trollhaguen. This is due to longer distance to the sources at Zeppelin and particularly Trollhaugen, and thus the sink through reaction with OH dominates the variation. Note that for Trollhaugen the annual minimum is in winter i.e., the Antarctic Summer, and that trend calculations for methane are not yet possible for this site, where only a short time series is available. The larger variations at Birkenes are explained by both the regional sources in Norway, as well as a stronger impact of pollution transported from central Europe or UK. Meanwhile the big difference between global mean (Figure 2.6), and the observations at Zeppelin and Birkenes is due higher emissions in the Northern hemisphere.

Note that year-to-year changes in methane (and all other greenhouse gases) at NILU's observatories are influenced by several short-term factors, which may partly obscure long-term trends. Drivers of short-term variability include changes in atmospheric transport patterns (e.g., how much air is received from high-emitting regions), changes in atmospheric chemistry (particularly due to emissions of other hydrocarbons and their influence on OH levels), and short-term fluctuations in emissions. Emission changes are also driven by climatological factors, such as precipitation patterns that affect methane emissions from wetlands. Hence, while smaller increases in CH_4 were seen in 2023 compared to 2022, these short-term factors make it challenging to draw conclusions based on annual variations alone.

[1] Time taken to decay to 1/e, 1/2.7, of original levels.

[2] Methanogenic bacteria produce methane in oxygen-deprived environments, such as waterlogged soils in tropical wetlands, where they break down organic material anaerobically, releasing methane as a byproduct.

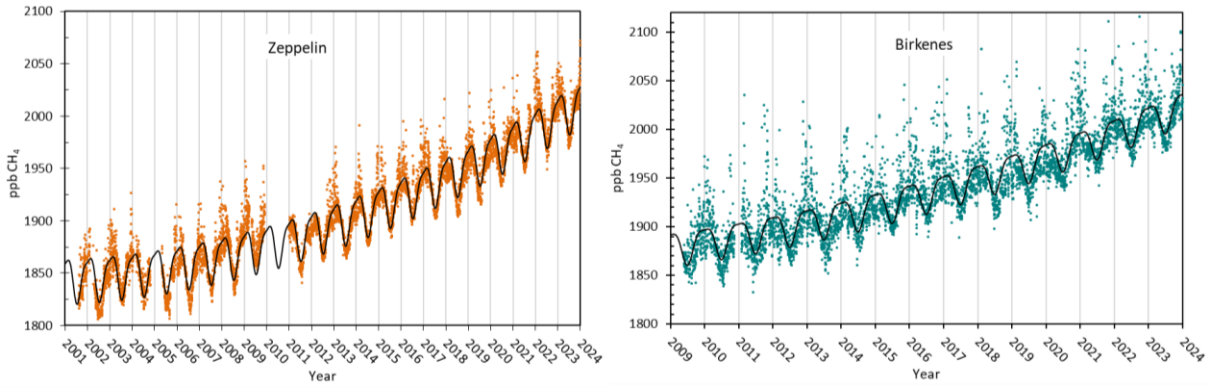

Figure 2.5: Left: daily averaged CH_4 mixing ratios for the period 2001 to 2024 at the Zeppelin Observatory and the empirical fitted methane mixing ratio (black). Right: daily averaged CH_4 mixing ratios for 2009 to 2024 at the Birkenes Observatory and the empirical fitted methane mixing ratio (black). The black solid lines for both are the empirical, fitted, mixing ratio, with fit coefficients yielding the trend. This trend calculation is described in Appendix II. The methane trend is too short for trend analysis or interpretation of longer term variation and is not included here.

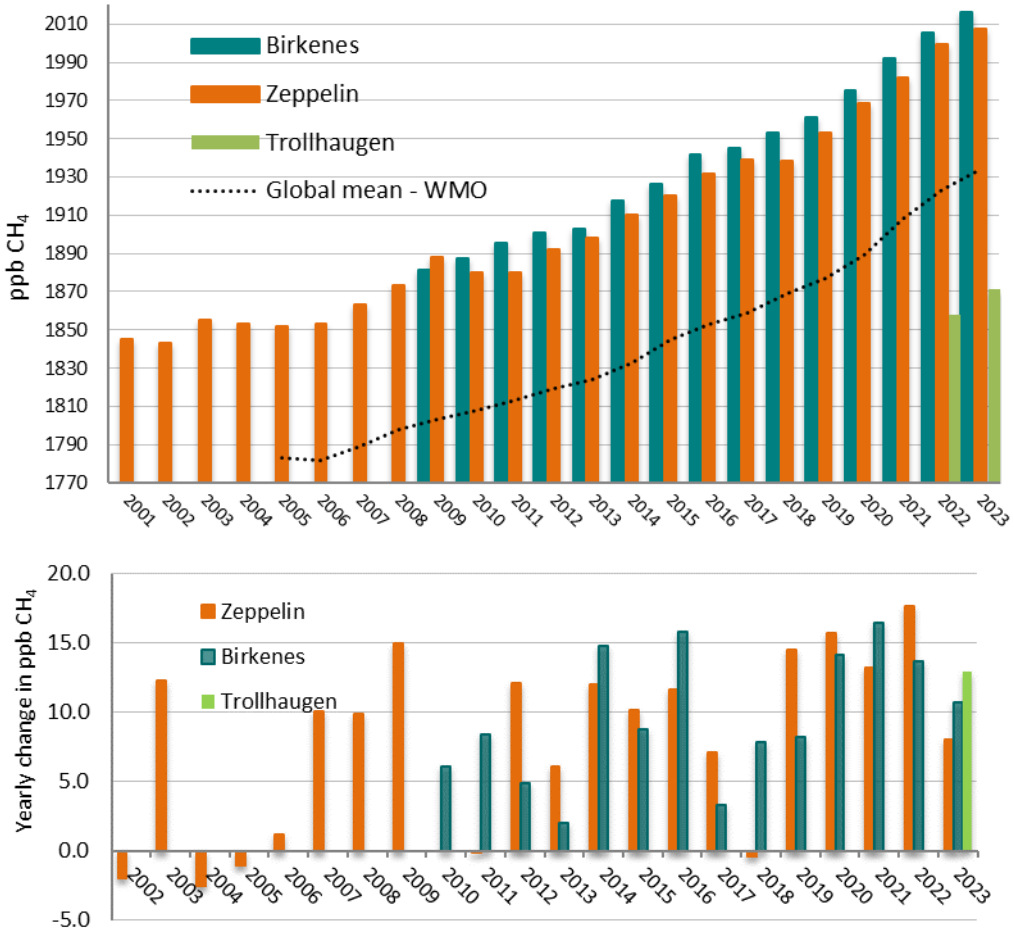

Figure 2.6: Upper: Development of the annual mean CH_4 mixing ratio at the Zeppelin Observatory (orange bars) for the period 2001 to 2024, Birkenes for the period 2010 to 2024 in dark green bars, and Trollhaugen 2022 to 2023 (light green bars), compared to global mean provided by WMO as black line (WMO, 2024). Lower: yearly increases for Zeppelin (orange), Birkenes (dark green), and Trollhaugen (light green). The annual means are based on the measured CH_4 values, however, model fitted values are used to fill in gaps if measurements are missing.

2.1.3 Methane isotopic signature

Key findings for CH_4 isotopic signature: The isotopic signature of CH_4 ($\delta^{13}C_{CH4}$) has decreased at the same time as the atmospheric CH_4 concentration has increased. This likely reflects increased emissions in tropical wetland regions. This is particularly concerning because it is more difficult to control natural emission sources compared to manmade emission sources.

The isotopic signature of CH_4 (written as $\delta^{13}C_{CH4}$) varies by emission source (France et al., 2016) and is also modified by the sink strength, hence measurements of the isotopic signature provide additional information on the changing balance of CH_4 sources and sinks (Table 4). Since $\delta^{13}C_{CH4}$ has shifted alongside the overall CH_4 concentrations, this implies that the change is being driven by a change in sources. Nisbet

et al. (2019) outline three non-mutually exclusive hypotheses compatible with observations of the isotopic signature:

1) Increased Biogenic Emissions: There may have been an increase in isotopically very negative biogenic emissions from sources such as wetlands, ruminants, and waste, or a combination of these. An increase in the proportion of global emissions from microbial sources could drive both the rise in methane levels and the shift towards a more negative $\delta^{13}C\text{-}CH_4$ signature.

2) Rise in Fossil Fuel Emissions with Altered Isotopic Characteristics: Methane emissions from the use of natural gas and oil may have increased. Typically, fossil fuel emissions have a $\delta^{13}C\text{-}CH_4$ signature less negative than biogenic sources. This hypothesis would align with the isotopic shift if either (a) recent fossil fuel emissions have a $\delta^{13}C\text{-}CH_4$ value markedly more negative than usual, (b) there has been a concurrent decline in a more ^{13}C-rich source, such as biomass burning, or (c) both changes have occurred. Both microbial and fossil fuel emissions could have increased, with the microbial increase being larger, driving the overall shift to a more negative $\delta^{13}C\text{-}CH_4$.

3) Reduced Atmospheric Oxidative Capacity: The oxidative capacity of the atmosphere, primarily governed by hydroxyl radicals (OH), may have declined, slowing methane's breakdown. A decrease in OH would have a strong isotopic impact, possibly resulting in a more negative $\delta^{13}C\text{-}CH_4$ signature even if total emissions changed little or potentially decreased. However, some studies suggest that OH variability during recent years may have been relatively small.

Increased biogenic emissions from wetlands are thought to be the main driver of increased CH_4 since this is consistent with the knowledge that methanogenic bacteria produce more methane at higher temperature and that wetland emission rates are increasing (Yuan et al., 2014b). Some increase in methane around 2020 to 2022 was driven by decreased OH levels due to changes in atmospheric chemistry (lower oxides of nitrogen, NO_X, emissions) during COVID lockdowns (Stevenson et al., 2022).

Careful interpretation of the signature is necessary, in combination with CH_4 observations in the previous section, and knowledge of relevant Earth Systems (e.g., land use change via models). This includes intercomparison of laboratory methods to harmonize data and increase interoperability of measurements and consideration of whether the isotopic signature of the sources themselves is also changing.

Changes in $\delta^{13}C_{CH4}$ signature at Zeppelin (Table 3) also support the hypothesis of an increase in microbial activity from wetlands (more negative signature, Figure 2.7). NILU's work on isotopes is also supported by Royal Holloway University of London (RHUL) light stable isotope laboratory.

Table 4: The main CH_4 sources and sinks in tera-grams (Tg) per year (yr) according to bottom-up estimations, from Saunois et al. (2024). The effect of a change in the sink is given in the right column. For example, increasing fossil fuel emission will tend to increase the background $\delta^{13}C_{CH4}$ signal to more positive values (a lower fraction of ^{13}C).

Source or Sink	Flux [Tg yr-1]	Effect on δ^{13}C-CH_4 of increased emission or increased sink
Fossil fuels	128	**More positive**
Agriculture and waste	211	**More negative**
Biomass burning	27	**More positive**
Wetlands and lakes	251	**More negative**
OH radical	-563	**More negative**
Oceanic	14	**More negative**

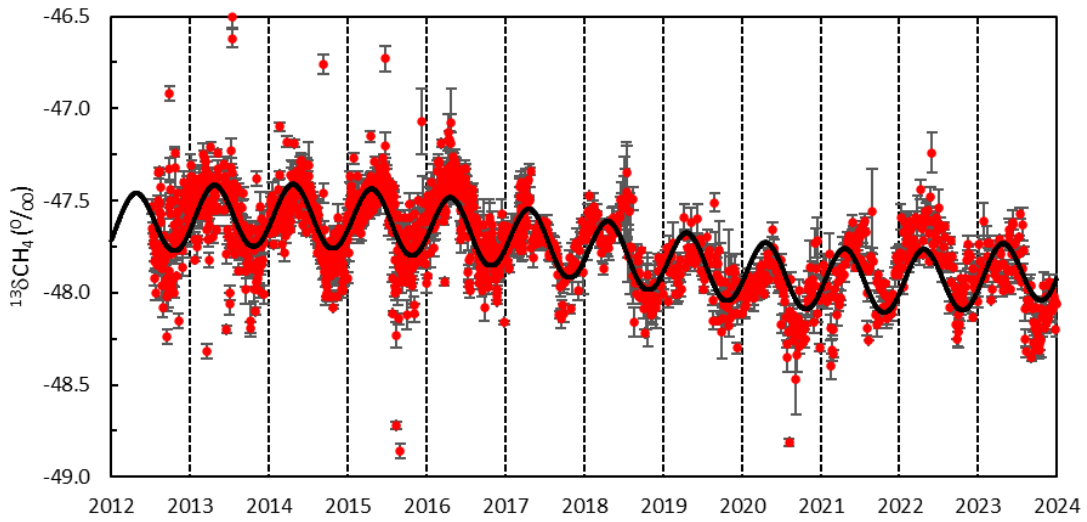

Figure 2.7: Long term measurements of the ^{13}C isotopic signature of CH_4 ($\delta^{13}C$-CH_4, red) at the Zeppelin Observatory, Svalbard 78°N. The black solid line is the empirical, fitted, mixing ratio, with fit coefficients yielding the trend. This trend calculation is described in Appendix II.

2.1.4 Nitrous Oxide (N_2O)

Key findings for N_2O: Nitrous Oxide (N_2O) is a powerful greenhouse gas, and levels continue to increase. Around half of emissions are manmade. The mean nitrous oxide concentration in ppb for 2023 and increase compared to the previous year (in parentheses) was 337.0 (1.18) at Zeppelin, a record high annual mean.

Nitrous Oxide (N_2O) is a greenhouse gas with both natural and anthropogenic sources including the oceans, tropical forests, soil, biomass burning, cultivated soil, animal manure, use of synthetic fertilizers, and various industrial processes. There are high uncertainties in the major soil, agricultural, combustion and oceanic sources of N_2O. Anthropogenic sources contribute approximately to 45% of total global N_2O emission according to the Global Carbon Project (https://www.globalcarbonproject.org/) Frozen peat soils in Arctic tundra are a potential source (Repo et al., 2009), but studies identify tropical and sub-tropical regions as the largest source regions (Thompson et al., 2013). N_2O is an important greenhouse gas with a high GWP of 273 and a radiative forcing of 0.21 W m^{-2} since 1750 (Masson-Delmotte et al., 2021). N_2O is also the major source of the ozone-depleting nitric oxide (NO) and nitrogen dioxide (NO_2) in the stratosphere, thus the component is also influencing the stratospheric ozone layer (WMO, 2024).

In 2009, NILU installed a new instrument at Zeppelin measuring N_2O with high time resolution of 15 minutes. The instrument was in full operation in April 2010 and has later been upgraded to comply with ICOS. NILU has experienced some technical difficulty with this instrument and for 2022 to 2023 the trend calculation is based on independent flask sample measurements at Zeppelin from NOAA. There has been a gradual increase in N_2O at Zeppelin since the measurements started in 2010 (Figure 2.8). Annual means at the Zeppelin Observatory compared to the WMO global data are shown in Figure 2.9.

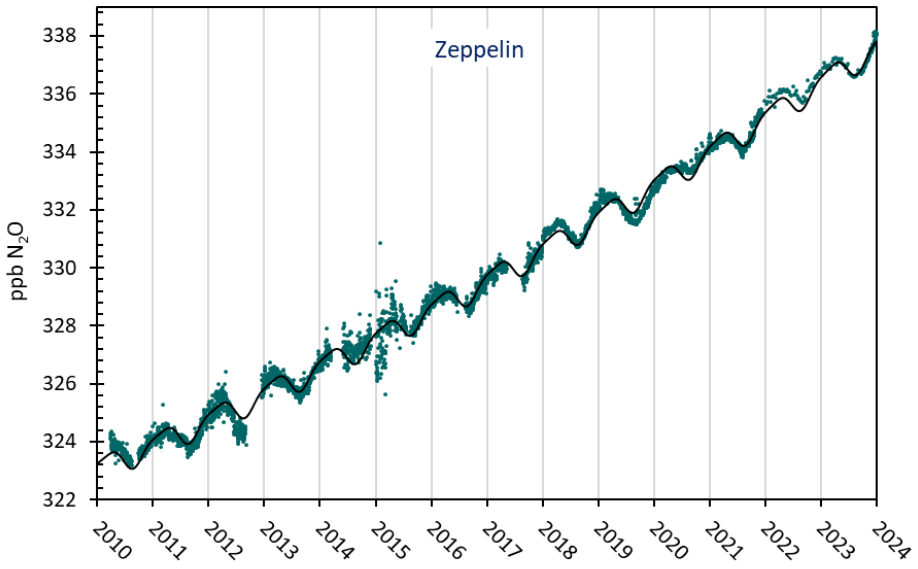

Figure 2.8: Measurements of N_2O at the Zeppelin Observatory for 2010 to 2024.The black line is empirical modelled N_2O mixing ratio. The black solid line is the empirical, fitted, mixing ratio, with fit coefficients yielding the trend. This trend calculation is described in Appendix II.

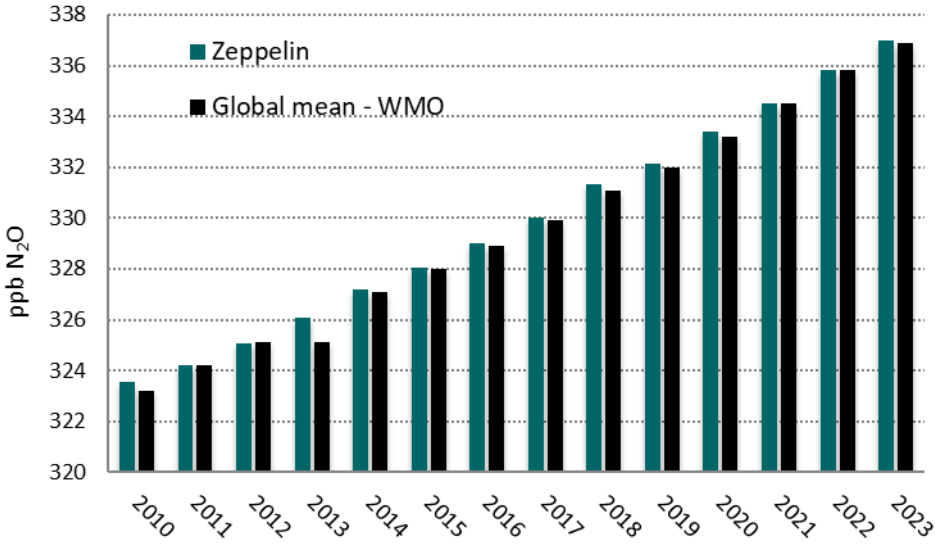

Figure 2.9: Annual mean concentration of N_2O at the Zeppelin Observatory for 2010 to 2024.

2.1.5 Volatile organic compounds (VOC)

Key findings for Volatile Organic Compounds (VOCs): Most VOC levels have declined recently, with the lowest levels observed in 2020 and 2021. It remains uncertain whether this decline is a lasting trend or was primarily influenced by the COVID-19 lockdowns. Notably, VOC levels have not returned to their pre-lockdown values, and the reasons for this sustained reduction are not yet fully understood. Potential factors driving these changes include shifts in the main sink (the OH radical), reductions in anthropogenic emissions—such as from oil and gas activities—and changes in atmospheric transport patterns from emission-heavy regions. Continued monitoring is essential to understand these developments.

Volatile Organic Compounds (VOCs) represent a large group of carbon-based compounds that have a high vapour pressure and easily evaporate at room temperature. Six different volatile VOCs have been measured at Zeppelin since September 2010: ethane, propane, butane, pentane, benzene, and toluene. VOC oxidation contributes to tropospheric ozone production and influences photochemical processes, both impacting climate and air quality. Sources of VOCs are both natural (mostly geological but also from wildfires) and anthropogenic (fossil fuels). CH_4 and VOCs are co-emitted from oil and natural gas sources.

In 2010 a Medusa-GCMS instrument was installed at Zeppelin, which made it possible to perform online high time resolution VOC measurements. Figure 2.10 shows the daily mean observations of the four non-methane hydrocarbons included in the programme in 2010: ethane, propane, butane, and pentane.

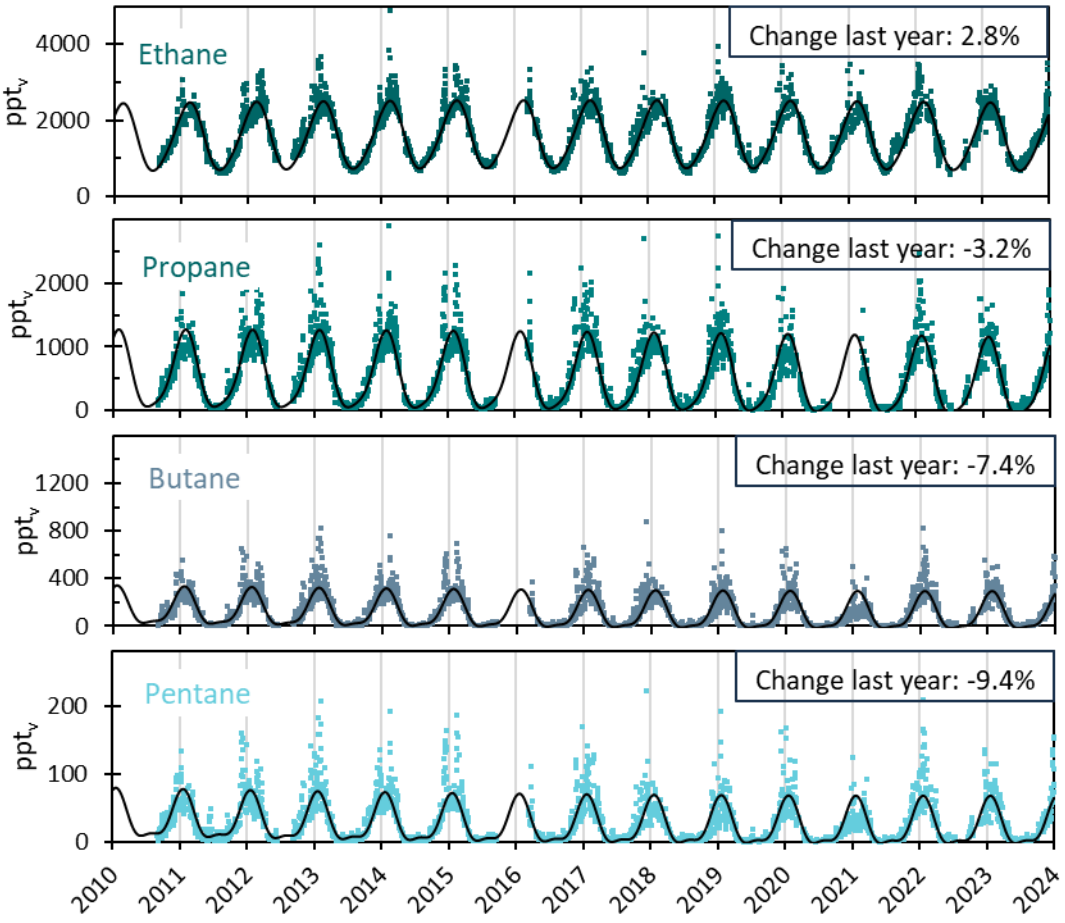

Figure 2.10: Observations of daily averaged mixing ratios of ethane, propane, butane, and pentane for the period September 2010 to 2024 at the Zeppelin Observatory. Due to a technical issue following a Medusa-GCMS upgrade in fall 2017, benzene and toluene measurements appeared unrealistically low. This did not affect actual background levels but resulted in missing data from 2018 to 2020. The black solid lines for both are the empirical, fitted, mixing ratio, with fit coefficients yielding the trend. This trend calculation is described in Appendix II.

Due to the short lifetimes, ranging from a few days for pentane to 2 to 3 months for ethane, the annual cycles are very strong and are regulated by OH reactions. The annual mean from 2011 to 2024 are shown in Figure 2.11. As seen from the figure the annual mean concentrations vary from one year to another and for most compounds it is not possible to draw any definite conclusions about development and trend. Figure 2.12 shows the daily mean observations of benzene and toluene at Zeppelin for the period 2010 to 2024. After an upgrade of the Medusa-GCMS in fall 2017, the benzene and toluene values became unrealistically low. This was purely a technical issue with no implication for the background levels of these gases. The upgrade was required to measure the low concentrations of the halogenated gases. Thus, the measurements performed in 2018 to 2020 are mainly missing.

Figure 2.11: Development of the annual means of the measured non-methane hydrocarbons at the Zeppelin Observatory for the period 2011 to 2024. Upper left panel in dark green: ethane, upper right panel: propane, and lower panel: butane and pentane. All values in ppt.

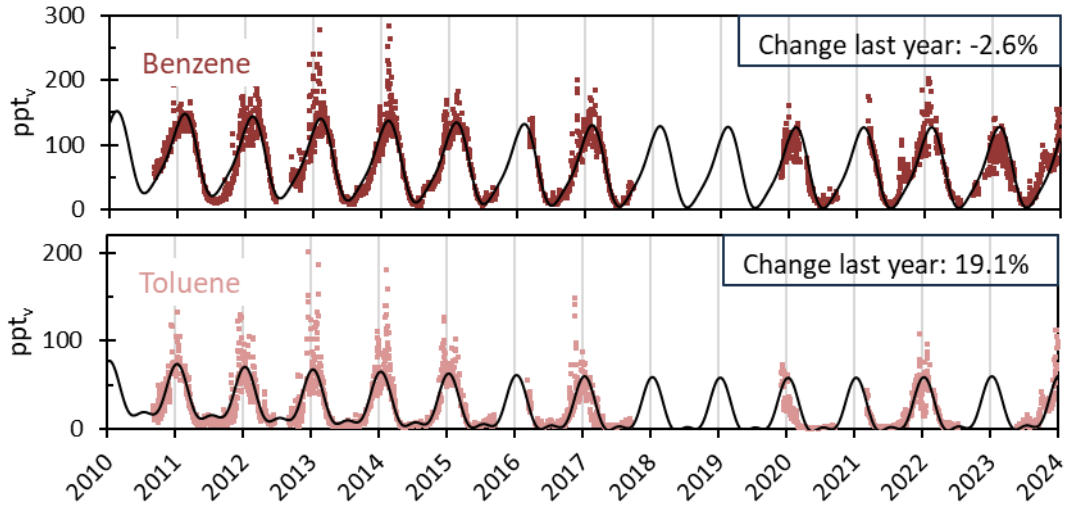

Figure 2.12: Daily averaged mixing ratio of benzene (upper panel) and toluene (lower panel) for the period September 2010 to 2024 at the Zeppelin Observatory (pink dots). The black solid lines for both are the empirical, fitted, mixing ratio, with fit coefficients yielding the trend. This trend calculation is described in Appendix II.

As can be seen from the figure there are strong annual variations, mainly explained by the reactions induced by sunlight. The annual means of benzene and toluene for the period 2011 to 2024 are presented in Figure 2.13. As explained above annual mean values were not calculated from the measurements in 2018 to 2020, which makes the trend estimates very uncertain. The shaded and patterned bars in Figure 2.13 imply that the annual means 2018 to 2020 primarily are based on model values (i.e., the black curve in Figure 2.12).

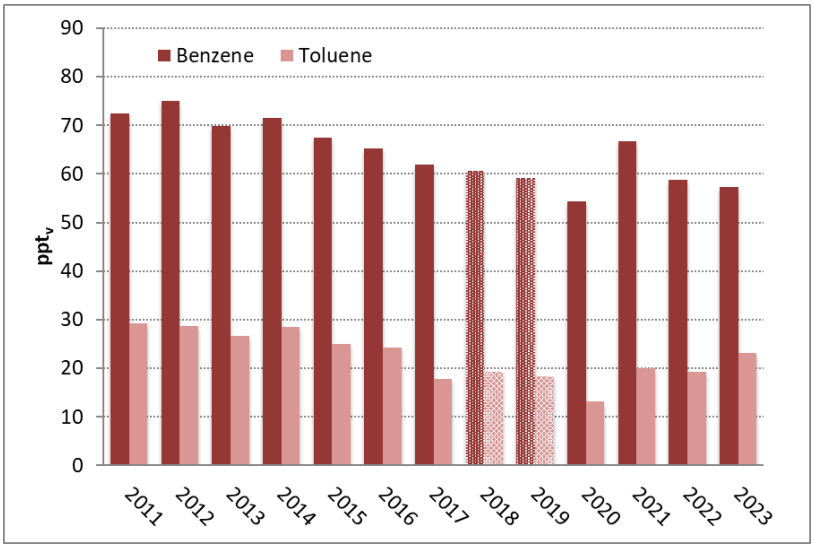

Figure 2.13: Development of the annual means of benzene (brown) and toluene (light red) for the period 2011 to 2024 at the Zeppelin Observatory. All concentrations are in ppt. Note that benzene and toluene in 2018 to 2020 mainly are based on data from the fitted trends.

2.1.6 Carbon monoxide (CO)

Key findings for Carbon monoxide (CO): CO levels are stable after a small decline between 2002 to 2010. Large spikes are often associated with long range transport.

Atmospheric carbon monoxide (CO) has both natural and anthropogenic sources. CO is produced when various organic gases are oxidized, such as methane, VOCs emitted from fossil fuel, and gases from biomass burning. Additionally, emissions from plants and ocean are important sources. CO is not considered as a direct greenhouse gas, as it does not absorb terrestrial thermal IR energy strongly enough. However, CO modulates the level of methane and the production of tropospheric ozone, which are both very important greenhouse gases. Hence, CO is considered as an indirect greenhouse gas. CO also plays a key role in the control of OH radicals. CO at Zeppelin is included in the current monitoring programme and for ICOS and the observed CO mixing ratios for the period September 2001 to 2024 are shown in Figure 2.14. CO concentrations show characteristic seasonal variations with a clear annual cycle with a late winter (February to March) maximum and a late summer (August) minimum. This seasonal cycle is driven by variations in OH concentration as a sink, emission by industries and biomass burning, and transport of air on a large scale. As seen from the figure there are also peak values which are due to long-range transport

of polluted air to Zeppelin and the Arctic, e.g., from Russia and Central and Northern Europe. The development of the annual CO means at Zeppelin for the period 2001 to 2024 is presented in Figure 2.15. Overall, the CO concentration at Zeppelin shows a decrease during the period 2003 to 2009, and stable levels the last years with a small peak in 2010.

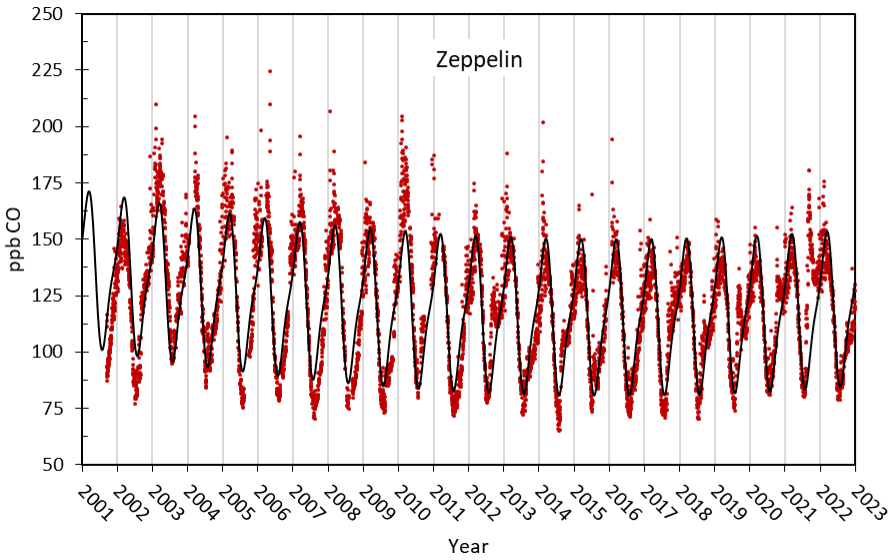

Figure 2.14: Daily averaged carbon monoxide (CO) from September 2001 to 2024 at the Zeppelin observatory (red dots). The black solid line is the empirical, fitted, mixing ratio, with fit coefficients yielding the trend. This trend calculation is described in Appendix II.

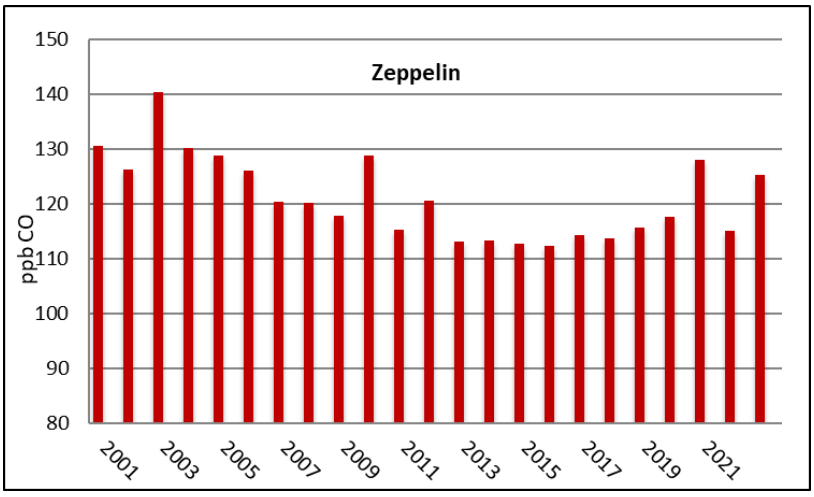

Figure 2.15: Development of the annual means of carbon monoxide at Zeppelin.

2.1.7 Chloromethane at the Zeppelin Observatory

Key findings for Chloromethane (CH_3Cl): CH_3Cl is ozone depleting but not regulated under the Kyoto and Montreal protocols because it is emitted naturally. Levels are stable and are lower at Zeppelin than the global average due to higher emissions in the Tropics.

Chloromethane (or methyl chloride, CH_3Cl) is the most abundant chlorine containing organic gas in the atmosphere, contributing ~16% of total chlorine from the well-mixed gases in the troposphere (WMO, 2014). It is a strong contributor to ozone depletion. Its main sources are natural, including the oceans, biomass burning, fungi, wetlands, rice paddies, and tropical forests and hence this compound is not regulated through the Montreal or the Kyoto protocols. CH_3Cl has a relatively high mixing ratio and contributes to the stratospheric chlorine burden. The results of the measurements of this gas for the period 2001 to 2024 are shown in Figure 2.16. The lifetime of chloromethane is only one year, resulting in large seasonal fluctuations due to rapid changes in emission, as shown in Figure 2.16.

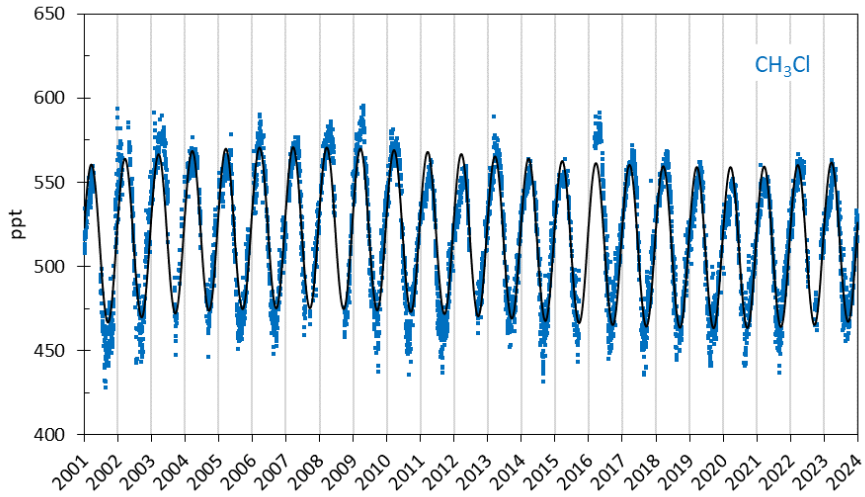

Figure 2.16: Daily averaged chloromethane, CH_3Cl, for the period 2001 to 2024 at the Zeppelin Observatory (blue dots). The black solid line is the empirical, fitted, mixing ratio, with fit coefficients yielding the trend. This trend calculation is described in Appendix II.

The annual means of chloromethane for the period 2001 to 2024 are shown in Figure 2.17. Days with missing observations are filled with empirically fitted data. Only small changes have been observed since the measurements started in 2001. The black bars in Figure 2.17 show that the global annual means, published by BAMS in the "State of Climate" report (2016 to 2023, last reported by Blunden et al., 2024), are 30 to 40 ppt (6 to 7%) higher than the annual mean values at the Zeppelin Observatory. This difference is likely due to strong emission sources in the tropics, which increase CH_3Cl levels at lower latitudes. As Zeppelin Observatory is located in the Arctic and further from these sources, it sees lower CH_3Cl levels, especially since chloromethane has a relatively short atmospheric lifetime and doesn't travel far from emission sources before being depleted in the atmosphere.

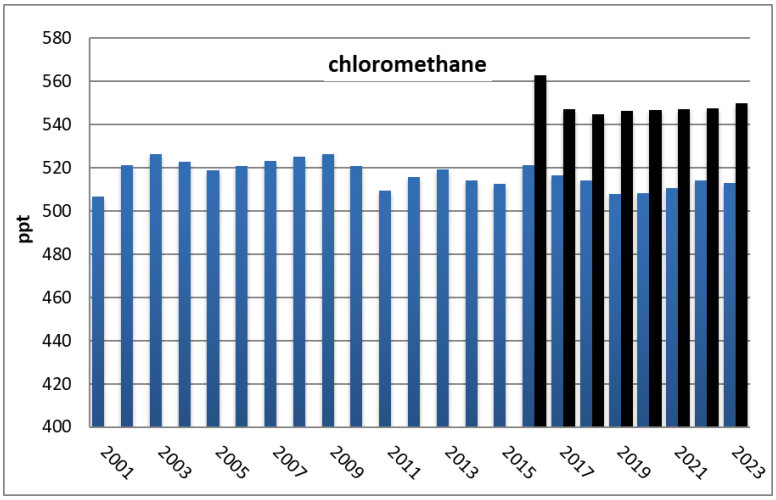

Figure 2.17: Development of Chloromethane annual means measured at the Zeppelin Observatory for the period 2001 to 2024. Global annual means for 2016 to 2024 are included as black bars. All units are in ppt.

2.1.8 Bromomethane at the Zeppelin Observatory

Key findings for Methyl bromide (CH_3Br): CH_3Br is a potent greenhouse gas and ozone depleting substance with both natural and anthropogenic sources. Levels have declined and are now stable following successful implantation of the Kyoto and Montreal protocols.

Bromomethane, also known as Methyl bromide (CH_3Br), is a significant atmospheric bromine reservoir, and is a key player in ozone layer depletion. This compound has dual origins—natural and anthropogenic— with natural sources such as the ocean, plants, and soil acting as both emitters and absorbers. The main anthropogenic source is fumigants for pest control. Additional anthropogenic contributors include leaded gasoline combustion, biomass burning, and emissions from specific crop species. Despite its natural occurrence, the human-induced release of bromomethane contributes to ozone layer depletion. The combined organic bromine levels from halons and bromomethane reached a peak in the mid-1990s and have declined and stabilised since 2001. Stratospheric bromide abundance has also started to decline (WMO, 2024). Figure 2.18 shows daily averaged CH_3Br mixing ratios from 2001 to 2024. CH_3Br is a potent greenhouse gas, twice as effective as CO_2, with a relatively short lifetime of 0.8 years (Myhre et al., 2013). This short lifespan accounts for the compound's annual and seasonal variations.

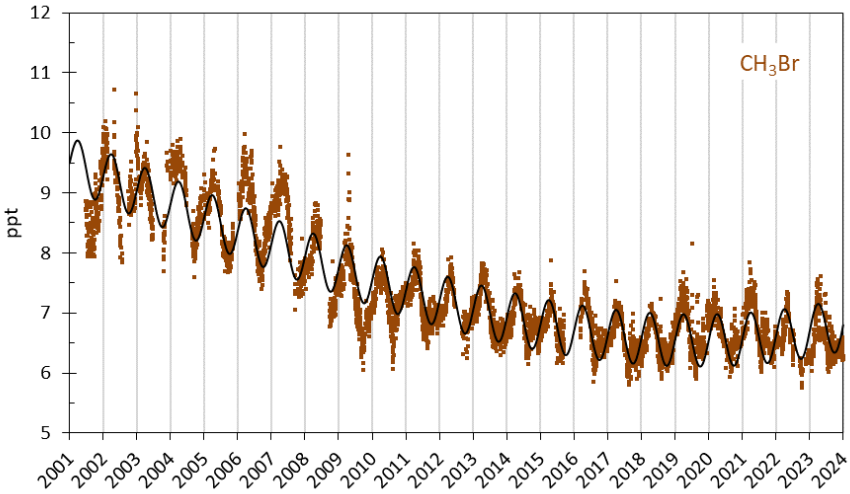

Figure 2.18: Observations of Bromomethane, CH_3Br, for the period 2001 to 2024 at the Zeppelin Observatory. Brown dots: daily averages mixing ratios from the observations. The black solid line is the empirical, fitted, mixing ratio, with fit coefficients yielding the trend. This trend calculation is described in Appendix II.

The development of the annual means for the period 2001 to 2024 is presented in Figure 2.19. The decline in bromomethane from 2001 to around 2015 is explained by a considerable reduction in emissions; the use of CH_3Br has decreased steadily following the implementation of the Montreal Protocol. The global mean mixing ratios published by BAMS in "State of the Climate" is close to the annual mean values observed at the Zeppelin Observatory.

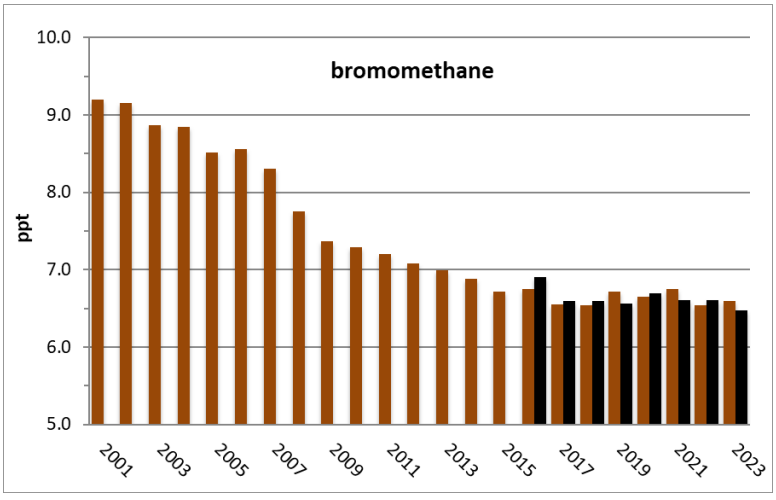

Figure 2.19: Development of the annual means of bromomethane measured at the Zeppelin Observatory for the period 2001 to 2024. The global annual mean for 2016 to 2024 are included as black bars.

2.1.9 Chlorofluorocarbons (CFCs) at the Zeppelin Observatory

Key findings for chlorofluorocarbons (CFCs): CFCs are regulated under the Montreal Protocol as ozone depleting substances. They are also potent greenhouse gases. Following the protocol, all four CFCs measured Zeppelin (-11, -12, -113, -115) declined. However, CFC-115 has begun to increase since ~2017, though it is still at a low concentration. The increase may be due to its use in HFC production. The Montreal Protocol does not forbid this use case, and future developments in CFC-115 should be followed closely.

NILU measures four chlorofluorocarbons (CFCs) at Zeppelin: CFCs -11, -12, -113, and -115 (Figure 2.20). These are the main four ozone depleting substances (ODS). The main sources of these compounds were foam blowing, aerosol propellant, refrigerants, solvents, and the electronics industry. Peak CFC production was ~1985, with peak emission two years later in 1987. Note however, that CFC-115 is used in the production of HFCs, and this use-case is not regulated under the Montreal Protocol (MP). The lifetimes of these compounds are long, from 52 to over five hundred years (Table 3) and combined with strong infrared absorption properties, their GWPs are high. However, the development of the CFC -11, -12, and - 113 levels, as seen at the global background site Zeppelin is promising and in accordance with the MP. While still not posing a threat due to low levels, and still in accordance with the MP, CFC-115 has increased since around 2017. This development must be followed closely.

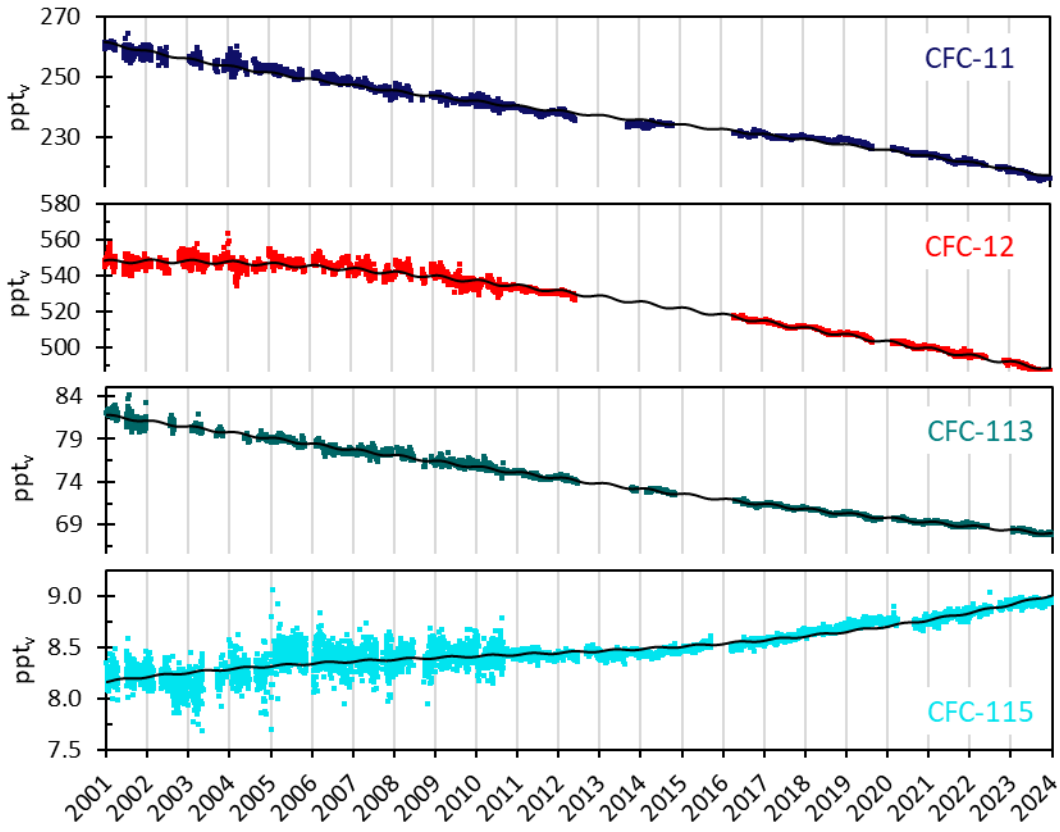

Figure 2.20: Daily averaged mixing ratios of the monitored CFCs at the Zeppelin observatory for the period 2001 to 2024: CFC-11 (dark blue), CFC-12 (red), CFC-113 (green) and CFC-115 (light blue). The black solid lines are the empirical, fitted, mixing ratios, with fit coefficients yielding the trend. This trend calculation is described in Appendix II.

The 2001 to 2024 annual means for all the observed CFCs at Zeppelin are shown in Figure 2.21. The global annual means in 2016 to 2024 as reported in "State of the Climate", BAMS (Blunden et al, 2024) are included as black bars for comparison. As can be seen, the observed concentrations at Zeppelin are close to the global mean for these compounds, as they are well mixed in the atmosphere since their lifetimes are long and there are hardly any present-day emissions.

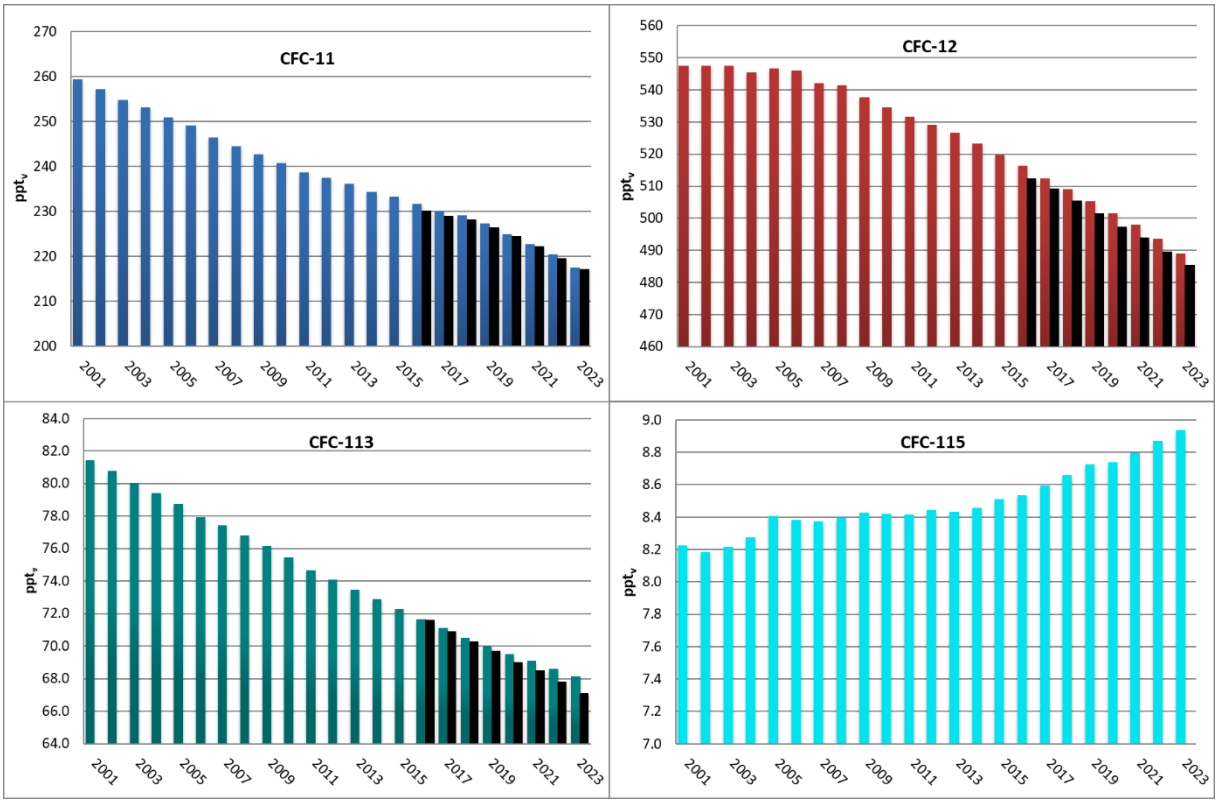

Figure 2.21: Development of CFC annual means at the Zeppelin Observatory for the period 2001 to 2024. Upper left panel: CFC-11, upper right panel: CFC-12, lower left panel: CFC-113, lower right panel: CFC-115. See Appendix I for data quality and uncertainty. The global annual means for 2016 to 2024 are included as black bars. All units are in ppt.

2.1.10 Hydrochlorofluorocarbons (HCFCs) at the Zeppelin Observatory

Key findings for hydrochlorofluorocarbons (HCFCs): HCFCs are stable or very recently in decline, in accordance with the Montreal Protocol.

Hydrochlorofluorocarbons (HCFCs) are the first-generation replacement gases for CFCs. Their lifetimes are rather long (Table 3), and although not as stable and persistent in the atmosphere as CFCs, they can still reach the stratosphere where they can destroy the ozone layer. Consequently, these gases are regulated through the Montreal Protocol. The Norwegian monitoring programme includes three HCFC species: HCFC-22 (removed from AGAGE since 2019), HCFC-141b and HCFC-142b. These compounds are mainly used as refrigerants, foam blowing agents and solvents. All these gases potentially have a strong warming effect due to their high GWPs, e.g., HCFC-142b has the highest GWP, with a warming potential 2300 times

stronger than CO_2, per kg gas emitted (Table 3). The daily averaged observations of the three HCFCs are shown in Figure 2.22 for 2001 to 2024.

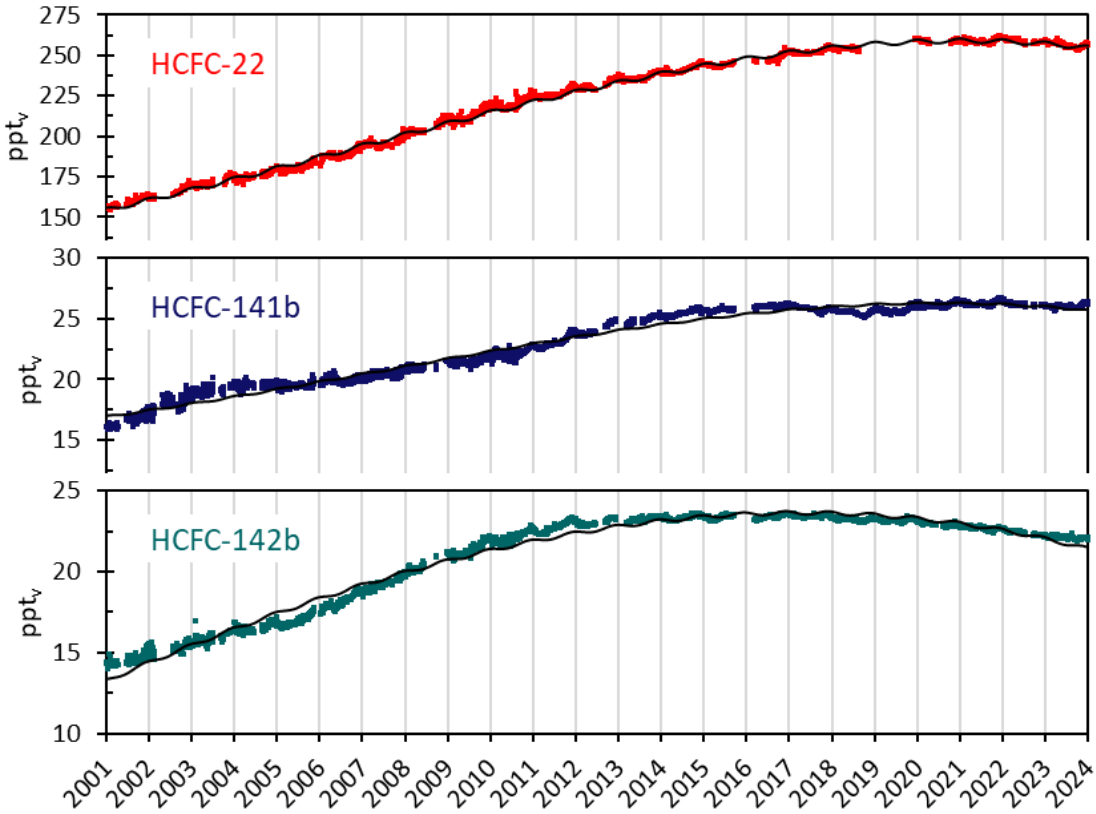

Figure 2.22: Daily averaged mixing ratios of the monitored HCFCs for the period 2001 to 2024 at the Zeppelin observatory: HCFC-22 (red), HCFC-141b (dark blue), and HCFC-142b (green). The black solid lines are the empirical, fitted, mixing ratios, with fit coefficients yielding the trend. This trend calculation is described in Appendix II.

Prior to ~2010 HCFC-22, HCFC-141b and HCFC-142b were increasing, see Figure 2.23, which also includes the global annual means for 2016 to 2024 (Blunden et al., 2024). The subsequent stabilisation or reduction in levels (for HCFC-142b and HCFC-22) is promising. The observed concentrations at Zeppelin are 4 to 6% higher than the global means, due to location in the Northern Hemisphere, closer to emission sources. Finally, however, despite the promising trend, with lifetimes in the order of 10 to 20 years, it is important to continue monitoring the development of the HCFCs for many years to come, as they have a significant influence on the ozone layer and are also strong greenhouse gases.

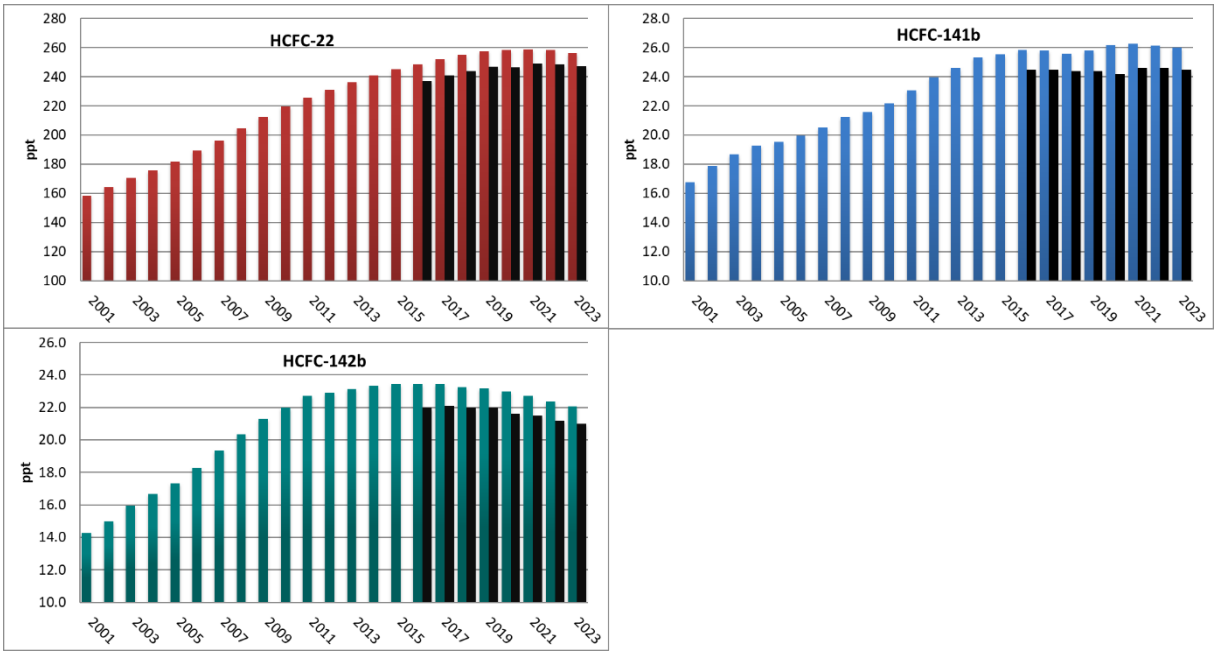

Figure 2.23: Development of the annual means of observed HCFCs at the Zeppelin Observatory for 2001 to 2024. HCFC-22 (red), HCFC-141b (blue), and HCFC-142b (green). The global annual means in 2016 to 2024 are included as black bars. All units are in ppt.

2.1.11 Hydrofluorocarbons (HFCs) at Zeppelin Observatory

Key findings for hydrofluorocarbons (HFCs): HFCs are second generation CFC replacements, with much lower ozone depleting potential than both CFCs and HCFCs. They are, however, strong greenhouse gases. Almost all are increasing in concentration, albeit from a low level at present, and these compounds should be monitored closely.

HFCs are second generation replacements of CFCs, meaning that they are considered as better alternatives to the CFCs with respect to the ozone layer than HCFCs, as they do not contain chlorine or bromine. However, many of these compounds are strong greenhouse gases. For example, HFC-23 has a GWP of 14600 (Table 3). The phase-out of HFCs under the Montreal Protocol was under negotiation for many years and the successful agreement in Kigali, October 2016, was an important step. Presently, the contribution to global warming posed by HFCs is very limited. However, most of the compounds are increasing rapidly. The compounds are strong infrared absorbers with high GWP hence it is crucial to reduce future emissions.

For the period 2001 to 2024, three compounds have been measured at the Zeppelin Observatory: HFC-125, HFC-134a, and HFC-152a. HFC-125 is mainly used as a refrigerant and fire suppression agent. HFC-134a is used as a temperature control for domestic refrigeration and automobile air conditioners, whereas HFC-152a is used as a refrigerant and propellant for aerosol sprays and in gas duster products. Since 1990, when HFC-134a was almost undetectable in the atmosphere, the concentration of this gas has risen massively, and HFC-134a is currently the HFC with highest atmospheric concentration.

In 2015 five new HFCs were included in the Norwegian monitoring programme: HFC-23, HFC-365mfc, HFC-227ea, HFC-236fa, and HFC-245fa. In 2016, three additional HFCs were introduced to the programme: HFC-32, HFC-143a, and HFC-4310mee. All these species have been measured at Zeppelin since 2010, but they have not been analysed or reported to an international data base until 2016. The development of HFC-23

should be followed carefully since this gas has a relatively high concentration and an extremely high GWP of 228. HFC-23 is a by-product of the production of HCFC-22 and is also used in the semiconductor industry. In addition, it is a useful refrigerant and fire suppressant.

Generally, the new HFCs are used for refrigeration and air conditioning, foam blowing, and fire extinguishing. Both HFC-245fa and HFC-365mfc are substitutes for HCFC-141b in foam blowing applications. HFC-236fa is also a foaming agent, in addition to a fire suppression agent and a refrigerant. HFC-227ea is mainly used to suppress fire in data equipment and telecommunication facilities, and in protection of flammable liquids and gases. HFC-227ea is also used as an aerosol propellant in pharmaceutical dose inhalers for e.g., asthma medication.

The three new HFCs introduced to the monitoring programme in 2016, are mainly used for refrigeration (HFC-32 and HFC-143a). In addition, HFC-143a is applied as propellant in canned air products for cleaning electronic equipment. HFC-4310mee is mainly used as a cleaning solvent in the electronics industry.

The seasonal cycles in HFC mixing ratios are closely linked to the lifetimes and variations in the incoming solar radiation. HFC-152a has the shortest lifetime (1.6 year), and as seen in Figure 2.24, HFC-152a has the most distinct seasonal cycle. The gas is mainly destroyed in the lowest part of the atmosphere by photolysis and reactions with OH.

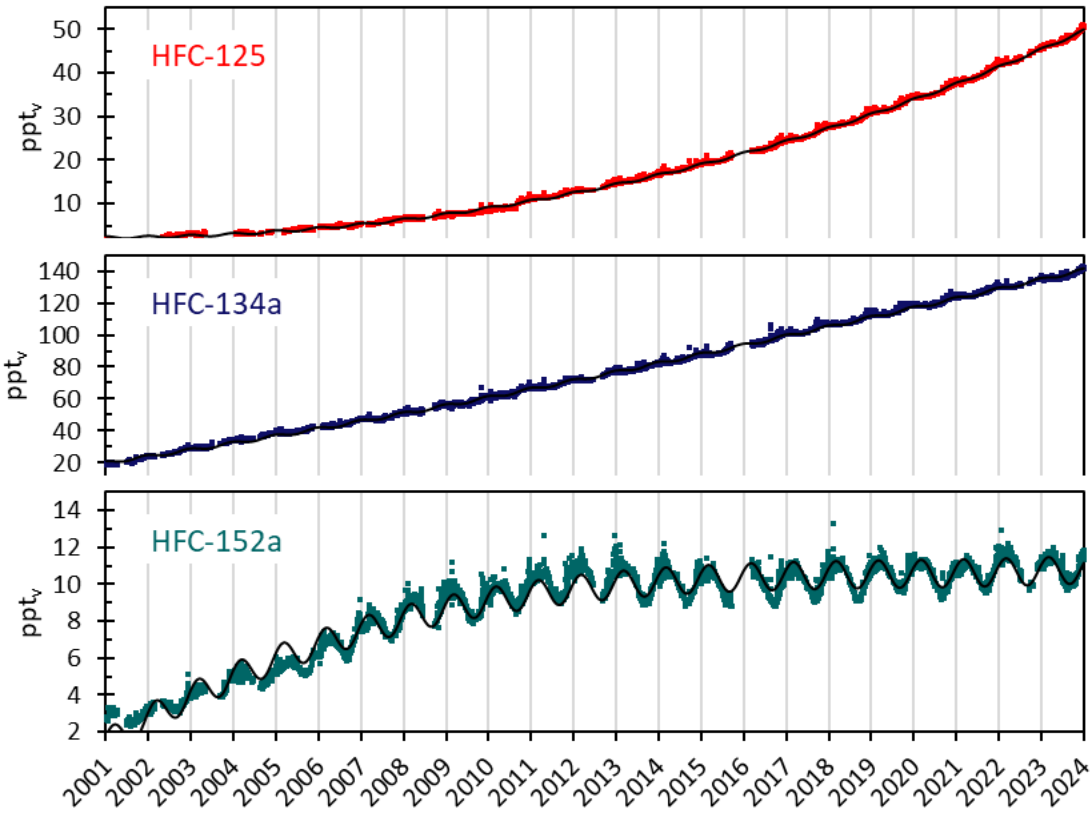

Figure 2.24: Daily averaged concentrations of the monitored HFCs for the period 2001 to 2024 at the Zeppelin observatory: HFC-125 (red), HFC-134a (dark blue), and HFC-152a (green). The black solid lines are the empirical, fitted, mixing ratios, with fit coefficients yielding the trend. This trend calculation is described in Appendix II.

HFCs shown in Figure 2.24 have increased significantly since 2001. HFC-152a has a shorter lifetime than the other HCFCs and hence the response to emissions changes is faster. This is clearly illustrated in Figure 2.25 and Figure 2.26 where there are apparent changes in the growth rate.

The eight new HFCs included in the programme in 2015 and 2016 are shown in Figure 2.25, which clearly demonstrates that the concentrations of all HFCs have increased steadily since 2010. The compounds generally increase by 4-10%/yr, except from HFC-32 which has an average increase of 17%/yr.

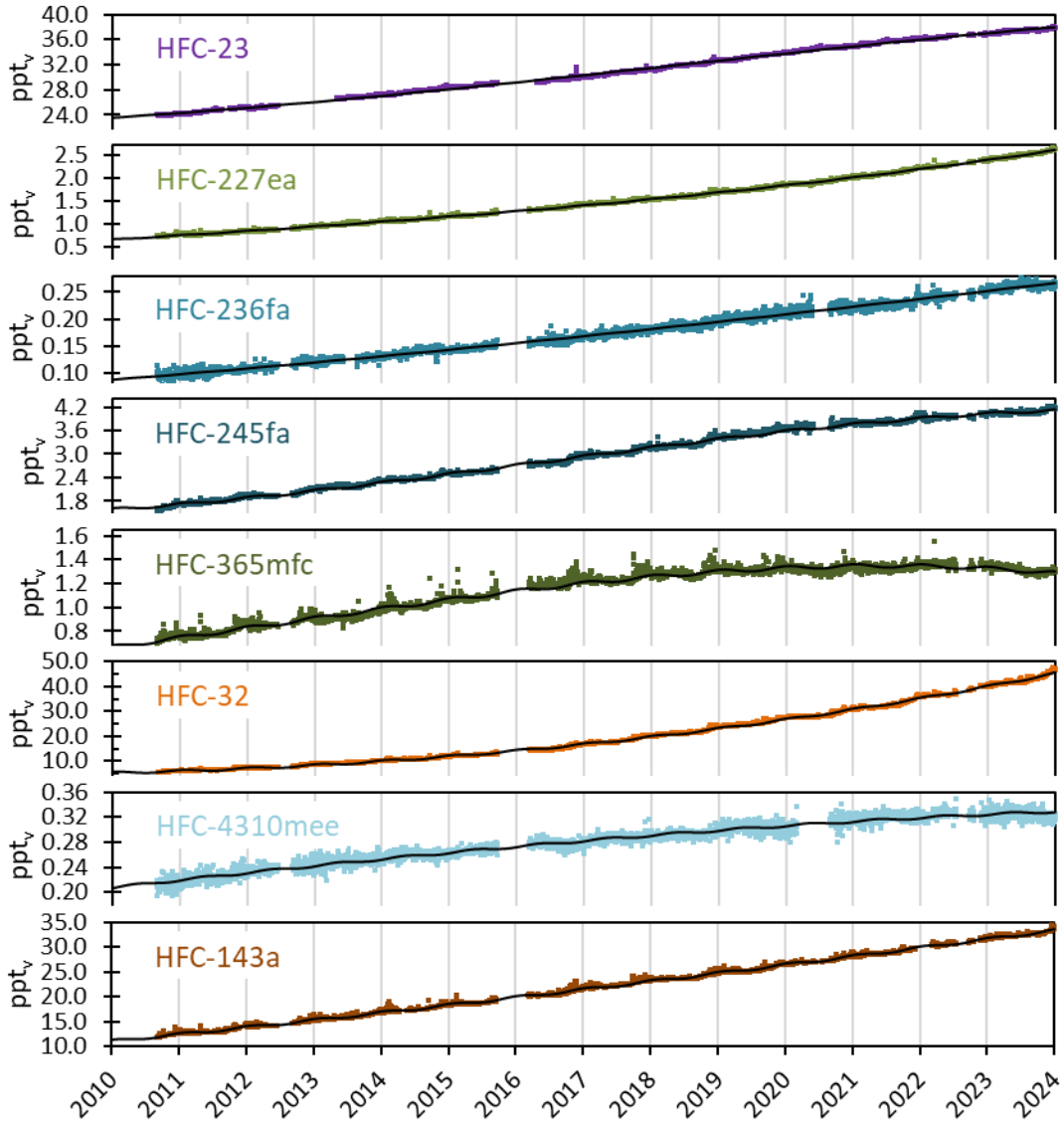

Figure 2.25: Daily averaged concentrations of monitored HFCs at the Zeppelin observatory for the period 2010 to 2024: HFC-23 (violet), HFC-227ea (light green), HFC-236fa (blue), HFC-245fa (dark blue), HFC-365mfc (dark green), HFC-32 (orange), HFC-4310mee (light blue), and HFC-143a (brown). The black solid lines are the empirical, fitted, mixing ratios, with fit coefficients yielding the trend. This trend calculation is described in Appendix II.

The development of annual means of all reported HFCs are shown in Figure 2.26. The global annual means of 2016 to 2024 as given in Hall et al. (2017; 2020), Dlugokencky et al. (2018; 2019), and Lan et al. (2021; 2022) are included as black bars for comparison. As for HCFCs the concentrations at Zeppelin are higher than the global means. Also, the increasing tendency for most HFCs is clear, even if the concentrations are still very low, particularly for the new HFC-365mfc, HFC-245fa, HFC-236fa, HFC-227ea, and HFC-4310mee.

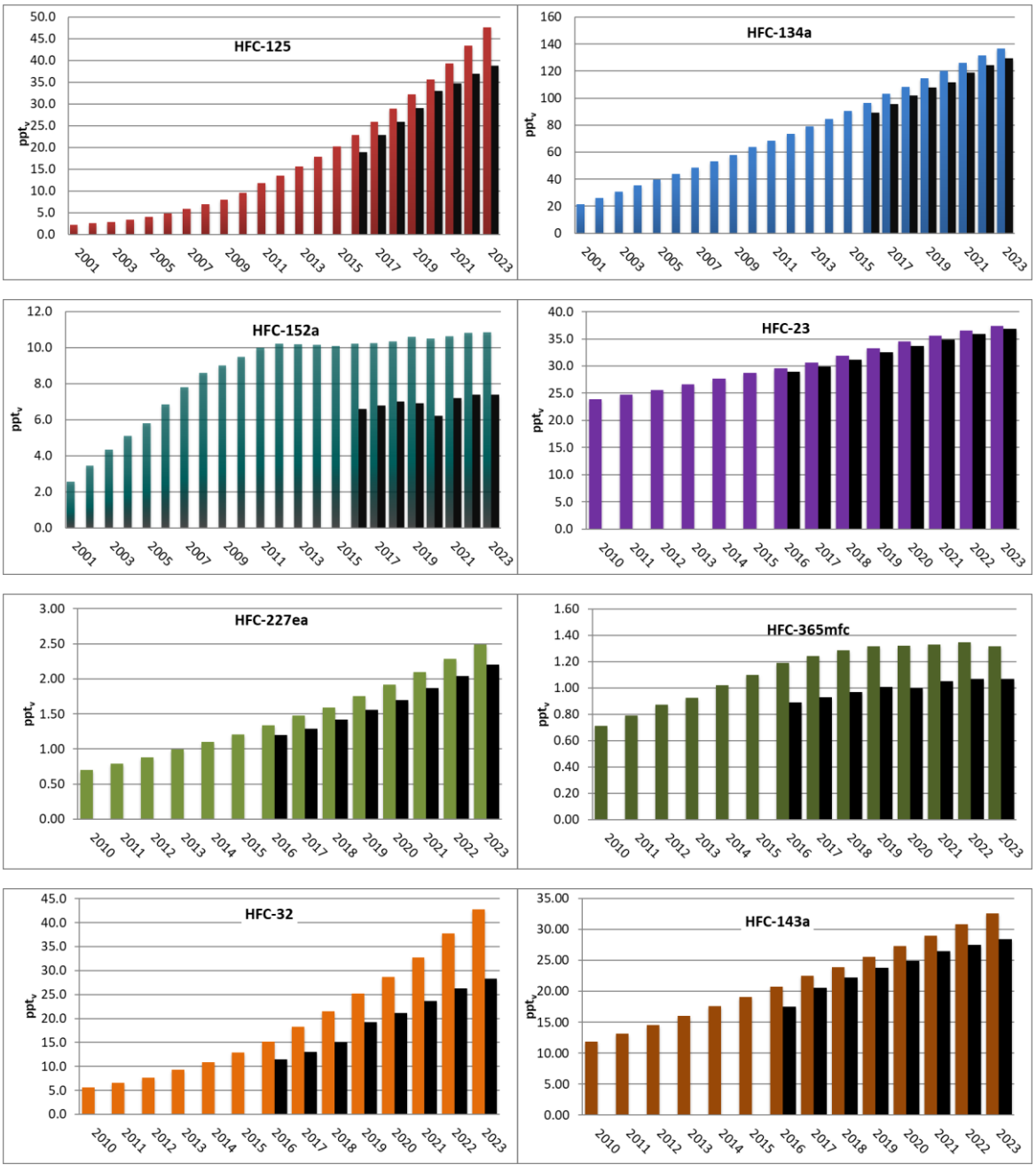

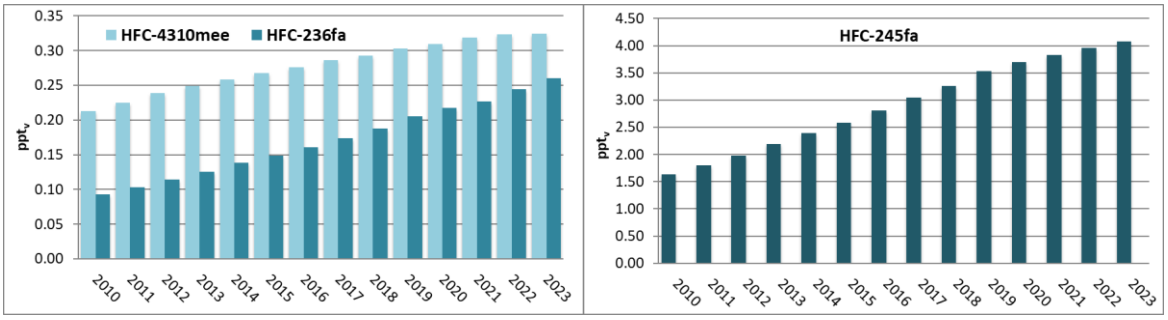

Figure 2.26: Development of the annual means of observed HFCs at the Zeppelin Observatory. For the period 2001 to 2024: HFC-125 (red), HFC-134a (blue), and HFC-152a (dark green). For the period 2010 to 2024: HFC-23 (violet), HFC-227ea (light green), HFC-365mfc (dark green), HFC-32 (orange), HFC-143 (brown), and light to dark blue: HFC-4310mee, HFC-236fa, and HFC-245fa. The global annual means in 2016 to 2024 included as black bars, when available.

2.1.12 Halons measured at the Zeppelin Observatory

Key findings for halons: Halons are bromine-containing greenhouse gases which are more ozone depleting than CFCs, though they are less likely to reach the stratosphere (location of the ozone layer). NILU measures three of these compounds at Zeppelin: H-1301 (levels of which are stable due to its long, 72-year lifetime), and H-1211 and H-2404 (levels of which are declining).

Halons are greenhouse gases containing bromine. Regulations for halons are also important to protect the ozone layer: If bromine reaches the stratosphere (high atmosphere), it is even more effective in destroying ozone than chlorine from CFCs. The halons are regulated through the Montreal Protocol and the concentration of most of these substances are decreasing. The main source of halons has been fire extinguishers. From 2001 to 2015 two halons were measured and analysed at the Zeppelin observatory: H-1301 and H-1211. In 2016 H-2402 was also included in the monitoring programme, where data were analysed back to 2010 (made possible since measurement chromatograms are stored and can be retrospectively analyzed for new compounds where peaks are present, identifiable, and represent robust measurements). H-2402 was used primarily in the former USSR and was the main halon fire suppressant in that region.

The ambient concentrations of the three halons are fairly low, below 4 ppt. Figure 2.27 shows the daily average concentrations of the monitored halons at Zeppelin. The halon trend analyses, listed in Table 3 are visualized in Figure 2.27. The annual mean of H-1301 is stable, while H-1211 and H-2404 are declining. This is explained by the shorter lifetime of the latter two compounds (16 years for H-1211, 28 years for H-2402) compared to H-1301 (72 years). A comparison to the global average of H-1211 and H-2402 is shown in Figure 2.28.

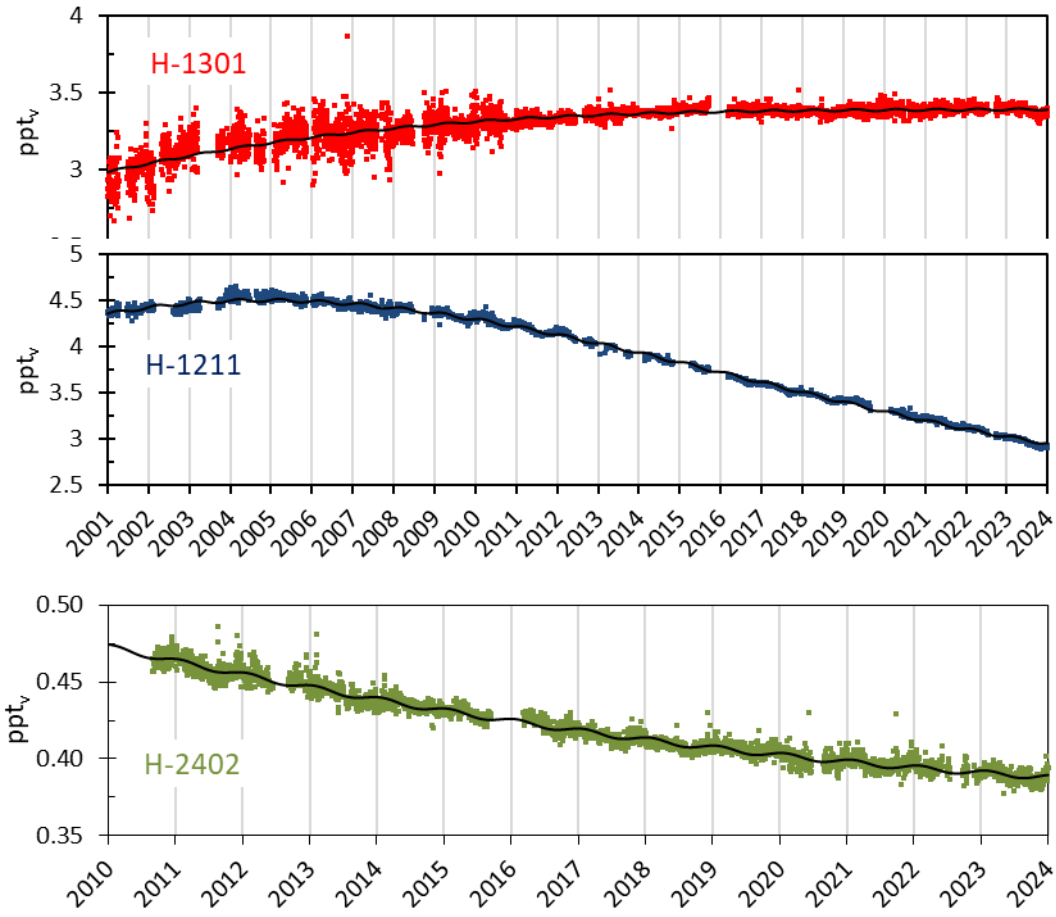

Figure 2.27: Daily averaged concentrations of the monitored halons at the Zeppelin Observatory. For the period 2001 to 2024: H-1301 (red) and H-1211 (blue). For the period 2010 to 2024: H-2402 (green). The black solid lines are the empirical, fitted, mixing ratios, with fit coefficients yielding the trend. This trend calculation is described in Appendix II.

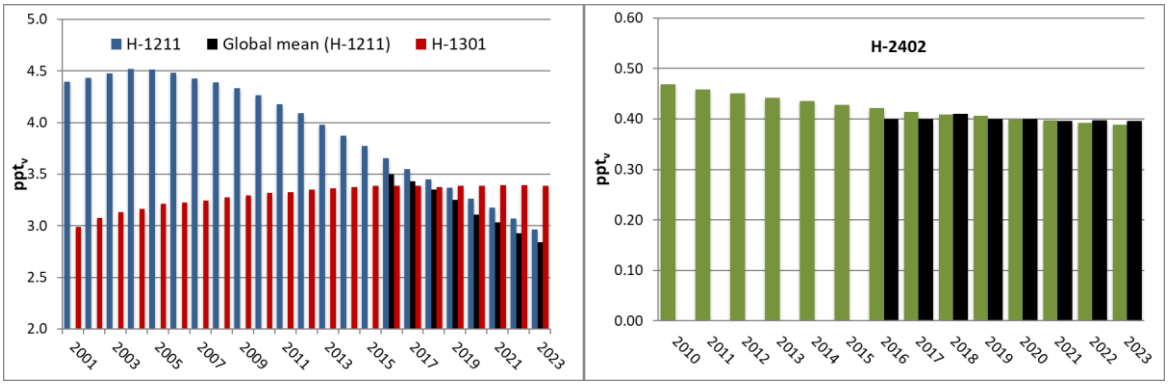

Figure 2.28: Development of the annual means of the observed halons at the Zeppelin Observatory. Red: H-1301, blue: H-1211, and green: H-2402. The global annual means in 2016 to 2024 are included as black bars. All units are in ppt.

2.1.13 Other chlorinated hydrocarbons at the Zeppelin Observatory

Key findings for other chlorinated hydrocarbons: Other chlorinated hydrocarbons at the Zeppelin Observatory are: Trichloroethane (or methyl chloroform, CH_3CCl_3), dichloromethane (CH_2Cl_2), trichloromethane (or chloroform, $CHCl_3$), trichloroethene (TCE, $CHClCCl_2$), carbon tetrachloride (CCL_4) and tetrachloroethene (PCE, CCl_2CCl_2). Levels of trichloroethane, PCE, TCE and carbon tetrachloride are all stable or in decline. Dichloromethane and trichloromethane levels have increased or fluctuated in recent years. The reason is unclear since both are from a mix of natural and anthropogenic sources. It is important to follow developments in all of these compounds since they are ozone depleting if they are able to reach the stratosphere despite their short lifetimes.

NILU measures the following additional chlorinated hydrocarbons at the Zeppelin Observatory: Trichloroethane (or methyl chloroform, CH_3CCl_3), dichloromethane (CH_2Cl_2), trichloromethane (or chloroform, $CHCl_3$), trichloroethene (TCE, $CHClCCl_2$), carbon tetrachloride (CCL_4), and tetrachloroethene (PCE, CCl_2CCl_2). The daily average concentrations and annual means are shown in Figure 2.29 and Figure 2.30. The main anthropogenic sources of all these substances are solvents, while some, such as trichloromethane have significant natural sources including vegetation and the oceans.

Trichloroethane (CH_3CCl_3), which is controlled under the Montreal Protocol, has been declining steadily since the peak the early 1990s. Dichloromethane has a lifetime of less than 6 months and responds rapidly to emissions changes. Levels are increasing. Natural dichloromethane sources, which account for ~10% of the total, are mainly from biomass burning and the oceans. Trichloromethane (light blue) has a lifetime of ~6 months, thus the response to emission changes is also relatively rapid. The reason for many of the rapid changes observed is not yet clear, but they are likely explained by variations in natural emissions, since these dominate the atmospheric trichloromethane burden (Laturnus et al., 2002).

Even if trichloromethane and dichloromethane have relatively short lifetimes, modelling studies imply that chlorine from these compounds can reach the lower stratosphere and potentially destroy stratospheric ozone (Hossaini et al., 2017). Thus, sustained growth in these compounds might offset some of the gains achieved by the Montreal Protocol, further delaying recovery of Earth's ozone layer.

The atmospheric concentrations of trichloroethene (TCE; green) and tetrachloroethene (PCE; grey) are low, and the measured annual variabilities are quite high, especially before 2011 due to instrumental limitations (see Appendix II). This makes it difficult to draw conclusions about trends and development of these species.

The concentration of carbon tetrachloride (CCl_4) has been measured at Zeppelin since 2010. This compound was once a popular solvent in organic chemistry, but because of its adverse health effects and ozone depleting potential it is rarely used any more, and hence levels are declining. Today CCl_4 is sometimes applied as a solvent for infrared spectroscopy. Note that measurements of CCl_4 are often complicated by drift in calibration flasks at the reference laboratory, co-eluting peaks in the chromatogram, and that this compound is very sensitive to overall instrument performance. For these reasons it is not possible to report CCl_4 for all years and that in these cases annual mean values are derived from the fitted trend line.

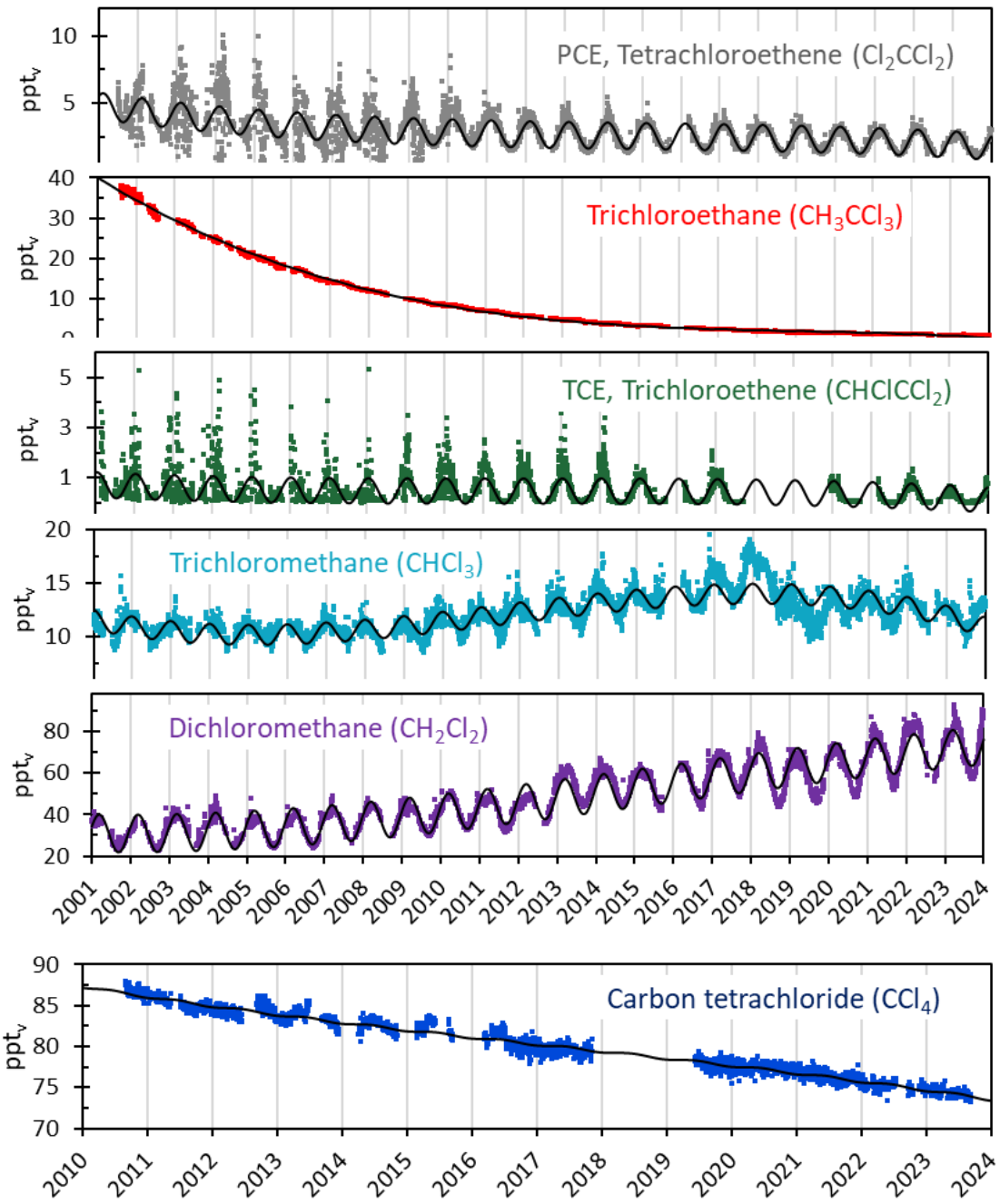

Figure 2.29: Daily averaged concentrations of chlorinated hydrocarbons at the Zeppelin observatory: For the period 2001 to 2024: Tetrachloroethene (grey), trichloroethane (red), trichloroethene (green), trichloromethane (light blue), and dichloromethane (violet). For the period 2010 to 2024: carbon tetrachloride (dark blue). Note that in some years carbon tetrachloride measurements are unvaailbale due to measurmeent issues (see main text), The black solid lines are the empirical, fitted, mixing ratios, with fit coefficients yielding the trend. This trend calculation is described in Appendix II.

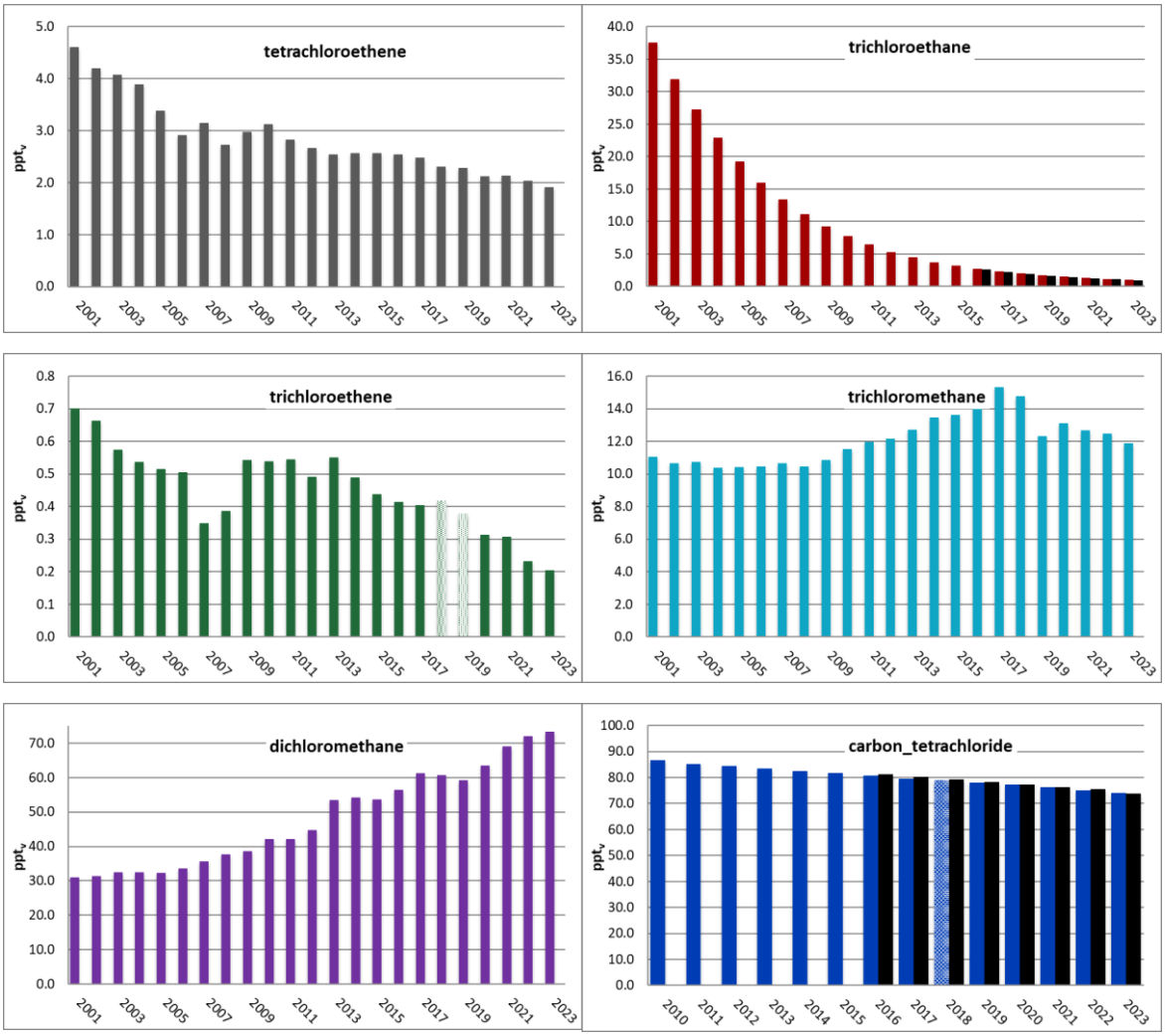

Figure 2.30: Annual means of the chlorinated hydrocarbons. Upper panel: tetrachloroethane (grey) and trichloroethane (red). Mid panel: trichloroethene (TCE, green) and trichloromethane (light blue). Lower panel: dichloromethane (violet) and carbon tetrachloride (CCl_4, dark blue). The global annual means for CH_3CCl_3 and CCl_4 in 2016 to 2024 are included as black bars, when available. All units are in ppt. Shaded bars indicate that annual means are derived from the fitted trend line in Figure 2.29.

2.1.14 Perfluorinated compounds at Zeppelin Observatory

Key findings for perfluorinated compounds: As a group, the perfluorinated compounds are some of the most extreme greenhouse gases. E.g., sulfur hexafluoride, SF_6, has a global warming potential of 25200. While all are currently at very low levels, the high warming potentials of these compounds means they must be followed closely. All are increasing in concentration.

Perfluorinated compounds, including SF_6, NF_3, and SO_2F_2 (Figure 2.31, Figure 2.32), are extremely potent and long-lived (up to 50000 years) greenhouse gases. For example, SF_6, emitted mainly from magnesium production and the electrical industry, has been monitored since 2001, and has a warming potential 25200 times greater than CO_2. SO_2F_2, used as a pesticide fumigant, has a lifetime of 36 years and a GWP of 4630,

while NF_3, employed in electronics manufacturing, has a 569-year lifetime and a GWP of 17400. These compounds raise concerns due to their extended atmospheric persistence and strong infrared absorption, impacting climate change. Monitoring improvements in 2015 and 2016 enabled the inclusion of NF_3 data from 2016 onwards. The concentration of SF_6 at Zeppelin is slightly higher than the global means due to lower emissions in the Southern Hemisphere.

NILU also monitors PFCs - 14, -116, -218, and -318, at Zeppelin. PFC-14, used in refrigeration and electronics, has a 50000-year atmospheric lifetime and a GWP of 7380. PFC-116, found in semiconductor manufacturing, has a 10000-year lifetime and a GWP of 12400. PFC-218, used in electronics and medicine, has a 2600-year lifetime and a GWP of 9290. PFC-318, a by-product of fluorochemical production, has a 3200-year lifetime and a GWP of 10200. Daily means are shown in Figure 2.33 and the yearly averages at Zeppelin alongside global means in Figure 2.34.

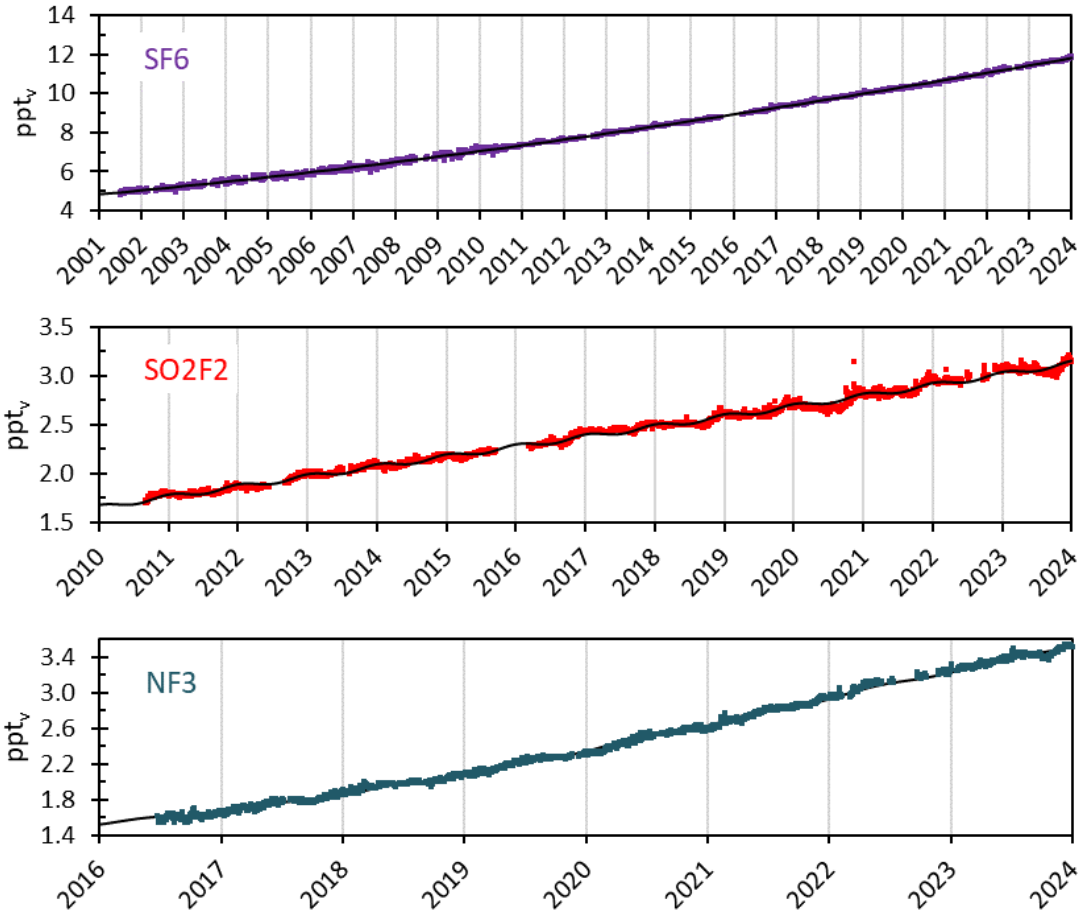

Figure 2.31: Daily averaged concentrations at the Zeppelin Observatory. Upper panel: SF_6 for the period 2001 to 2024. Middle panel: SO_2F_2 for the period 2010 to 2024. Lower panel: NF_3 from mid-2016 to 2024. The black solid lines are the empirical, fitted, mixing ratios, with fit coefficients yielding the trend. This trend calculation is described in Appendix II.

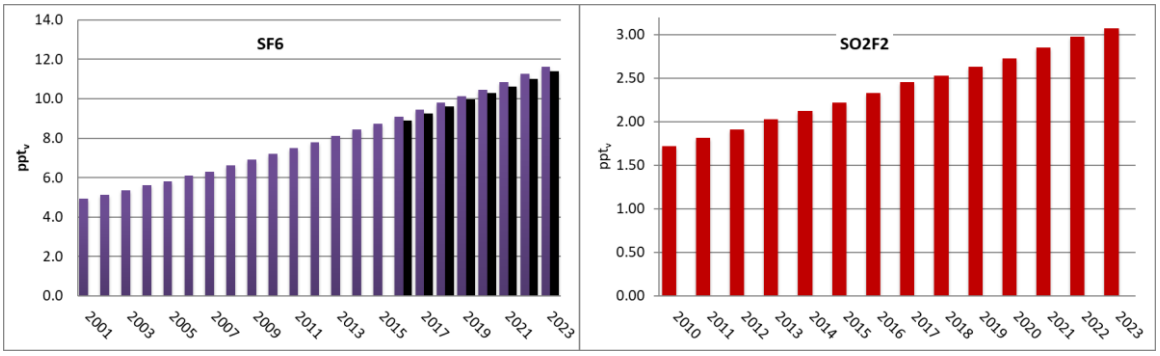

Figure 2.32: Annual means of SF_6 for the period 2001 to 2024 (left) and SO_2F_2 for the period 2010 to 2024 (right) at the Zeppelin observatory. The global annual means for SF_6 in 2016 to 2024 are included as black bars.

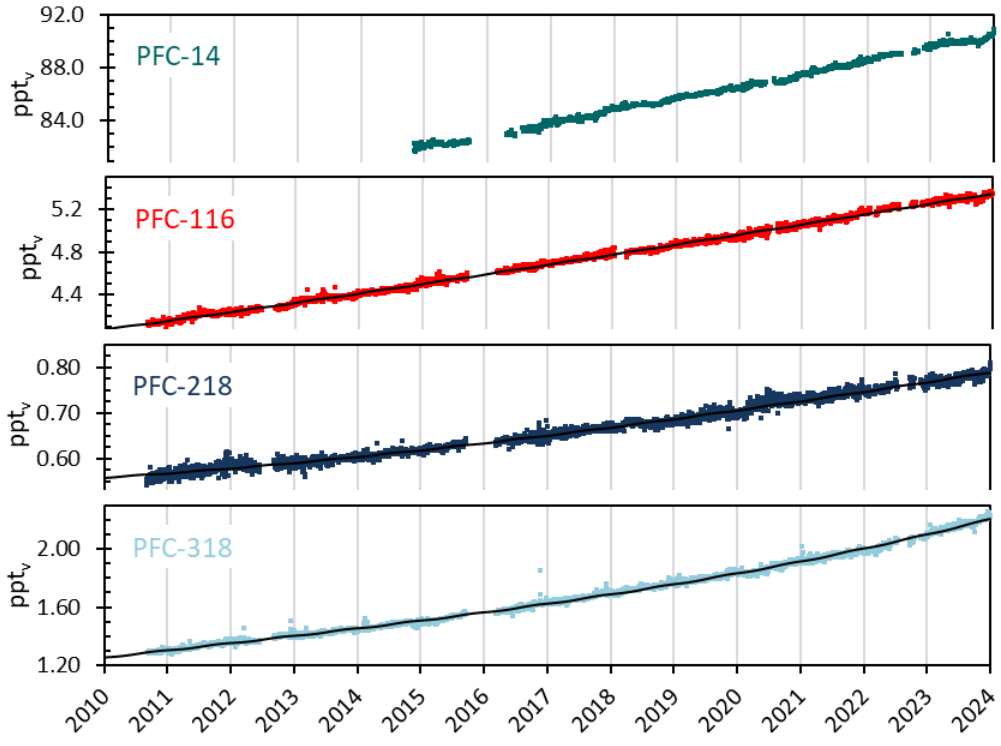

Figure 2.33: Daily averaged concentrations of perfluorocarbons at the Zeppelin observatory for the period 2010 to 2024: PFC-14 (green), PFC-116 (red), PFC-218 (dark blue), and PFC-318 (light blue). PFC-14 is only ranging back to autumn 2014. The black solid lines are the empirical, fitted, mixing ratios, with fit coefficients yielding the trend. This trend calculation is described in Appendix II.

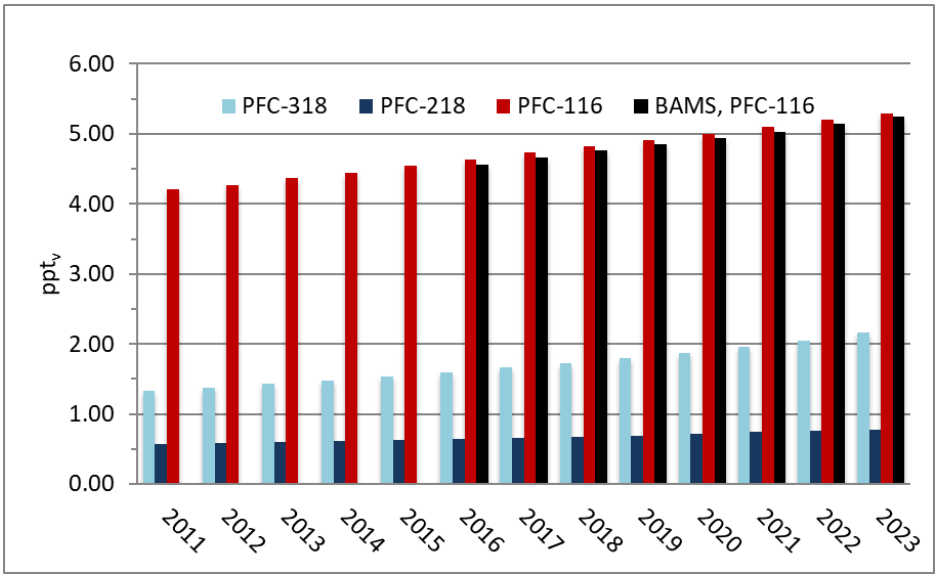

Figure 2.34: Annual mean concentrations of perfluorocarbons for the period 2010 to 2024 at the Zeppelin observatory: PFC-116 (red), PFC-218 (dark blue), and PFC-318 (light blue). The global annual means for PFC-116 in 2016 to 2024 are included as black bars.

2.2 Aerosol properties

Atmospheric aerosol particles directly influence climate change by absorbing incoming solar radiation causing warming or by scattering sunlight passing through the atmosphere, causing cooling. Aerosol particles also have indirect effects, mainly due to their influence on cloud formation and cloud properties, changing the amount of sunlight being reflected into space. The net effect of aerosol particles is to cool the climate, mainly due to the indirect effect. The balance of effects and how this will change in future is modified by the relative balance between scattering and absorption, the particle size, the total number of particles, and where in the atmosphere the particles are located. An overview of aerosol optical and physical properties in the monitoring programme for greenhouse gases and aerosol and their relevance to climate is provided in Table 5.

Table 5: Aerosol observations at Zeppelin, Birkenes and Troll Observatory. "X" mark funded by the Norwegian Environment Agency and Ministry of Climate and Environment. The rest, marked "O", is funded by NILU and other institutes. See also Appendix II for detailed methodology.

Parameter	Relevance	Zeppelin	Birkenes	Trollhaugen
Aerosol Scattering Coefficient	**Direct climate effect (cooling)**	**O**	**X**	**X**
Aerosol Absorption Coefficient, equivalent black carbon	**Direct climate effect (warming), proxy for black carbon**	**O, X**	**X**	**X**
Single scattering albedo	**Direct climate effect (balance of warming vs cooling)**	**O**	**X**	**X**
Scattering Ångström coefficient	**Direct climate effect**	**O, X**	**X**	**X**
Absorption Ångström coefficient	**Direct climate effect**	**O**	**X**	**X**
Aerosol Optical Depth, Column Ångström coefficient	**Direct climate effect**	**X**	**X**	**O**
Particle number	**Direct and indirect effects (overall magnitude)**	**X**	**X**	**X**
Particle Number Size Distribution (PNSD)	**fundamental to all aerosol processes**	**X**	**X**	**X**

2.2.1 Aerosol Scattering coefficient

Key findings for aerosol scattering: The aerosol scattering coefficient measures how much atmospheric particles reflect and diffuse sunlight, thereby creating a cooling effect. At Trollhaugen, this coefficient has been increasing by approximately 4% per decade, enhancing the cooling effect in that region. In contrast, at Birkenes, it has been decreasing by about 9% per decade, which reduces the cooling effect and potentially contributes to regional warming. These contrasting trends reflect the different conditions at each observatory. The decline at Birkenes is particularly notable on a global scale, indicating the success of Europe's sulfate reduction efforts under the Gothenburg Protocol.

How much light is scattered by aerosol particles depends on their composition and size. Particles with a similar diameter to the wavelength of the incoming sunlight scatter more efficiently. Inorganic species such as sulfate, nitrate, and ammonium, sea salt, and mineral dust increase scattering since they absorb less radiation than other aerosol chemical components such as black carbon.

At Trollhaugen, the polar vortex drives aerosol patterns, with stable air masses in the austral winter (May-August) limiting long-range aerosol transport, while Austral summer (December to February) brings mid-latitude emissions via long range transport (Figure 2.35). The scattering minima tends to occur in Austral autumn when aerosol concentration is lowest. The peak is in Austral winter and spring, likely due to increased biological activity, e.g., due to phytoplankton blooms (Virkula et al., 2022). The increase in scattering in Antarctica may be unique to the region possibly driven by increased biological activity due to climate change, which also affects weather patterns and sea ice cover (Yan et al., 2020).

At Birkenes the scattering coefficient is more variable. The long-term decline of around 9% per decade likely reflects the successful implementation of the Gothenburg protocol and a reduction in sulfate and

other inorganic aerosol, also reported in the monitoring programme in Aas et al. (2024). Birkenes, while regarded as a relatively unpolluted location is affected by regional and European anthropogenic emissions. With higher aerosol levels in Europe and the Northern Hemisphere due to population density and biogenic activity, Birkenes' trend is more representative of the global picture than that of Trollhaugen.

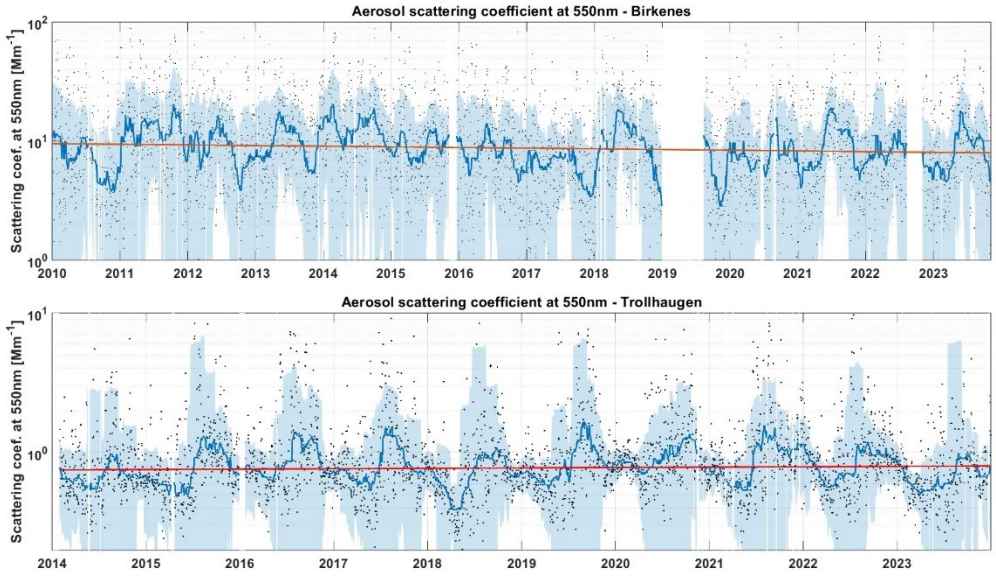

Figure 2.35: The aerosol daily scattering coefficient at 550 nm (blue dots) and standard deviation (blue shaded area) for Birkenes from 2010 to 2024 and Trollhaugen from 2015 to 2024. The red line shows the long-term trend according to the Senn's slope. All plots also depict the running 55-day medians of the respective properties as heavy lines to visualize seasonal variations.

2.2.2 Aerosol absorption coefficient and equivalent black carbon

Key findings for the aerosol absorption coefficient and equivalent black carbon: The aerosol absorption coefficient quantifies how much sunlight is absorbed by aerosols, contributing to atmospheric warming. The main light absorber is black carbon and hence absorption is directly related to black carbon concentrations. Absorption coefficients, and hence black carbon levels, are decreasing at Zeppelin, Birkenes, and Troll by 10 to 16% per decade due to stricter air quality regulations across different sectors. This yields a net cooling effect alongside a decrease in negative health effects.

While the net effect of light absorbing aerosols and black carbon is to warm the planet, the uncertainty in this effect is large (Figure 2.2) due to black carbon's influence on cloud formation, melting ice and snow, and modifying regional temperature patterns (Masson-Delmotte et al., 2021). Further uncertainty arises due to difficulty in modelling emissions over time as well as the operational nature of the definition of 'black carbon'. Absorption, converted to an 'equivalent black carbon, eBC' concentration using a conversion factor called a 'mass absorption cross section (MAC)' is used in this report (please see appendix B for details of this calculation), but note that other definitions exist, which may in turn influence the expected effect on climate. eBC is from combustion sources e.g., fossil fuels, residential heating, industry, as well as from wildfires.

The formation of a polar vortex in winter at Zeppelin and summer at Trollhaugen (during Austral winter) influences absorption. Trollhaugen experiences lower values during the austral winter (Figure 2.36) due to reduced biomass burning and human activities, and higher values in the austral summer when mid-latitude pollution and black carbon emissions are transported to the region. This seasonal variation is closely tied to atmospheric circulation patterns and changes in aerosol sources affecting the Antarctic region (Virkula et al., 2022). Absorption is at or below instrument detection levels in Austral winter. Meanwhile at Zeppelin, absorption peaks in late winter and early spring due to long-range transport from mid-latitude sources. In summer, concentrations drop because of less atmospheric transport and increased wet scavenging processes. These seasonal variations are driven by both natural processes and anthropogenic emissions, which are more prominent in the colder months and during the so called 'Arctic Haze' period (Platt et al., 2022). Stohl et al. (2013) indicate that high latitude gas flaring makes an important contribution to anthropogenic eBC in the Arctic during the haze period. At Birkenes, eBC is generally higher in winter due to residential heating (Yttri et al., 2024).

The decrease seen across all sites reflects the impact of successful regulations to reduce black carbon emission across several sectors, motivated by black carbon's negative health impacts (e.g., Sun et al., 2020). These regulations include, for example, vehicle emission regulations, cleaner household energy, and reduced open burning in the agricultural sector.

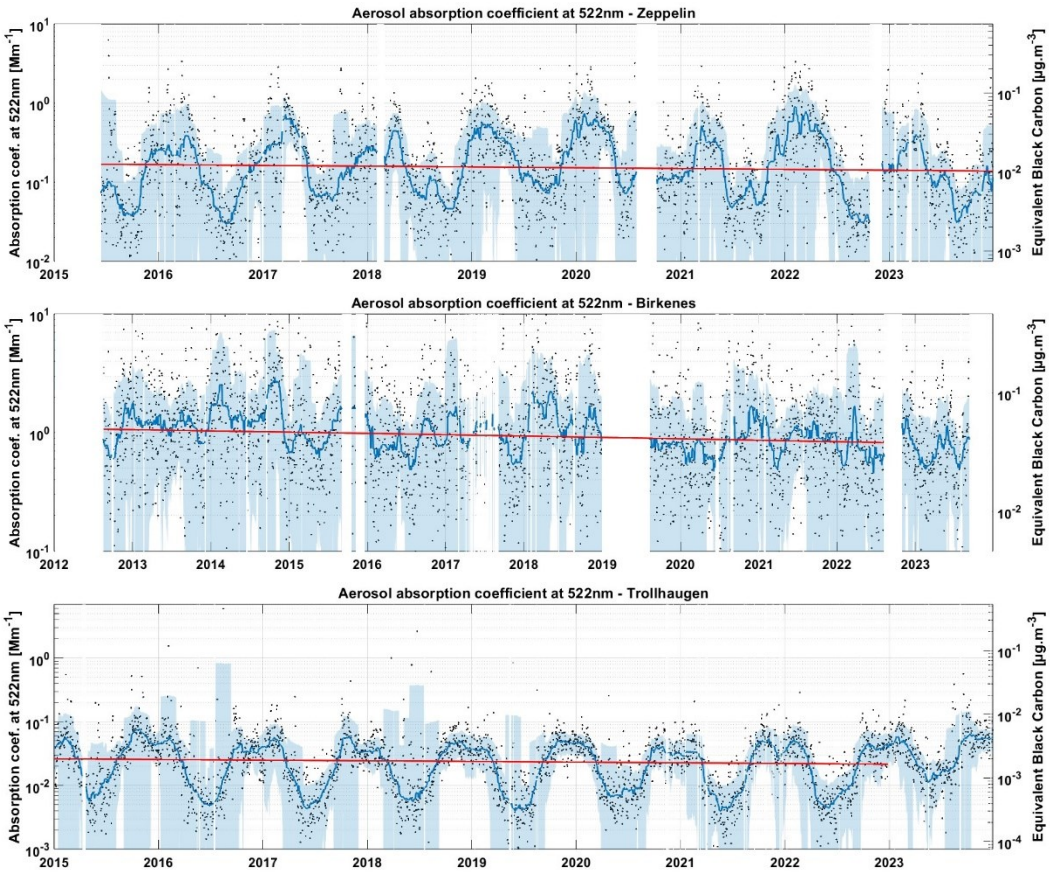

Figure 2.36: The aerosol daily absorption coefficient at 522 nm (blue dots) and standard deviation (blue shaded area) for Zeppelin from 2015 to 2024, Birkenes from 2012 to 2024, and Trollhaugen from 2015 to 2024. The red line shows the long-term trend according to the Senn's slope. The equivalent black carbon (eBC) concentration is on the right axis (representing a simple normalisation of the absorption coefficient by the mass absorption cross section, MAC). Due to an instrument change in 2023 at Birkenes and Trollhaugen there has been a small shift in the observed parameters and data from this period onwards is not included in the fit for both sites. All plots also depict the running 55-day medians of the respective properties as heavy lines to visualize seasonal variations.

2.2.3 Single scattering albedo

Key findings for the single scattering albedo: The single scattering albedo (SSA) quantifies the balance between scattering and absorption, with 1 representing pure scattering and 0 representing pure absorption. SSA has been increasing slightly (around 1% per decade) at both Trollhaugen and Birkenes due to the significant decrease in absorbing aerosols. As a result, the atmospheric aerosol composition is becoming more cooling. However, this relative increase in scattering may be offset by overall changes in aerosol concentrations, potentially reducing the total cooling effect.

The SSA variability at Birkenes is high due to competing effects from absorption and scattering which vary widely with weather patterns and seasonal variations in emissions. The overall trend is positive (relatively more scattering), despite a long-term decrease in the scattering coefficient, since the change in absorption

has been large enough to offset this. At Trollhaugen there is a clear seasonal pattern. SSA is close to one, i.e. purely scattering, in Austral winter, where the polar vortex prevents the intrusion of mid latitude emissions of black carbon. The SSA increase is slightly larger than at Birkenes, since the scattering is also increasing alongside decreasing absorption.

Even though the trends at Birkenes and Trollhaugen are towards relatively increased scattering, this does not mean that aerosol particles are causing increased cooling or offsetting increased forcing from, e.g., CO_2. SSA is only a relative parameter, and it is likely that the total reduction in aerosol due to clean air regulations and the Gothenburg Protocol is having a net warming effect (Kramer et al., 2021).

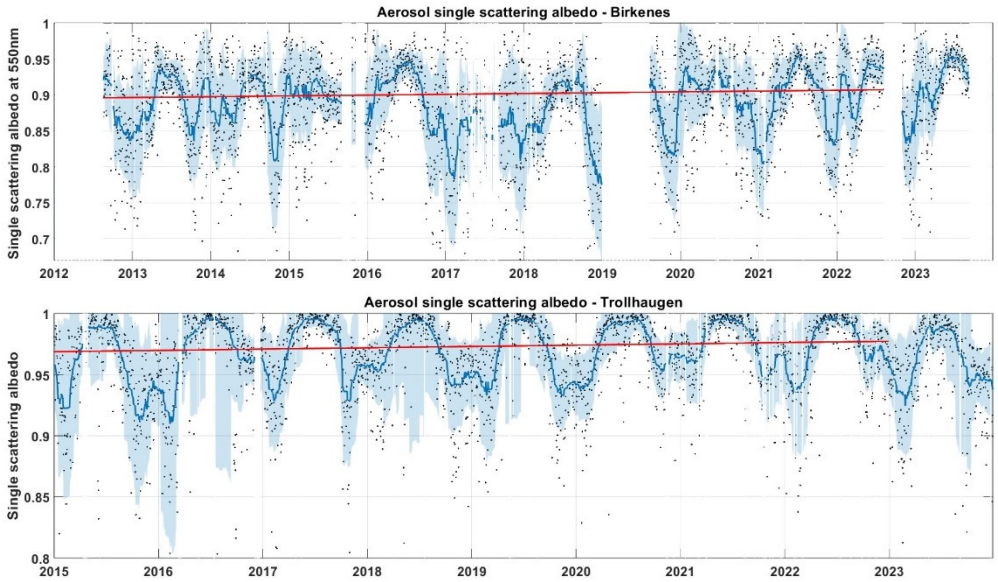

Figure 2.37: The aerosol single scattering albedo at 550 nm (blue dots) and standard deviation (blue shaded area) for Birkenes from 2012 to 2024 and Trollhaugen from 2015 to 2024. The red line shows the long-term trend based on Senn's slope, indicating an increase in SSA at both sites. Due to an instrument change in 2023 at Birkenes and Trollhaugen there has been a small shift in the observed parameters and data from this period onwards is not included in the fit for both sites. All plots also depict the running 55-day medians of the respective properties as heavy lines to visualize seasonal variations.

2.2.4 Absorption Ångström exponent

Key findings for the Absorption Ångström exponent (AAE): The AAE quantifies how aerosol absorption varies with wavelength and can be used to infer the relative contribution of liquid fuel combustion sources (mainly traffic) and solid fuel sources (mainly woodburning) to absorption and eBC. The AAE is increasing by 3 to 4 % per decade at Birkenes and Zeppelin, indicating that an important driver of the reductions seen in absorption is a reduction in eBC from liquid fuel combustion.

The AAE captures the wavelength dependence of absorption by comparison of the absorption coefficient at a minimum of two wavelengths. It increases when the absorption is higher at shorter wavelengths, which is typically due to the presence of organic compounds present in the absorbing aerosol particles, e.g. due to fuel rich combustion such as might be found in residential wood stoves (Zotter et al., 2017). The

presence of aerosol from woodburning emissions thus likely explains the seasonal peak in AAE seen at Birkenes (Figure 2.38) around winter and the 'residential heating season' (Yttri et al., 2021). The AAE is generally higher in winter than summer at Zeppelin, though the remote location of the observatory minimizes the impact of residential heating emissions.

It should be noted that while AAE is determined from absorption measurements, the measurement principle for this determination is a light extinction technique (see Appendix II). At very high SSA the AAE may be perturbed by scattering due to instrumental effects, e.g., Collaud Coen et al. (2010). This likely explains the extreme minima seen in Figure 2.38, which coincide with the peak SSA in Figure 2.37, seen in the Trollhaugen data.

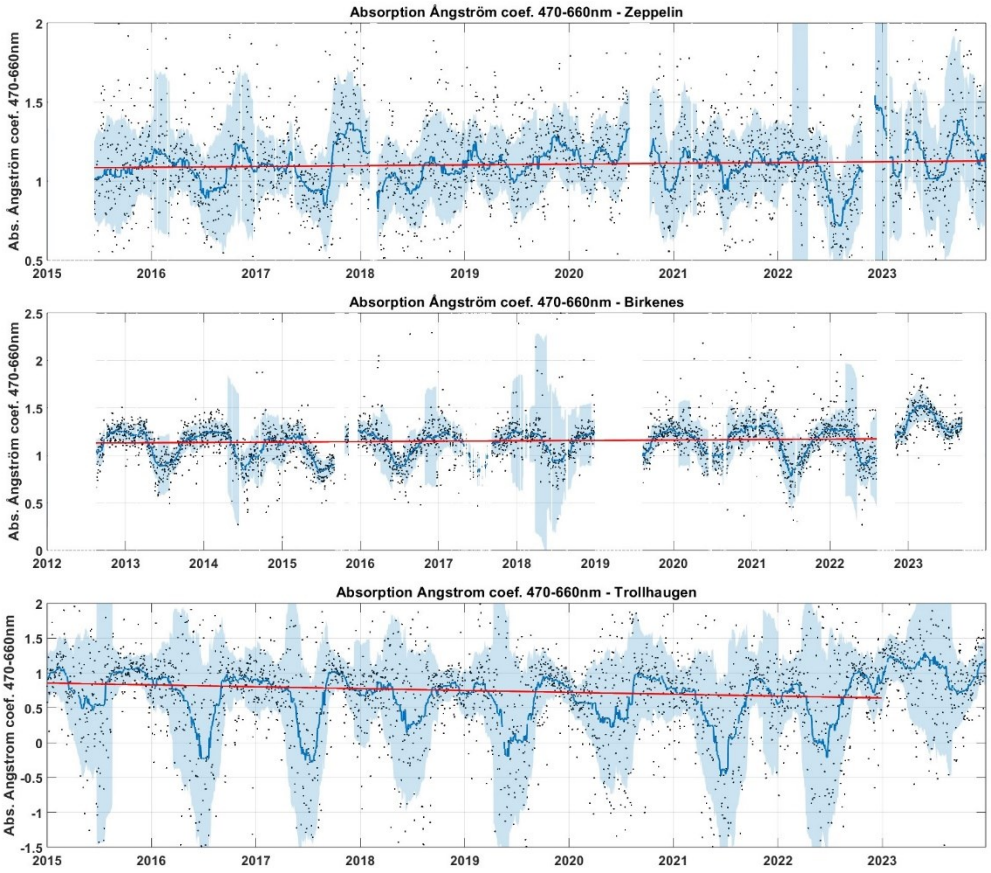

Figure 2.38: The Absorption Ångström exponent (470-660 nm) (blue dots) and standard deviation (blue shaded area) for Zeppelin, Birkenes, and Trollhaugen. The red line represents the long-term trend based on Senn's slope. Note that at Birkenes, the instrument type was changed (to the same as at Trollhaugen and Zeppelin), resulting in an offset of the AAE. Newer data for Birkenes are not included in the trend calculations. Due to an instrument change in 2023 at Birkenes and Trollhaugen there has been a small shift in the observed parameters and data from this period onwards is not included in the fit for both sites.

2.2.5 Particle number

Key findings for particle number: In the monitoring program, particle numbers are segregated by size: 0-0.1 µm (Aitken mode or ultrafine), 0.1 to 1 µm (accumulation mode or PM1 excluding ultrafine), and 1 to 10 µm (coarse mode or PM_{10} excluding PM_1). There is a statistically significant trend of increasing ultrafine particles (UFPs) at Birkenes, with an increase of around 10% per decade, and a decrease of 9% per decade at Zeppelin. Accumulation mode particles have decreased significantly across all sites, with reductions of 20 to 30%. The increase in UFPs at Birkenes may decrease net warming by modifying cloud properties, but negatively impact human health, while the decrease in accumulation mode particles may increase net warming and benefit human health.

Ultrafine particles (UFPs) are those with a diameter (D_P) less than 0.1 µm. They are not regulated, though they can have significant health impacts since their small size allows them to penetrate deep into the respiratory system. UFPs can also influence cloud formation by acting as cloud condensation nuclei (CCN), affecting cloud properties and albedo, potentially cooling the atmosphere. Since UFPs may be produced by natural chemical processes, e.g. oxidation of VOCs, and man-made processes, e.g., combustion it is difficult to elucidate the main driver of growth. The seasonal trend, with peaks during the summer (when oxidation is highest) suggests a large natural contribution, e.g. from plant-emitted VOCs. Nevertheless, the upward trend in UFPs of 10% per decade at Birkenes (Figure 2.39), combined with health effects supports the need for legislation to reduce atmospheric concentrations. It should be noted that the mass of UFPs is much lower than particles in the larger size bins such that particle number, rather than mass should be the focus of measures to improve air quality.

Accumulation mode particles have been decreasing, likely because of measures to improve air quality by emissions reductions across various sectors, as well as because of the Gothenburg Protocol. Since the mass of the accumulation mode is much larger than the Aitken/ ultrafine mode, it represents a significant fraction of the mass of particles of diameter less than 2.5 µm. I.e., measures aimed at reducing PM2.5 would likely also affect the accumulation mode. While the health effects of the decreasing number of accumulation mode particles are positive, the climate impact is likely to represent a net positive forcing i.e., warming. As for ultrafine particles, there is also a clear seasonal trend, likely driven by increased photooxidation of VOCs in summer.

There was no significant trend in the coarse mode particles. The main sources of these particles are primary biogenic aerosol particles such as plant fragments, fungal spores, and pollen, mineral dust, sea salt and sea spray or other any particles generated by mechanical abrasion processes.

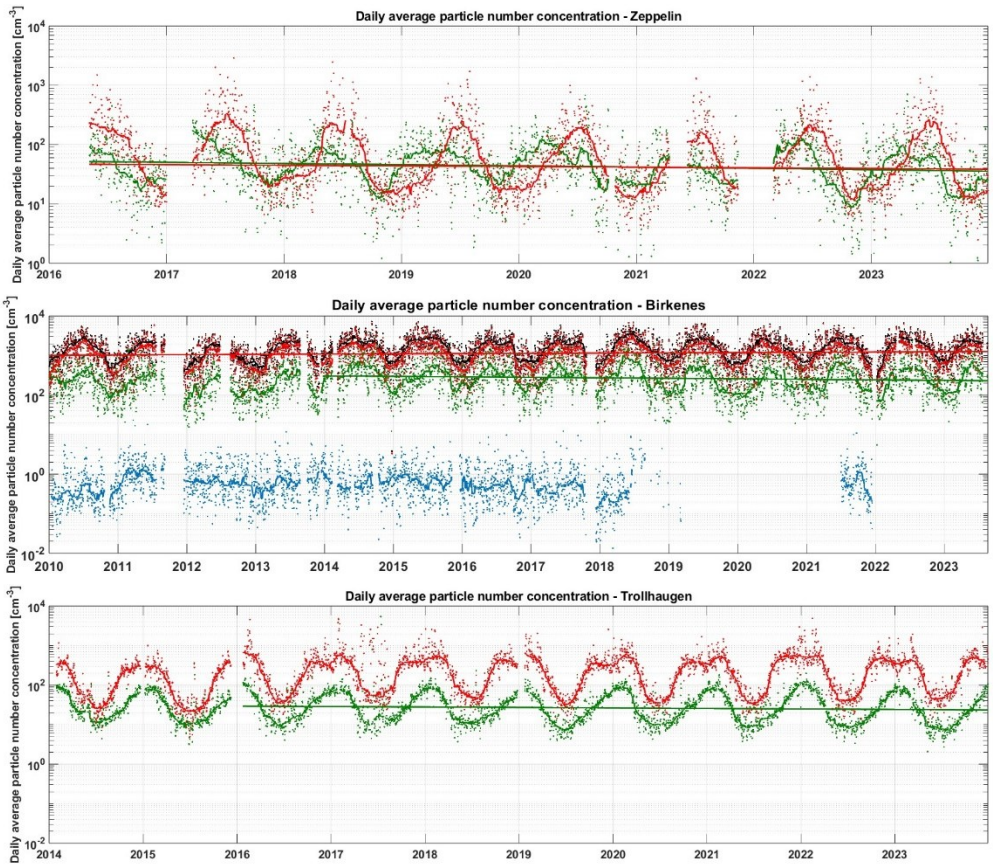

Figure 2.39: Daily average particle number concentrations (colored dots) for different particle size modes at Zeppelin, Birkenes, and Trollhaugen. Red dots and lines show ultrafine particles (Aitken mode: 0-0.1 µm) and their trends, green dots and lines show accumulation mode particles (0.1-1 µm) and their trends, and blue dots and lines show coarse mode particles (1-10 µm) and their trends. Trend lines are based on Sen's slope.

2.2.6 Particle number size distribution

Key findings for the particle number size distribution: The particle number size distribution (PNSD) is a fundamental aerosol property critical for climate, as particle size determines the direct effect (scattering and absorption) and influences cloud formation. The PNSD has been stable at Zeppelin, Birkenes, and Trollhaugen, when comparing data from 2024 to previous years. There is a pronounced seasonal variation at all sites. At Zeppelin the PNSD is bimodal with a pronounced peak at the 'accumulation mode' (100 to 1000 nm), which is highest during spring, linked to Arctic haze.

The Particle Number Size Distribution (PNSD) represents the concentration of aerosol particles as a function of size and is crucial for understanding their atmospheric behavior, such as scattering or absorbing light, influencing cloud formation, and impacting air quality and human health. The PNSD is often expressed as dN/dlogDp (Figure 2.40), which normalizes the particle number concentration by the logarithmic interval of particle diameter (Dp). This logarithmic approach allows for clearer representation across the wide range of particle sizes, as particle diameters span several orders of magnitude.

Peaks in the distribution indicate size ranges where particle concentrations are highest, reflecting the dominant particle sources or processes at that time. For example, peaks in smaller sizes might indicate recent particle formation, while peaks in larger sizes could result from processes like coagulation or condensation. Troughs, on the other hand, show size ranges with fewer particles, often due to losses from settling or transformation processes. Using the dlogDp scale makes it possible to capture these relative changes in particle size, making it easier to compare the behavior and effects of small and large particles within the same framework.

In general, the PNSD is monomodal at Birkenes and Trollhaugen, while for Zeppelin there is a pronounced second mode at 100 to 1000 nm (the so-called 'accumulation mode') in winter and particularly spring due to the Arctic Haze phenomenon. Arctic haze is characterised by the long-range transport of aerosols and pollutants into the Arctic, typically during late winter and early spring. These aerosols, which include sulfates, nitrates, and black carbon, originate from industrial and biomass burning activities in lower latitudes and accumulate in the Arctic atmosphere due to stable air masses and limited precipitation during these months. Artic haze modifies the optical properties described in the previous sections also affecting health in the region. The late spring and summer PNSD at Zeppelin are somewhat more variable than in winter due to less stable atmospheric conditions.

At Trollhaugen, the PNSD reflects the clean, remote Antarctic atmosphere. The size distribution at Troll is typically dominated by smaller particles (Aitken mode) during certain periods, likely due to limited local sources of pollution and aerosol production from natural processes, such as sea salt aerosols from the ocean or particles resulting from photochemical reactions. The scarcity of accumulation mode particles here highlights the pristine nature of the atmosphere and the lack of significant anthropogenic influence. At Birkenes, the PNSD shows more variability due to the site's closer proximity to Europe and regional pollution sources. Figure 2.40 shows that 2024 was typical with respect to the long-term average PNSD across all sites.

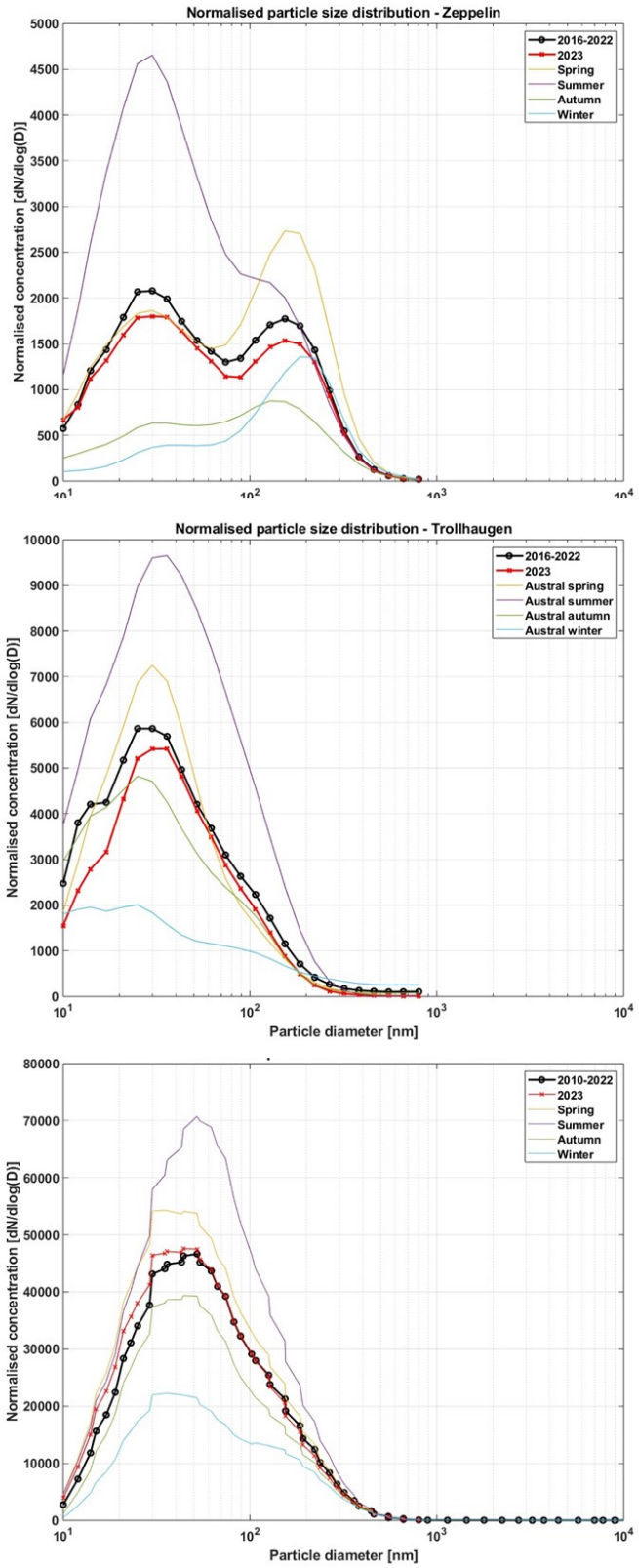

Figure 2.40: The normalized particle size distribution for Zeppelin, Birkenes, and Trollhaugen, showing seasonal variations (spring, summer, autumn, and winter) in particle concentrations across different size ranges (10 to 10000 nm, or 0.01 to 10 µm). The black line represents the long-term averages (2016 to 2023. for Zeppelin and Trollhaugen, 2010 to 2023 for Birkenes), while the red line shows the data for 2024).

2.2.7 Aerosol Optical Depth

Key findings for the AOD observations: Aerosol Optical Thickness (AOD) is a measure of how much light is scattered or absorbed by aerosol particles as it passes through the atmosphere. AOD is dimensionless, ranging from 0 (clear sky, no clouds or haze) to values greater than 1 (very hazy, enough cloud or dust to obscure all direct incoming light), and is an essential variable for determining the net direct climatic impact of aerosols AOD in Ny-Ålesund shows a stable annual trend (the net result of opposing seasonal trends), with values ranging mostly between 0.05 and 0.15, and prominent peaks in 2019 due to volcanic eruptions and forest fires. At Birkenes AOD shows a slight downward trend, likely correlating with reduced anthropogenic emissions in Europe. The low AOD loading at Trollhaugen (0.01 to 0.04) showed a gradual increase in the last 10 years, likely linked to climate change and biological activity.

In Figure 2.41, timeseries of monthly mean AOD at 500 nm measured at Ny-Ålesund, Birkenes, and Trollhaugen are shown. At all sites, observations were made with sun-photometers (in dark blue), complemented by lunar observations at Ny-Ålesund and Birkenes during the most recent years (in cyan). Note, the y-axis is adapted to make the range of AOD visible at the various sides. In addition, a Theil-Sen regression line, based on sun-photometer observations, is overlayed to indicate trends in the datasets.

Observations in Ny-Ålesund started in 2002. AOD values fluctuate, they are mostly in the range between 0.05 and 0.15, with some higher peaks. 2019 shows particularly enhanced values of up to 0.2, which was caused by volcanic activity (eruption of the Raikoke volcano end of June 2019, Kuril Islands, Russia) and forest fires occurring in Northern latitudes. On an annual based the trend looks stable, with no essential increase or decrease over the 20-year period. Existing opposite seasonal trends, i.e., a decrease in springtime due to the reduction of Arctic haze and an increase in summer and autumn due to increased forest fire activities, are averaged out in the annual perspective.

The AOD monitoring at the Birkenes observatory started in 2009, and since 2019 regular lunar observations were made. AOD shows episodic behaviour over time and lies mostly in the range between 0.05 and 0.2, but some stronger peaks, especially after 2019. Between 2009 and 2023, a light downward trend in AOD can be observed. This is consistent with the decrease in ground-based in situ aerosol scattering at the location, likely reflecting the reduction in anthropogenic emissions in Europe (see Section 2.2.1). Moon photometer measurements complement the sun-photometer at Ny-Ålesund and Birkenes and were added during recent years to cover the annual cycle (see Table A 5 and Table A 6).

At Trollhaugen, AOD data from sun-photometer observations started in 2014, after moving the observations from Troll to the new observatory. AOD values at Trollhaugen in Antarctica are much lower than those at Birkenes and Ny-Ålesund, reflecting the significantly lower aerosol concentration in the Antarctic region. AOD typically ranges between 0.01 and 0.04, with occasional peaks above 0.04, particularly around 2020, when Australian bushfire smoke affected the polar observations. While the primary climate effect of the bushfires is likely to have been regional warming, such fire events can have wide ranging effects in addition, e.g., darkening the Earth's surface (reducing albedo) particularly via deposition on snow causing warming, modifying cloud formation, and even effecting plankton growth and hence CO_2 uptake in the Southern Ocean (Weis et al., 2022).

The trends analysis shows a gradual increase in AOD over the 10-year period. This behaviour seems linked to the observed increase in ground-based observations of aerosol scattering observed at Trollhaugen (see Section 2.2.1) and may be driven by increased biological activity due to climate change, which also affects weather patterns and sea ice cover. The net climate impact of this is likely to be enhanced cooling (in opposition to the global trend where declining aerosol is having a likely warming effect). However, more research is needed to confirm this trend across the wider Antarctic region, where there are few measurements, and to determine all of the mechanisms whereby climate is affected.

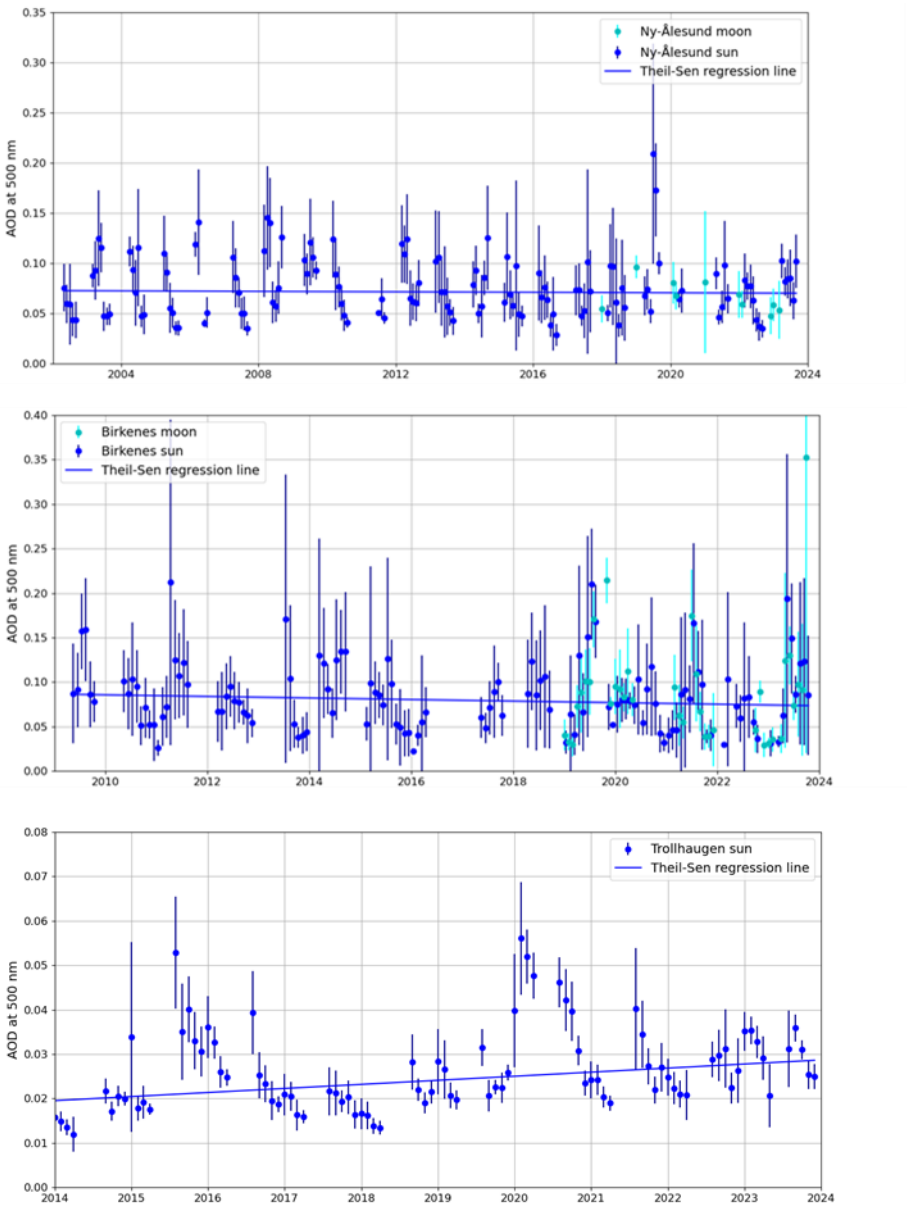

Figure 2.41: Time series of AOD at 500 nm wavelength in the atmospheric column above Ny-Ålesund (2002 to 2023, upper panel), Birkenes (2009 to *2023, middle panel), and Trollhaugen (2014* to *2023, lower panel, sun photometer only). Monthly mean values and standard deviations are given. Sun- and moon photometer observations are shown in dark blue and cyan, respectively.*

2.2.8 Total column Ångström coefficient

Key findings for the total column Ångström coefficient: The Ångström coefficients are a measure that describes the wavelength dependence of the AOD. Higher values indicating smaller particles (for example smoke or urban pollution) and lower values are observed for larger particles (such as sea salt, dust or volcanic ash). Data at the polar sites are slightly higher than observations at Birkenes, indicating smaller particles. No significant changes are seen at Ny-Ålesund and Trollhaugen, while the Ångström coefficients at Birkenes shows a slight positive trend with high variability.

The Ångström coefficients for AOD is derived from the spectral variation of AOD and is dimensionless. The Ångström coefficient is related to the size of the aerosol particles in the total column of the atmosphere. Ångström coefficients were calculated for Ny-Ålesund, Birkenes, and Trollhaugen using sun-photometers, with lunar data added for Ny-Ålesund and Birkenes recently (see Table A 5 and Table A 6).

In Figure 2.42, timeseries of monthly mean Ångström coefficient measured at Ny-Ålesund, Birkenes, and Trollhaugen are shown. At all sites, observations were derived from sun-photometers (in dark green), complemented by lunar observations at Ny-Ålesund and Birkenes during the most recent years (in light green). In addition, a Theil-Sen regression line, based on solar observations, is overlayed to indicate trends in the datasets.

The Ångström coefficient from the Precision Filter Radiometer (PFR) used in Ny-Ålesund (upper panel) and at Trollhaugen (lower panel) vary mainly between 1.0 and 2.0, while the values for Birkenes vary between 0.5 and 2.0. The variability is highest at Birkenes. Differences in the evaluation of the Ångström coefficient in the GAW-PFR network (Ny-Ålesund, Trollhaugen) and AERONET (Birkenes) may partly be responsible for the fewer low values at sites associated with the former network. Ångström coefficient at the polar sites are generally higher, indicating the presence of smaller particles. Exceptions are the observations from 2023, which have significantly lower values, generally indicating larger particles. Whether this is due to atmospheric events, e.g. local dust, caused by unresolved cloud contamination of the data, could not yet be fully resolved. Therefore, the trend analysis includes data until 2022 only. Values at polar sites are generally higher, indicating smaller particles.

At Ny-Ålesund, the regression shows a stable trend, with no major increase or decrease of the Ångström coefficient over the last 20 years. As for the AOD, underlying seasonal trends may be averaged out in the annual perspective. Over the last decade the Ångström coefficient remained stable with minor fluctuations, indicating no major change in the aerosol size distributions in the atmospheric column above the Antarctic location. For Birkenes, a slight positive trend of the Ångström coefficient is observed, although the fluctuations are very high, so the effect is marginal.

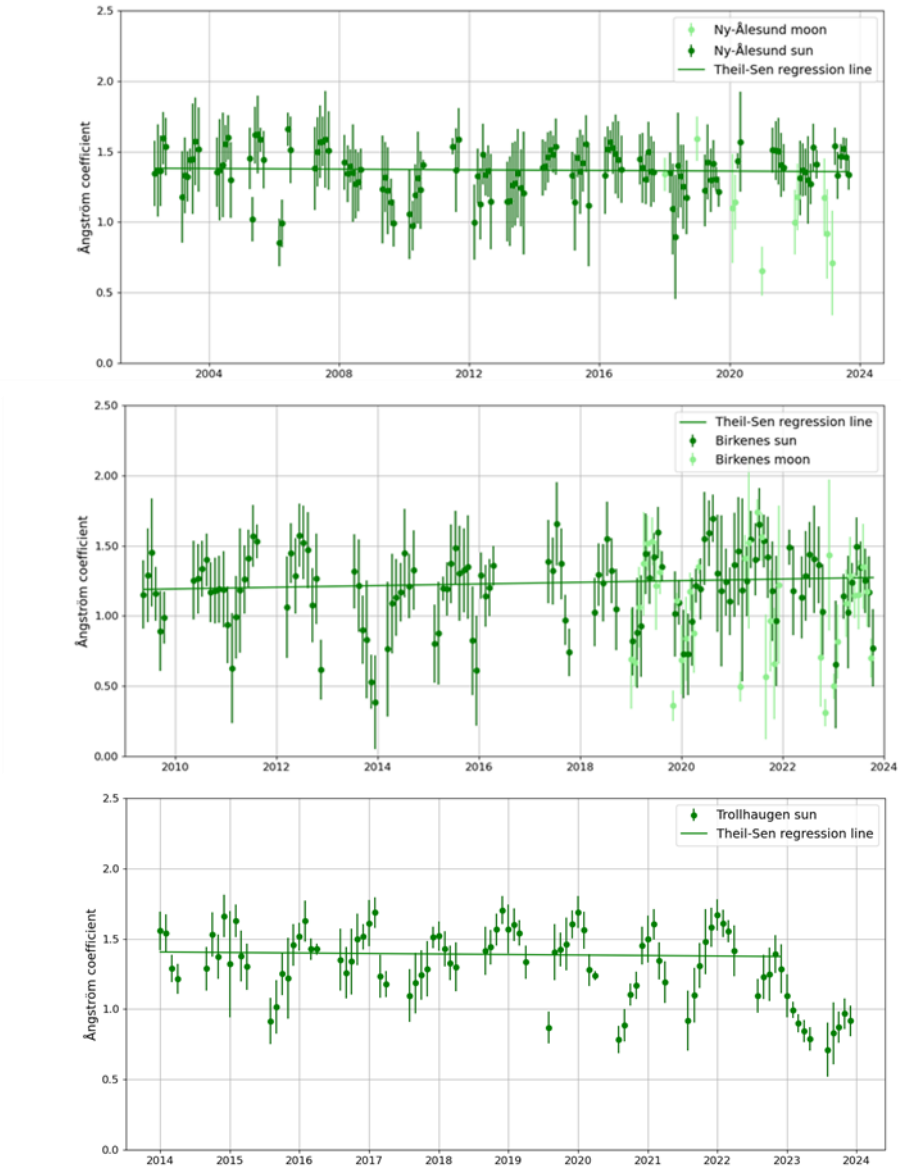

Figure 2.42: Time series of Ångström coefficient in the atmospheric column above Ny-Ålesund (2002 to 2023, upper panel), Birkenes (2009 to 2023, middle panel), and Trollhaugen (2014 to 2023, lower panel). Monthly mean values and standard deviations are given. Sun- and moon photometer observations are shown in dark green and light green, respectively.

2.3 Conclusion

The report *Monitoring of greenhouse gases and aerosols at Svalbard and Birkenes in 2024* describes the latest developments in atmospheric greenhouse gases and aerosol properties measured at the Zeppelin and Birkenes Observatories and includes information from the Trollhaugen Observatory for comparison. This report underscores the critical role these sites play in assessing global atmospheric trends. The continued rise in carbon dioxide (CO_2), methane (CH_4), and nitrous oxide (N_2O) levels—despite global and national efforts to reduce emissions—serves as a stark reminder of the challenges that remain in meeting climate temperature goals such as the Paris Agreement aspirational goal of limiting warming to 1.5 °C, and other national and EU climate targets. Methane poses a significant challenge, with concentrations increasing at an accelerated rate. This reinforces the need for urgent, more aggressive mitigation strategies to reduce emissions of this potent greenhouse gas.

The steady decline in chlorofluorocarbon (CFC) concentrations demonstrates the success of international agreements like the Montreal Protocol in curbing ozone-depleting substances. However, the slight increase in CFC-115 levels since 2017 highlights the need for continued vigilance in monitoring potential new fluorinated hydrocarbon and halon sources and ensuring compliance with global agreements. This is particularly true for several compounds, such as SF_6, with global warming potentials many thousands of times higher than CO_2.

A significant achievement in this year's report is the fitting of trends for aerosols. These trends offer new insights into the long-term changes in aerosol scattering and absorption properties, which are key drivers of cooling and warming effects in the atmosphere. The successful reduction in aerosol absorption (and its analogue, equivalent black carbon, eBC) at all sites, driven by air quality regulations, is an encouraging sign. However, the contrasting trend at Trollhaugen, where aerosol scattering has been increasing, implying regional cooling underlines the complexity of aerosol-climate interactions and the need for further investigation into the biological processes potentially influencing this trend.

The inclusion of aerosol observations from Trollhaugen, combined with the integration of the ACTRIS framework, enhances the comprehensiveness of the monitoring program. These data not only improve the quality and comparability of measurements but also place Norway’s monitoring efforts at the forefront of European atmospheric research.

Annual reporting is a vital final step in the quality assurance process of the atmospheric data collected on behalf of the Norwegian Environment Agency. With ongoing changes in atmospheric composition, continued support for Norway’s monitoring infrastructure is vital to inform national and international policies. The data from Zeppelin, Birkenes, and Trollhaugen remain indispensable in both tracking the impacts of climate change and ensuring that Norway fulfills its national and international obligations to mitigate these effects, as well as providing data to the international research community.

3 References

Aas, W., Eckhardt, S., Evangeliou, N., Hjellbrekke, A.-G., Platt, S. M., Solberg, S., Yttri, K. E. (2024). *Monitoring of long-range transported air pollutants in Norway. Annual report 2023* (NILU rapport 19/2024). Kjeller: NILU.

Blunden, J., Boyer, T. (2024). State of the Climate in 2023. *Bulletin of the American Meteorological Society, 105*(8), S1-S484.

Bondur, V. G., Mokhov, I. I., Voronova, O. S., Sitnov, S. A. (2020). Satellite Monitoring of Siberian Wildfires and Their Effects: Features of 2019 Anomalies and Trends of 20-Year Changes. *Doklady Earth Sciences*, *492*(1), 370-375.

Byrne, B., Liu, J., Bowman, K. W., Pascolini-Campbell, M., Chatterjee, A., Pandey, S., Miyazaki, K., van der Werf, G. R., Wunch, D., Wennberg, P. O., Roehl, C. M., Sinha, S. (2024). Carbon emissions from the 2023 Canadian wildfires. *Nature*, *633*(8031), 835-839.

Collaud Coen, M., Weingartner, E., Apituley, A., Ceburnis, D., Fierz-Schmidhauser, R., Flentje, H., Henzing, J. S., Jennings, S. G., Moerman, M., Petzold, A., Schmid, O., Baltensperger, U. (2010). Minimizing light absorption measurement artifacts of the Aethalometer: evaluation of five correction algorithms. *Atmospheric Measurement Techniques*, *3*(2), 457-474.

Cunningham, C. X., Williamson, G. J., Bowman, D. M. J. S. (2024). Increasing frequency and intensity of the most extreme wildfires on Earth. *Nature Ecology & Evolution*, *8*(8), 1420-1425.

Ehhalt, D., Prather, M., Dentener, F., Derwent, R., Dlugokencky, E., Holland, E., Isaksen, I., Katima, J., Kirchhoff, V., Matson, P., Midgley, P., Wang, M., Berntsen, T., Bey, I., Brasseur, G., Buja, L., Collins, W. J., Daniel, J., Demore, W. B., Dickerson, R., Etheridge, D., Feichter, J., Fraser, P., Friedl, R., Fuglestvedt, J., Gauss, M., Grenfell, L., Grübler, A., Harris, N., Hauglustaine, D., Horowitz, L., Jackman, C., Jacob, D., Jaeglé, L., Jain, A., Karlsdottir, S., Ko, M., Kurylo, M., Lawrence, M., Logan, J. A., Manning, A., Mauzerall, D., Mcconnell, J., Mickley, L., Montzka, S., Olivier, J., Pickering, K., Pitari, G., Roelofs, G. J., Rogers, H., Rognerud, B., Smith, S., Solomon, S., Staehelin, J., Steele, P., Stevenson, D., Sundet, J., Thompson, A., van Weele, M., von Kuhlmann, R., Wang, Y., Weisenstein, D., Wigley, T., Wild, O., Wuebbles, D., Yantosca, R., Joos, F., Mcfarland, M. (2001). Atmospheric Chemistry and Greenhouse Gases. In J.T. Houghton, Y. Ding, D.J. Griggs, M. Noguer, P.J. van der Linden, X. Dai, K. Maskell, C.A. Johnson (Eds.). *Climate Change 2001: The Scientific Basis. Contribution of Working Group I to the Third Assessment Report of the Intergovernmental Panel on Climate Change* (pp. 239-287). Cambridge University Press.

France, J. L., Cain, M., Fisher, R. E., Lowry, D., Allen, G., O'Shea, S. J., Illingworth, S., Pyle, J., Warwick, N., Jones, B. T., Gallagher, M. W., Bower, K. B., Le Breton, M., Percival, C., Muller, J., Welpott, A., Bauguitte, S., George, C., Hayman, G. D., Manning, A. J., Myhre, C. L., Lanoisellé, M., Nisbet, E. G. (2016). Measurements of δ13C in CH4 and using particle dispersion modeling to characterize sources of Arctic methane within an air mass. *Global Biogeochemical Cycles*, *121*(23), 14257-14270.

Gilbert, R. (1987). *Statistical methods for environmental pollution monitoring*. New York: Van Nostrand Reinhold.

Hossaini, R., Chipperfield, M. P., Montzka, S. A., Leeson, A. A., Dhomse, S. S., Pyle, J. A. (2017). The increasing threat to stratospheric ozone from dichloromethane. *Nature Communications*, *8*(1), 15962.

Isaksen, I. S. A., Hov, Ø. (1987). Calculation of trends in the tropospheric concentration of O3, OH, CO, CH4 and NOx. *Tellus B*, *39B*(3), 271-285.

Kramer, R. J., He, H., Soden, B. J., Oreopoulos, L., Myhre, G., Forster, P. M., Smith, C. J. (2021). Observational Evidence of Increasing Global Radiative Forcing. *Geophysical Research Letters*, *48*(7), e2020GL091585.

Laturnus, F., Haselmann, K. F., Borch, T., Grøn, C. (2002). Terrestrial natural sources of trichloromethane (chloroform, CHCl3) – An overview. *Biogeochemistry*, *60*(2), 121-139.

Masson-Delmotte, V., Zhai, P., Pirani, A., Connors, S.L., Péan, C., Berger, S., Caud, N., Chen, Y., Goldfarb, L., Gomis, M.I., Huang, M., Leitzell, K., Lonnoy, E., Matthews, J.B.R., Maycock, T.K., Waterfield, T., Yelekçi, O., Yu, R., Zhou, B. (Eds.). (2021). *IPCC: Climate Change 2021: The Physical Science Basis. Contribution of Working Group I to the Sixth Assessment Report of the Intergovernmental Panel on Climate Change*. Cambridge University Press.

Myhre, G., Shindell, D., Bréon, F. M., Collins, W., Fuglestvedt, J., Huang, J., Koch, D., Lamarque, J. F., Lee, D., Mendoza, B., Nakajima, T., Robock, A., Stephens, G., Takemura, T., Zhang, H. (2013). Anthropogenic and natural radiative forcing. In T.F Stocker, D. Qin, G.-K. Plattner, M. Tignor, S.K. Allen, J. Boschung, A. Nauels, Y. Xia, V. Bex and P.M. Midgley (Eds.), *Climate Change 2013: The Physical Science Basis. Contribution of Working Group I to the Fifth Assessment Report of the Intergovernmental Panel on Climate Change* (pp. 659-740). Cambridge University Press.

Nisbet, E. G., Manning, M. R., Dlugokencky, E. J., Fisher, R. E., Lowry, D., Michel, S. E., Myhre, C. L., Platt, S. M., Allen, G., Bousquet, P., Brownlow, R., Cain, M., France, J. L., Hermansen, O., Hossaini, R., Jones, A. E., Levin, I., Manning, A. C., Myhre, G., Pyle, J. A., Vaughn, B. H., Warwick, N. J., White, J. W. C. (2019). Very Strong Atmospheric Methane Growth in the 4 Years 2014–2017: Implications for the Paris Agreement. *Global Biogeochemical Cycles*, *33*(3), 318-342.

Persad, G., Samset, B. H., Wilcox, L. J., Allen, R. J., Bollasina, M. A., Booth, B. B. B., Bonfils, C., Crocker, T., Joshi, M., Lund, M. T., Marvel, K., Merikanto, J., Nordling, K., Undorf, S., van Vuuren, D. P., Westervelt, D. M., Zhao, A. (2023). Rapidly evolving aerosol emissions are a dangerous omission from near-term climate risk assessments. *Environmental Research: Climate*, *2*(3), 032001.

Platt, S. M., Hov, Ø., Berg, T., Breivik, K., Eckhardt, S., Eleftheriadis, K., Evangeliou, N., Fiebig, M., Fisher, R., Hansen, G., Hansson, H. C., Heintzenberg, J., Hermansen, O., Heslin-Rees, D., Holmén, K., Hudson, S., Kallenborn, R., Krejci, R., Krognes, T., Larssen, S., Lowry, D., Lund Myhre, C., Lunder, C., Nisbet, E., Nizzetto, P. B., Park, K. T., Pedersen, C. A., Pfaffhuber, K. Aspmo, Röckmann, T., Schmidbauer, N., Solberg, S., Stohl, A., Ström, J., Svendby, T., Tunved, P., Tørnkvist, K., van der Veen, C., Vratolis, S., Yoon, Y. J., Yttri, K. E., Zieger, P., Aas, W., Tørseth, K. (2022). Atmospheric composition in the European Arctic and 30 years of the Zeppelin Observatory, Ny-Ålesund. *Atmospheric Chemistry and Physics*, *22*(5), 3321-3369.

Repo, M. E., Susiluoto, S., Lind, S. E., Jokinen, S., Elsakov, V., Biasi, C., Virtanen, T., Martikainen, P. J. (2009). Large N_2O emissions from cryoturbated peat soil in tundra. *Nature Geoscience*, *2*(3), 189-192.

Saunois, M., Martinez, A., Poulter, B., Zhang, Z., Raymond, P., Regnier, P., Canadell, J. G., Jackson, R. B., Patra, P. K., Bousquet, P., Ciais, P., Dlugokencky, E. J., Lan, X., Allen, G. H., Bastviken, D., Beerling, D. J., Belikov, D. A., Blake, D. R., Castaldi, S., Crippa, M., Deemer, B. R., Dennison, F., Etiope, G., Gedney, N., Höglund-Isaksson, L., Holgerson, M. A., Hopcroft, P. O., Hugelius, G., Ito, A., Jain, A. K., Janardanan, R.,

Johnson, M. S., Kleinen, T., Krummel, P., Lauerwald, R., Li, T., Liu, X., McDonald, K. C., Melton, J. R., Mühle, J., Müller, J., Murguia-Flores, F., Niwa, Y., Noce, S., Pan, S., Parker, R. J., Peng, C., Ramonet, M., Riley, W. J., Rocher-Ros, G., Rosentreter, J. A., Sasakawa, M., Segers, A., Smith, S. J., Stanley, E. H., Thanwerdas, J., Tian, H., Tsuruta, A., Tubiello, F. N., Weber, T. S., van der Werf, G., Worthy, D. E., Xi, Y., Yoshida, Y., Zhang, W., Zheng, B., Zhu, Q., Zhu, Q., Zhuang, Q. (2024). Global Methane Budget 2000-2020. *Earth System Science Data Discussions*, 2024, 1-147.

Sirois, A. (1999). A brief and biased overview of time-series analysis of how to find that evasive trend. Annex E, *WMO EMEP Workshop on Advanced Statistical Methods and their Application to Air Quality Data Sets, Helsinki*, (4–18 September 1998), Global Atmosphere Watch.

Stevenson, D. S., Derwent, R. G., Wild, O., Collins, W. J. (2022). COVID-19 lockdown emission reductions have the potential to explain over half of the coincident increase in global atmospheric methane. *Atmospheric Chemistry and Physics*, *22*(21), 14243-14252.

Stohl, A., Klimont, Z., Eckhardt, S., Kupiainen, K., Shevchenko, V. P., Kopeikin, V. M., Novigatsky, A. N. (2013). Black carbon in the Arctic: the underestimated role of gas flaring and residential combustion emissions. *Atmospheric Chemistry and Physics*, *13*(17), 8833-8855.

Sun, J., Birmili, W., Hermann, M., Tuch, T., Weinhold, K., Merkel, M., Rasch, F., Müller, T., Schladitz, A., Bastian, S., Löschau, G., Cyrys, J., Gu, J., Flentje, H., Briel, B., Asbach, C., Kaminski, H., Ries, L., Sohmer, R., Gerwig, H., Wirtz, K., Meinhardt, F., Schwerin, A., Bath, O., Ma, N., Wiedensohler, A. (2020). Decreasing trends of particle number and black carbon mass concentrations at 16 observational sites in Germany from 2009 to 2018. *Atmospheric Chemistry and Physics*, *20*(11), 7049-7068.

Svendby, T. F., Schulze, D., Bäcklund, A., Johnsen, B. (2024). *Monitoring of the atmospheric ozone layer and natural ultraviolet radiation. Annual Report 2023* (NILU rapport 20/2024). Kjeller: NILU.

Thompson, R. L., Dlugokencky, E., Chevallier, F., Ciais, P., Dutton, G., Elkins, J. W., Langenfelds, R. L., Prinn, R. G., Weiss, R. F., Tohjima, Y., O'Doherty, S., Krummel, P. B., Fraser, P., Steele, L. P. (2013). Interannual variability in tropospheric nitrous oxide. *Journal of Geophysical Research: Atmospheres*, *40*(16), 4426-4431.

Virkkula, A., Grythe, H., Backman, J., Petäjä, T., Busetto, M., Lanconelli, C., Lupi, A., Becagli, S., Traversi, R., Severi, M., Vitale, V., Sheridan, P., Andrews, E. (2022). Aerosol optical properties calculated from size distributions, filter samples and absorption photometer data at Dome C, Antarctica, and their relationships with seasonal cycles of sources. *Atmospheric Chemistry and Physics*, *22*(7), 5033-5069.

Weis, J., Schallenberg, C., Chase, Z., Bowie, A. R., Wojtasiewicz, B., Perron, M. M. G., Mallet, M. D., Strutton, P. G. (2022). Southern Ocean Phytoplankton Stimulated by Wildfire Emissions and Sustained by Iron Recycling. *Geophysical Research Letters*, *49*(11), e2021GL097538.

WMO (2024) Greenhouse Gas Bulletin. The State of Greenhouse Gases in the Atmosphere Based on Global Observations through 2023. (GHG Bulletin No. 20, 28 October 2024). Geneva: World Meteorological Organization.

World Meteorological Organization (2014). *Scientific Assessment of Ozone Depletion: 2014*. Geneva: World Meteorological Organization.

Yan, J., Jung, J., Lin, Q., Zhang, M., Xu, S., Zhao, S. (2020). Effect of sea ice retreat on marine aerosol emissions in the Southern Ocean, Antarctica. *Science of The Total Environment, 745,* 140773.

Yttri, K. E., Bäcklund, A., Conen, F., Eckhardt, S., Evangeliou, N., Fiebig, M., Kasper-Giebl, A., Gold, A., Gundersen, H., Myhre, C. L., Platt, S. M., Simpson, D., Surratt, J. D., Szidat, S., Rauber, M., Tørseth, K., Ytre-Eide, M. A., Zhang, Z., Aas, W. (2024). Composition and sources of carbonaceous aerosol in the European Arctic at Zeppelin Observatory, Svalbard (2017 to 2020). *Atmospheric Chemistry and Physics, 24*(4), 2731-2758.

Yttri, K. E., Canonaco, F., Eckhardt, S., Evangeliou, N., Fiebig, M., Gundersen, H., Hjellbrekke, A. G., Lund Myhre, C., Platt, S. M., Prévôt, A. S. H., Simpson, D., Solberg, S., Surratt, J., Tørseth, K., Uggerud, H., Vadset, M., Wan, X., Aas, W. (2021). Trends, composition, and sources of carbonaceous aerosol at the Birkenes Observatory, northern Europe, 2001–2018. *Atmospheric Chemistry and Physics*, *21*(9), 7149-7170.

Yuan, K., Li, F., McNicol, G., Chen, M., Hoyt, A., Knox, S., Riley, W. J., Jackson, R., Zhu, Q. (2024). Boreal–Arctic wetland methane emissions modulated by warming and vegetation activity. *Nature Climate Change*, 14(3), 282-288.

Yuan, T., Song, H., Oreopoulos, L., Wood, R., Bian, H., Breen, K., Chin, M., Yu, H., Barahona, D., Meyer, K., Platnick, S. (2024). Abrupt reduction in shipping emission as an inadvertent geoengineering termination shock produces substantial radiative warming. *Communications Earth & Environment*, *5*(1), 281.

Yver-Kwok, C., Philippon, C., Bergamaschi, P., Biermann, T., Calzolari, F., Chen, H., Conil, S., Cristofanelli, P., Delmotte, M., Hatakka, J., Heliasz, M., Hermansen, O., Komínková, K., Kubistin, D., Kumps, N., Laurent, O., Laurila, T., Lehner, I., Levula, J., Lindauer, M., Lopez, M., Mammarella, I., Manca, G., Marklund, P., Metzger, J.-M., Mölder, M., Platt, S.M., Ramonet, M., Rivier, L., Scheeren, B., Kumar , M.S., Smith, P., Steinbacher, M., Vítková, G., and Wyss, S. (2021). Evaluation and optimization of ICOS atmosphere station data as part of the labeling process. *Atmospheric Measurement Techniques*, 14(1), 89-116.

Zeileis A. (2004) Econometric Computing with HC and HAC Covariance Matrix Estimators. *J. Stat. Software*, *11,* 1-17.

Zeileis, A. (2006) Object-oriented computation of sandwich estimators. *J. Stat. Software*, *16,* 1-16.

Zotter, P., Herich, H., Gysel, M., El-Haddad, I., Zhang, Y., Močnik, G., Hüglin, C., Baltensperger, U., Szidat, S., Prévôt, A. S. H. (2017). Evaluation of the absorption Ångström exponents for traffic and wood burning in the Aethalometer-based source apportionment using radiocarbon measurements of ambient aerosol. *Atmospheric Chemistry and Physics*, *17*(6), 4229-4249

Appendix A
Data Tables

Table A 1: Annual mean concentration for all greenhouse gases included in the programme at Zeppelin and Birkenes. All concentrations are mixing ratios in ppt, except for methane and carbon monoxide (ppb) and carbon dioxide (ppm). The annual means are based on a combination of the measurements and the fitted values; during periods with lacking observations the fitted mixing ratios in the calculation of the annual mean are used. All underlying measurement data are open and accessible and can be downloaded directly from the database: http://ebas.nilu.no/

Component	2001	2002	2003	2004	2005	2006	2007	2008	2009	2010	2011	2012	2013	2014	2015	2016	2017	2018	2019	2020	2021	2022	2023
CO_2 - Zeppelin	370,9	372,2	376,3	378,9	380,5	383,0	384,0	386,4	387,6	390,2	392,5	394,9	397,6	399,8	401,2	404,6	408,2	409,6	412,2	414,8	417,5	419,6	421,5
CO_2 - Birkenes									391,7	394,7	397,5	398,0	400,9	403,0	405,4	409,9	411,4	415,4	416,3	419,0	421,3	423,9	426,0
CO_2 - Trollhaugen														395,3	397,7	400,7	402,5	405,0	407,6	409,9	412,1	414,3	416,4
Methane - Zeppelin	1845,2	1843,2	1855,5	1853,0	1852,0	1853,2	1863,3	1873,2	1888,2	1880,0	1879,8	1891,9	1898,0	1910,0	1920,2	1931,8	1938,9	1938,5	1953,1	1968,8	1982,0	1999,6	2007,6
Methane - Birkenes									1881,1	1887,2	1895,6	1900,5	1902,5	1917,3	1926,1	1941,9	1945,2	1953,1	1961,2	1975,3	1991,8	2005,5	2016,2
Methane - Trollhaugen																						1858,2	1871,1
Carbon monoxide	130,6	126,2	140,3	130,3	128,8	126,0	120,3	120,0	117,9	128,9	115,2	120,6	113,1	113,4	112,8	112,3	114,3	113,6	115,6	117,7	128,0	115,0	125,2
Nitrous oxide										323,6	324,2	325,1	326,1	327,2	328,0	329,0	330,0	331,3	332,1	333,4	334,5	335,8	337,0
Chlorofluorocarbons																							
CFC-11	259,4	257,2	254,9	253,2	250,9	249,2	246,4	244,5	242,7	240,8	238,6	237,5	236,1	234,3	233,3	231,6	230,1	229,2	227,3	225,0	222,7	220,4	217,5
CFC-12	547,5	547,6	547,6	545,5	546,7	546,1	542,2	541,4	537,7	534,6	531,6	529,2	526,6	523,3	519,8	516,4	512,5	509,2	505,4	501,4	497,9	493,5	488,9
CFC-113	81,4	80,8	80,0	79,4	78,8	77,9	77,5	76,8	76,2	75,4	74,7	74,1	73,5	72,9	72,3	71,7	71,1	70,5	70,0	69,5	69,1	68,6	68,1
CFC-115	8,22	8,18	8,22	8,28	8,41	8,38	8,37	8,39	8,43	8,42	8,42	8,44	8,43	8,46	8,51	8,54	8,59	8,66	8,73	8,74	8,80	8,87	8,94
Hydrochlorofluorocarbons																							
HCFC-22	158,4	164,1	170,8	175,9	181,5	189,2	196,4	204,6	212,5	219,7	225,8	231,0	236,4	241,2	245,3	248,7	252,2	255,2	257,8	258,5	258,8	258,5	256,4
HCFC-141b	16,7	17,9	18,7	19,3	19,5	20,0	20,5	21,2	21,6	22,2	23,1	24,0	24,6	25,3	25,5	25,9	25,8	25,6	25,8	26,2	26,3	26,1	26,0
HCFC-142b	14,3	15,0	16,0	16,7	17,3	18,3	19,4	20,4	21,3	22,0	22,7	22,9	23,2	23,3	23,4	23,5	23,4	23,3	23,2	23,0	22,7	22,4	22,1
Hydrofluorocarbons																							

Component	2001	2002	2003	2004	2005	2006	2007	2008	2009	2010	2011	2012	2013	2014	2015	2016	2017	2018	2019	2020	2021	2022	2023
HFC-125	2,2	2,6	2,9	3,3	4,0	4,9	5,8	6,9	8,0	9,6	11,8	13,5	15,6	17,9	20,3	22,9	25,8	28,9	32,3	35,6	39,4	43,4	47,6
HFC-134a	21,2	26,1	30,6	35,3	39,7	44,1	48,5	53,4	57,8	63,6	68,6	73,7	79,0	84,6	90,3	96,6	103,1	108,5	114,6	120,1	126,1	131,8	136,9
HFC-152a	2,6	3,4	4,3	5,1	5,8	6,8	7,8	8,6	9,0	9,5	10,0	10,2	10,2	10,1	10,1	10,2	10,3	10,3	10,6	10,5	10,6	10,8	10,8
HFC-23										23,9	24,7	25,5	26,6	27,7	28,7	29,6	30,7	31,9	33,2	34,5	35,6	36,5	37,4
HFC-365mfc										0,71	0,79	0,87	0,93	1,02	1,10	1,19	1,24	1,29	1,32	1,32	1,33	1,35	1,32
HFC-227ea										0,70	0,79	0,88	0,99	1,10	1,21	1,34	1,47	1,59	1,75	1,91	2,09	2,29	2,49
HFC-236fa										0,09	0,10	0,11	0,13	0,14	0,15	0,16	0,17	0,19	0,21	0,22	0,23	0,24	0,26
HFC-245fa										1,64	1,80	1,98	2,19	2,39	2,58	2,80	3,04	3,26	3,53	3,70	3,83	3,96	4,07
HFC-32										5,61	6,57	7,66	9,29	10,93	12,89	15,23	18,25	21,54	25,21	28,66	32,69	37,70	42,73
HFC-4310mee										0,21	0,23	0,24	0,25	0,26	0,27	0,28	0,29	0,29	0,30	0,31	0,32	0,32	0,32
HFC-143a										11,85	13,17	14,58	16,03	17,63	19,08	20,72	22,51	23,93	25,58	27,29	29,00	30,79	32,54
Perfluorinated compounds																							
PFC-14															82,42	83,32	84,27	85,25	86,12	86,98	88,02	89,00	89,93
PFC-116										4,11	4,20	4,27	4,37	4,45	4,55	4,64	4,74	4,82	4,91	5,00	5,11	5,21	5,30
PFC-218										0,56	0,57	0,59	0,60	0,61	0,63	0,64	0,66	0,68	0,69	0,72	0,74	0,76	0,78
PFC-318										1,28	1,33	1,38	1,43	1,47	1,53	1,59	1,66	1,73	1,80	1,87	1,95	2,04	2,16
Sulphurhexafluoride	4,94	5,14	5,37	5,61	5,82	6,09	6,31	6,64	6,93	7,19	7,50	7,78	8,11	8,43	8,75	9,08	9,46	9,80	10,14	10,45	10,84	11,26	11,63
Nitrogen trifluoride																1,61	1,76	1,98	2,21	2,49	2,79	3,11	3,39
Sulfuryl fluoride										1,72	1,81	1,91	2,03	2,12	2,22	2,33	2,45	2,52	2,63	2,72	2,85	2,98	3,07
Halons																							
H-1211	4,39	4,44	4,47	4,52	4,52	4,48	4,43	4,39	4,33	4,26	4,18	4,09	3,98	3,87	3,77	3,66	3,55	3,45	3,37	3,26	3,17	3,07	2,97
H-1301	2,99	3,07	3,13	3,17	3,21	3,22	3,24	3,28	3,29	3,32	3,33	3,35	3,36	3,38	3,39	3,39	3,39	3,38	3,39	3,39	3,40	3,40	3,39

Component	2001	2002	2003	2004	2005	2006	2007	2008	2009	2010	2011	2012	2013	2014	2015	2016	2017	2018	2019	2020	2021	2022	2023
H-2402										0,47	0,46	0,45	0,44	0,44	0,43	0,42	0,41	0,41	0,41	0,40	0,40	0,39	0,39
Other halocarbons																							
Chloromethane	506,7	521,1	526,5	522,7	519,0	520,7	523,3	525,3	526,3	520,7	509,6	515,6	519,2	514,4	512,7	521,3	516,7	514,2	507,7	508,4	510,8	514,3	512,8
Bromomethane	9,20	9,16	8,87	8,85	8,51	8,56	8,30	7,76	7,37	7,29	7,20	7,08	6,99	6,88	6,71	6,75	6,56	6,54	6,71	6,65	6,75	6,54	6,59
Dichloromethane	31,07	31,40	32,51	32,56	32,38	33,58	35,63	37,65	38,62	42,20	42,05	44,77	53,54	54,20	53,56	56,41	61,21	60,75	59,20	63,41	69,02	72,08	73,24
Trichloromethane	11,06	10,66	10,72	10,37	10,42	10,45	10,65	10,47	10,88	11,52	11,98	12,18	12,73	13,47	13,62	14,17	15,32	14,79	12,32	13,13	12,69	12,48	11,87
Carbon tetrachloride										86,81	85,28	84,42	83,46	82,52	81,74	80,65	79,49	78,98	78,10	77,34	76,38	75,14	74,07
Trichloroethane	37,56	31,90	27,30	22,94	19,27	15,99	13,41	11,16	9,24	7,74	6,47	5,32	4,46	3,74	3,22	2,76	2,35	2,01	1,72	1,57	1,37	1,16	1,05
Trichloroethene	0,70	0,66	0,57	0,54	0,52	0,50	0,35	0,39	0,54	0,54	0,54	0,49	0,55	0,49	0,44	0,41	0,40	0,42	0,38	0,31	0,31	0,23	0,20
Tetrachloroethene	4,61	4,20	4,07	3,89	3,39	2,92	3,15	2,73	2,97	3,13	2,82	2,67	2,55	2,57	2,57	2,54	2,48	2,31	2,29	2,13	2,14	2,04	1,91
Volatile Organic Compounds (VOC)																							
Ethane										1505,6	1473,1	1586,4	1566,8	1640,6	1628,9	1565,7	1576,4	1524,6	1607,1	1528,4	1544,0	1516,6	1559,8
Propane										548,7	530,6	570,0	578,0	565,2	527,3	551,1	583,1	498,6	457,7	417,0	436,6	492,3	476,8
Butane										140,3	128,4	137,0	139,1	130,9	118,1	110,0	132,1	98,7	96,9	84,0	81,3	120,8	111,8
Pentane										33,3	29,7	30,5	32,4	30,7	28,2	26,6	29,3	18,9	21,3	20,4	20,3	27,5	24,9
Benzene										86,1	72,4	75,0	69,8	71,5	67,5	65,3	61,9	60,7	59,2	54,3	66,8	58,9	57,4
Toluene										36,8	29,3	28,8	26,6	28,5	25,1	24,2	17,7	19,2	18,3	13,1	20,0	19,4	23,1

*Trichloroethene: Larger uncertainties in the numbers due to low concentrations, memory effects and blanks in the instrument. The reference numbers (scale UB-98) have also larger uncertainties for the same reasons.

**Tetrachloroethene: Larger uncertainties in the 2001-2010 numbers due to larger variability in the measurements with the ADS-GCMS instrument.

Table A 2: All calculated trends per year, error and regression coefficient for the fit. The trends are all in ppt per year, except for CH_4, N_2O, and CO which are in ppb and CO_2 is in ppm. The negative trends are in blue, and the positive trends are shown in red.

Component	Formula	Trend/yr	Error	R^2
Carbon dioxide - Zeppelin	CO_2	2.47	0.02	0.98
Carbon dioxide - Birkenes		2.49	0.04	0.83
Methane - Zeppelin	CH_4	7.33	0.08	0.95
Methane - Birkenes		9.65	0.15	0.81
Carbon monoxide	CO	-0.65	0.23	0.73
Nitrous oxide	N_2O	1.04	0.00	0.99
Chlorofluorocarbons				
CFC-11	CCl_3F	-1.78	0.013	0.99
CFC-12	CF_2Cl_2	-2.79	0.018	0.99
CFC-113	CF2ClCFCl2	-0.61	0.002	1.00
CFC-115	CF_3CF_2Cl	0.03	0.001	0.85
Hydrochlorofluorocarbons				
HCFC-22	$CHClF_2$	4.95	0.030	0.997
HCFC-141b	$C_2H_3FCl_2$	0.44	0.012	0.973
HCFC-142b	CH_3CF_2Cl	0.38	0.014	0.979
Hydrofluorocarbons				
HFC-125	CHF_2CF_3	2.03	0.005	0.999
HFC-134a	CH_2FCF_3	5.31	0.014	0.999
HFC-152a	CH_3CHF_2	0.34	0.009	0.964
HFC-23	CHF_3	1.08	0.005	0.998
HFC-365mfc	$CH_3CF_2CH_2CF_3$	0.05	0.0003	0.980
HFC-227ea	CF_3CHFCF_3	0.14	0.0002	0.999
HFC-236fa	$CF_3CH_2CF_3$	0.01	0.00004	0.991
HFC-245fa	$CHF_2CH_2CF_3$	0.20	0.001	0.997
HFC-32	CH_2F_2	2.83	0.009	0.999
HFC-4310mee	$C_5H_2F_{10}$	0.01	0.000	0.965
HFC-143a	CH_3CF_3	1.60	0.003	0.999
Perfluorinated compounds				
PFC-14	CF_4	0.933	0.0242	0.997
PFC-116	C_2F_6	0.092	0.0002	0.998
PFC-218	C_3F_8	0.017	0.0001	0.989
PFC-318	$c\text{-}C_4F_8$	0.066	0.0002	0.997
Sulphurhexafluoride	SF_6	0.306	0.0004	0.999
Nitrogen trifluoride	NF_3	0.260	0.0143	0.998
Sulfuryl fluoride	SO_2F_2	0.104	0.0008	0.994
Halons				
H-1211	$CBrClF_2$	-0.074	0.0003	0.997

Component	Formula	Trend/yr	Error	R^2
H-1301	$CBrF_3$	0.015	0.0003	0.794
H-2402	$CBrF_2CBrF_2$	-0.006	0.00004	0.972
Chloromethane	CH_3Cl	-0.448	0.1566	0.868
Bromomethane	CH_3Br	-0.130	0.0054	0.875
Dichloromethane	CH_2Cl_2	2.058	0.0563	0.940
Trichloromethane	$CHCl_3$	0.155	0.0132	0.667
Carbon tetrachloride	CCl_4	-0.931	0.0084	0.974
Trichloroethane	CH_3CCl_3	-1.421	0.0099	0.998
Trichloroethene*	$CHClCCl_2$	-0.015	0.0027	0.414
Tetrachloroethene**	CCl_2CCl_2	-0.100	0.0060	0.561
Volatile Organic Compounds (VOC)				
Ethane***	C_2H_6	0.30	3.18	0.87
Propane***	C_3H_8	-9.35	2.22	0.81
Butane***	C_4H_{10}	-3.42	0.80	0.72
Pentane***	C_5H_{12}	-0.83	0.19	0.66
Benzene***	C_6H_6	-1.73	0.41	0.82
Toluene***	$C_6H_5CH_3$	-1.18	0.24	0.67
Isotopes				
Methane d13C isotope	d13C-CH_4	-0.037	0.003	0.52

**Trichloroethene: Larger uncertainties in the numbers due to low concentrations, memory effects and blanks in the instrument. The reference numbers (scale UB-98) have also larger uncertainties for the same reasons.*

***Tetrachloroethene: Larger uncertainties in the 2001-2010 numbers due to larger variability in the measurements with the ADS-GCMS instrument.*

**** Larger uncertainty for VOC due to shorter timeseries*

Table A 3: 2010 to 2024 seasonal and annual means of integral particle concentrations in the ultrafine (0.02 to 0.1 µm), fine (0.1 to 1 µm) and coarse (1 to 10 µm) particle size range for Birkenes, Trollhaugen, and Zeppelin stations.

		Birkenes				Trollhaugen[1]		Zeppelin	
Year	Season	N_{ait}/ cm^{-3}	N_{acc}/ cm^{-3}	N_{coa}/ cm^{-3}	N_{tot}/ cm^{-3}	N_{ait} / cm^{-3}	$^{2}N_{acc}$/ cm^{-3}	N_{ait}/ cm^{-3}	$^{2}N_{acc}$/ cm^{-3}
2009/10	Winter	467	433	0.296	967				
2010	Spring	1249	372	0.704	1633				
2010	Summer	1807	555	0.643	2381				
2010	Autumn	912	343	0.562	1358				
2010	Whole Year	1101	412	0.575	1593				
2010/11	Winter	544	320	0.974	863				
2011	Spring	1341	422	1.620	1765				
2011	Summer	1661	497	1.250	2161				
2011	Autumn	1908	560	1.844	2470				
2011	Whole Year	1215	417	1.427	1644				
2011/12	Winter	433	217	0.927	664				
2012	Spring	1179	303	0.982	1523				
2012	Summer	1447	435	1.041	1892				
2012	Autumn	722	169	0.918	898				
2012	Whole Year	951	288	0.912	1258				
2012/13	Winter	421	203	0.550	626				
2013	Spring	1314	392	1.012	1711				
2013	Summer	1680	497	0.951	2182				
2013	Autumn	785	183	0.952	968				
2013	Whole Year	1107	335	0.951	1454				
2013/14	Winter	737	342	1.246	1079				
2014	Spring	1569	429	0.823	1998	183	32		
2014	Summer	1717	642	0.757	2358	43	19		
2014	Autumn	1286	532	0.950	1818	207	28		
2014	Whole Year	1333	488	0.859	1821	183	34		
2014/15	Winter	567	203	1.038	770	368	67		
2015	Spring	1571	360	1.030	1931	134	25		
2015	Summer	2198	614	0.866	2812	38	23		
2015	Autumn	1081	378	0.766	1459	221	28		
2015	Whole Year	1363	395	0.963	1758	171	32		
2015/16	Winter	594	245	0.867	839				
2016	Spring	1471	483	0.848	1954	170	26		
2016	Summer	1608	535	0.876	2143	47	18	156	64
2016	Autumn	983	319	0.707	1302	262	35	47	31
2016	Whole Year	1167	391	0.804	1558	231	37	---	---
2016/17	Winter	585	219	0.717	804	473	74	---	---
2017	Spring	1474	476	0.564	1950	157	31	96	126
2017	Summer	1599	537	1.013	2136	51	20	282	70
2017	Autumn	1291	440	0.734	1731	265	27	56	63
2017	Whole Year	1256	424	0.721	1679	238	38	---	---
2017/18	Winter	517	275	0.399	792	482	78	27	44
2018	Spring	1511	649	---	2159	170	24	107	85
2018	Summer	1948	617	---	2565	45	18	225	66
2018	Autumn	986	300	---	1286	273	28	30	25
2018	Whole Year	1255	460	---	1715	233	35	92	55
2018/19	Winter	578	229	---	806	427	64	18	60

Year	Season	Birkenes				Trollhaugen[1]		Zeppelin	
		N_{ait}/ cm^{-3}	N_{acc}/ cm^{-3}	N_{coa}/ cm^{-3}	N_{tot}/ cm^{-3}	N_{ait} / cm^{-3}	$^{2}N_{acc}$/ cm^{-3}	N_{ait}/ cm^{-3}	$^{2}N_{acc}$/ cm^{-3}
2019	Spring	1406	500	---	1906	183	25	78	95
2019	Summer	1867	509	---	2376	34	14	224	68
2019	Autumn	805	185	---	990	233	29	29	28
2019	Whole Year	1163	356	---	1519	202	31	87	64
2019/20	Winter	567	133	---	700	398	78	25	78
2020	Spring	1480	291	---	1770	187	27	90	88
2020	Summer	1570	554	---	2125	36	13	148	96
2020	Autumn	907	251	---	1158	237	28	34	38
2020	Whole Year	1133	306	---	1439	219	37	77	75
2020/2021	Winter	503	160	---	721	395	72	16	23
2021	Spring	1107	255	---	1490	213	29	38	54
2021	Summer	1560	548	0.608	2217	46	11	127	39
2021	Autumn	977	195	0.703	1236	429	33	35	23
2021	Whole Year	1062	294	---	1445	289	38	61	34
2021/2022	Winter	457	97	---	593	528	91	---	---
2022	Spring	1664	308	---	2185	251	29	77	93
2022	Summer	1860	457	---	2512	49	10	164	61
2022	Autumn	1061	184	---	1319	360	24	28	13
2022	Whole Year	1298	273	---	1711	285	36	83	53
2022/2023	Winter	684	167	---	977	389	72	24	49
2023	Spring	1348	391	---	2037	209	24	86	102
2023	Summer	1230	393	---	1793	44	12	213	58
2023	Autumn	---	---	---	---	333	25	28	13
2023	Whole Year	1142	335	---	1684	238	33	83	53

[1] Cells shaded in grey mark values obtained with an older instrument version that can't be compared directly with later values. Numbers given for the time when the respective season is present in the Northern hemisphere. Actual seasons in Southern hemisphere are shifted by 6 months. In 2020, numbers for Birkenes have been reprocessed for all years since 2010 taking into account recent intercalibrations.

[2] The accumulation mode integral particle concentration N_{acc} at Trollhaugen and Zeppelin extends only up to 0.8 µm particle diameter due to lack of an instrument covering larger particles. For Birkenes, N_{acc} includes particles up to 1 µm diameter

Table A 4: 2010 to 2024 seasonal and annual means of optical aerosol properties scattering coefficient, absorption coefficient, and single scattering albedo (all at 550 nm) for Birkenes, Trollhaugen, and Zeppelin stations, as far as available.

		Birkenes			Trollhaugen[1]			Zeppelin		
Year	Season	σ_{sp} Mm^{-1}	σ_{ap} Mm^{-1}	v_0	σ_{sp} Mm^{-1}	σ_{ap} Mm^{-1}	v_0	σ_{sp} Mm^{-1}	σ_{ap} Mm^{-1}	v_0
2009/10	Winter	16.82	3.09	0.88						
2010	Spring	12.33	0.78	0.93						
2010	Summer	11.30	0.70	0.94						
2010	Autumn	7.26	0.71	0.90						
2010	Whole Year	11.52	1.24	0.91						
2010/11	Winter	16.96	2.18	0.89						
2011	Spring	18.67	1.26	0.93						
2011	Summer	15.43	0.74	0.95						
2011	Autumn	29.74	2.87	0.92						
2011	Whole Year	20.26	1.69	0.93						
2011/12	Winter	11.29	1.00	0.91						
2012	Spring	15.10	0.86	0.93						
2012	Summer	12.62	0.67	0.95						
2012	Autumn	9.80	0.65	0.92						
2012	Whole Year	12.22	0.83	0.92						
2012/13	Winter	12.48	1.84	0.84						
2013	Spring	17.03	1.48	0.90						
2013	Summer	13.81	1.15	0.92						
2013	Autumn	8.89	1.25	0.85						
2013	Whole Year	13.73	1.40	0.88						
2013/14	Winter	22.89	2.64	0.87						
2014	Spring	12.95	2.09	0.87	0.74	-0.05	0.95			
2014	Summer	15.85	1.26	0.92	1.39	0.04	0.98			
2014	Autumn	18.76	3.41	0.82	1.02	0.15	0.93			
2014	Whole Year	16.99	2.30	0.87	1.01	0.09	0.95			
2014/15	Winter	13.98	1.30	0.89	0.74	0.04	0.94			
2015	Spring	12.72	1.48	0.89	0.65	0.02	0.97			
2015	Summer	12.45	1.46	0.90	2.44	0.02	0.98			0.30
2015	Autumn	15.69	2.45	0.95	1.32	0.07	0.94			0.14
2015	Whole Year	14.36	1.56	0.90	1.32	0.04	0.96			
2015/16	Winter	13.59	1.24	0.88	0.87	0.05	0.94			0.38
2016	Spring	14.86	1.10	0.91	0.78	0.17	0.97			0.39
2016	Summer	11.93	0.77	0.94	2.01	0.00	0.99			0.09
2016	Autumn	11.47	1.46	0.85	1.54	0.04	0.95			0.12
2016	Whole Year	12.26	1.12	0.89	1.31	0.06	0.97			0.24
2016/17	Winter	12.27	2.24	0.81	0.82	0.05	0.94			0.40
2017	Spring	8.71			0.76	0.02	0.97			0.48
2017	Summer	8.58			1.57	0.01	0.99			0.10
2017	Autumn	8.09	1.21	0.85	1.22	0.05	0.94			0.29
2017	Whole Year	9.07			1.10	0.03	0.96			0.33

		Birkenes			Trollhaugen[1]			Zeppelin		
Year	Season	σ_{sp} Mm^{-1}	σ_{ap} Mm^{-1}	v_0	σ_{sp} Mm^{-1}	σ_{ap} Mm^{-1}	v_0	σ_{sp} Mm^{-1}	σ_{ap} Mm^{-1}	v_0
2017/18	Winter	13.56	1.66	0.83	0.72	0.04	0.95		0.34	
2018	Spring	17.10	2.45	0.87	0.60	0.03	0.97		0.32	
2018	Summer	13.62	1.23	0.91	1.78	0.06	0.98		0.12	
2018	Autumn	14.08	2.04	0.86	1.31	0.04	0.95		0.10	
2018	Whole Year	14.54	1.90	0.86	1.10	0.04	0.96		0.21	
2018/19	Winter	---	---	---	0.73	0.04	0.94		0.45	
2019	Spring	---	---	---	0.81	0.03	0.97		0.46	
2019	Summer	---	---	---	1.81	0.01	0.99		0.19	
2019	Autumn	6.26	0.93	0.85	1.61	0.04	0.96		0.13	
2019	Whole Year	---	---	---	1.26	0.03	0.97		0.33	
2019/20	Winter	10.15	0.96	0.87	0.88	0.04	0.95		0.73	
2020	Spring	10.84	1.03	0.90	0.89	0.02	0.98		0.36	
2020	Summer	11.28	1.07	0.91	1.43	0.01	0.99		0.24	
2020	Autumn	12.63	1.53	0.88	1.60	0.04	0.97		0.13	
2020	Whole Year	11.62	1.21	0.89	1.19	0.03	0.97		0.36	
2020/21	Winter	9.81	1.76	0.80	0.80	0.11	0.95		0.17	
2021	Spring	8.38	0.76	0.87	0.66	0.02	0.98		0.50	
2021	Summer	17.36	1.08	0.93	1.88	0.02	0.99		0.08	
2021	Autumn	12.23	1.21	0.86	1.27	0.14	0.95		0.20	
2021	Whole Year	11.42	1.14	0.86	1.23	0.07	0.97		0.25	
2021/22	Winter	8.74	1.11	0.85	1.14	0.13	0.95			
2022	Spring	15.63	2.12	0.89	0.76	0.04	0.98			
2022	Summer	12.9	0.9	0.94	1.59	0.02	0.99			
2022	Autumn	12.43	1.41	0.87	1.15	0.12	0.96			
2022	Whole Year	12.43	1.4	0.89	1.12	0.08	0.97			
2022/23	Winter	7.76	0.98	0.87	0.84	0.06	0.94		0.33	
2023	Spring	10.81	1.01	0.91	0.62	0.03	0.96		0.38	
2023	Summer	13.61	0.78	0.95	1.55	0.03	0.98		0.12	
2023	Autumn	11.80	2.01	0.92	1.03	0.07	0.94		0.08	
2023	Whole Year	11.33	0.93	0.92	1.00	0.05	0.95		0.20	

Table A 5: Monthly means and standard deviation of AOD at 500 nm in Ny-Ålesund

Year	Month	Ny Ålesund			Birkenes			Trollhaugen		
		AOD	AE	N	AOD	AE	N	AOD	AE	N
2002	1									
2002	2									
2002	3									
2002	4									
2002	5	0.076±0.024	1.35±0.23	24						
2002	6	0.060±0.019	1.36±0.33	19						
2002	7	0.059±0.040	1.36±0.25	13						
2002	8	0.043±0.016	1.60±0.19	12						
2002	9	0.044±0.018	1.53±0.20	15						
2002	10									
2002	11									
2002	12									
2003	1									
2003	2									
2003	3	0.088±0.012	1.18±0.32	4						
2003	4	0.093±0.029	1.33±0.27	12						
2003	5	0.125±0.047	1.32±0.18	15						
2003	6	0.116±0.024	1.44±0.08	16						
2003	7	0.047±0.014	1.45±0.39	17						
2003	8	0.047±0.009	1.57±0.31	19						
2003	9	0.049±0.011	1.51±0.30	9						
2003	10									
2003	11									
2003	12									
2004	1									
2004	2									
2004	3									
2004	4	0.112±0.015	1.36±0.25	7						
2004	5	0.094±0.024	1.37±0.36	21						
2004	6	0.071±0.033	1.40±0.37	14						
2004	7	0.116±0.058	1.56±0.13	17						
2004	8	0.047±0.010	1.60±0.16	14						
2004	9	0.049±0.020	1.30±0.27	8						
2004	10									
2004	11									

Year	Month	Ny Ålesund			Birkenes			Trollhaugen		
		AOD	AE	N	AOD	AE	N	AOD	AE	N
2004	12									
2005	1									
2005	2									
2005	3	0.058±0.017	1.32±0.18	3						
2005	4	0.110±0.038	1.45±0.22	17						
2005	5	0.091±0.019	1.02±0.16	25						
2005	6	0.055±0.025	1.62±0.20	15						
2005	7	0.051±0.015	1.62±0.28	11						
2005	8	0.036±0.007	1.59±0.09	6						
2005	9	0.035±0.007	1.44±0.20	11						
2005	10									
2005	11									
2005	12									
2006	1									
2006	2									
2006	3	0.119±0.012	0.86±0.17	7						
2006	4	0.141±0.053	0.99±0.17	12						
2006	5									
2006	6	0.040±0.004	1.66±0.12	5						
2006	7	0.051±0.015	1.51±0.24	9						
2006	8									
2006	9									
2006	10									
2006	11									
2006	12									
2007	1									
2007	2									
2007	3									
2007	4	0.106±0.036	1.38±0.29	14						
2007	5	0.085±0.029	1.50±0.25	14						
2007	6	0.071±0.015	1.57±0.26	15						
2007	7	0.050±0.015	1.57±0.18	16						
2007	8	0.050±0.017	1.59±0.34	15						
2007	9	0.035±0.007	1.51±0.28	9						
2007	10									
2007	11									
2007	12									

Year	Month	Ny Ålesund			Birkenes			Trollhaugen		
		AOD	AE	N	AOD	AE	N	AOD	AE	N
2008	1									
2008	2									
2008	3	0.112±0.046	1.42±0.20	16						
2008	4	0.145±0.051	1.34±0.20	22						
2008	5	0.141±0.044	1.40±0.12	15						
2008	6	0.061±0.021	1.35±0.35	21						
2008	7	0.057±0.016	1.27±0.25	16						
2008	8	0.075±0.026	1.29±0.21	12						
2008	9	0.126±0.031	1.37±0.15	7						
2008	10									
2008	11									
2008	12									
2009	1									
2009	2									
2009	3									
2009	4	0.165±0.008	1.54±0.07	2						
2009	5	0.103±0.026	1.23±0.38	14	0.087±0.056	1.15±0.24	20			
2009	6	0.089±0.021	1.32±0.25	13	0.091±0.042	1.29±0.33	24			
2009	7	0.121±0.043	1.22±0.31	19	0.157±0.043	1.45±0.39	10			
2009	8	0.106±0.020	1.14±0.17	12	0.159±0.058	1.16±0.19	12			
2009	9	0.093±0.009	0.99±0.17	10	0.086±0.037	0.89±0.28	13			
2009	10				0.078±0.023	0.99±0.18	13			
2009	11									
2009	12									
2010	1									
2010	2									
2010	3	0.124±0.039	1.06±0.32	13						
2010	4	0.089±0.036	0.97±0.18	24						
2010	5	0.076±0.020	1.19±0.22	11	0.101±0.035	1.25±0.28	13			
2010	6	0.059±0.017	1.31±0.33	12	0.087±0.040	1.27±0.25	16			
2010	7	0.048±0.016	1.23±0.28	12	0.103±0.064	1.34±0.20	18			
2010	8	0.041±0.005	1.41±0.03	5	0.095±0.041	1.40±0.19	19			
2010	9	0.022±0.000	1.13±0.00	1	0.051±0.022	1.17±0.21	16			
2010	10				0.071±0.034	1.18±0.23	10			
2010	11				0.052±0.016	1.19±0.24	11			
2010	12				0.052±0.041	1.19±0.27	13			
2011	1				0.026±0.009	0.94±0.27	13			

Year	Month	Ny Ålesund			Birkenes			Trollhaugen		
		AOD	AE	N	AOD	AE	N	AOD	AE	N
2011	2				0.061±0.033	0.63±0.39	4			
2011	3				0.072±0.035	0.99±0.29	19			
2011	4				0.212±0.183	1.18±0.44	22			
2011	5	0.088±0.012	1.62±0.09	3	0.125±0.067	1.26±0.24	19			
2011	6	0.096±0.023	1.50±0.38	3	0.107±0.048	1.41±0.20	23			
2011	7	0.050±0.003	1.54±0.06	6	0.122±0.060	1.57±0.22	15			
2011	8	0.064±0.021	1.37±0.30	11	0.097±0.049	1.53±0.12	15			
2011	9	0.046±0.006	1.58±0.22	6						
2011	10									
2011	11									
2011	12									
2012	1									
2012	2									
2012	3	0.119±0.039	1.00±0.27	10	0.067±0.034	1.06±0.36	11			
2012	4	0.109±0.029	1.33±0.19	25	0.067±0.044	1.45±0.21	14			
2012	5	0.124±0.045	1.13±0.25	23	0.084±0.037	1.28±0.27	11			
2012	6	0.065±0.028	1.48±0.22	17	0.095±0.034	1.57±0.23	8			
2012	7	0.062±0.018	1.34±0.15	19	0.079±0.032	1.52±0.26	17			
2012	8	0.061±0.018	1.36±0.18	13	0.077±0.023	1.47±0.27	23			
2012	9	0.080±0.023	1.15±0.34	5	0.066±0.014	1.08±0.26	10			
2012	10				0.062±0.031	1.26±0.32	13			
2012	11				0.054±0.016	0.62±0.21	3			
2012	12									
2013	1									
2013	2									
2013	3	0.102±0.051	1.15±0.28	17						
2013	4	0.106±0.046	1.15±0.32	24						
2013	5	0.071±0.034	1.26±0.30	16						
2013	6	0.072±0.045	1.27±0.30	19						
2013	7	0.057±0.028	1.34±0.32	16	0.171±0.162	1.32±0.26	27			
2013	8	0.051±0.013	1.24±0.27	16	0.104±0.082	1.21±0.33	21			
2013	9	0.043±0.014	1.21±0.44	15	0.053±0.027	0.90±0.24	14			
2013	10				0.038±0.012	0.83±0.42	7			
2013	11				0.040±0.021	0.53±0.19	14			
2013	12				0.044±0.022	0.38±0.33	7			
2014	1							0.016±0.002	1.56±0.14	17
2014	2							0.015±0.002	1.54±0.13	24

Year	Month	Ny Ålesund			Birkenes			Trollhaugen		
		AOD	AE	N	AOD	AE	N	AOD	AE	N
2014	3				0.130±0.131	0.76±0.48	13	0.014±0.002	1.29±0.10	17
2014	4	0.079±0.023	1.39±0.20	16	0.121±0.062	1.09±0.35	19	0.012±0.004	1.21±0.11	19
2014	5	0.093±0.025	1.40±0.17	19	0.092±0.028	1.13±0.27	17			
2014	6	0.050±0.010	1.46±0.18	14	0.065±0.028	1.17±0.21	26			
2014	7	0.057±0.031	1.51±0.13	12	0.125±0.068	1.45±0.32	22			
2014	8	0.086±0.017	1.48±0.13	19	0.134±0.047	1.21±0.23	14			
2014	9	0.126±0.052	1.54±0.20	5	0.134±0.067	1.33±0.28	19	0.022±0.003	1.29±0.16	4
2014	10							0.017±0.002	1.53±0.16	11
2014	11							0.021±0.002	1.37±0.16	13
2014	12							0.020±0.002	1.66±0.15	16
2015	1							0.034±0.021	1.32±0.38	9
2015	2				0.053±0.019	0.80±0.28	7	0.018±0.003	1.63±0.12	19
2015	3	0.061±0.020	1.33±0.17	7	0.099±0.131	0.88±0.37	10	0.019±0.004	1.38±0.18	10
2015	4	0.107±0.044	1.14±0.34	21	0.088±0.035	1.20±0.09	3	0.018±0.001	1.30±0.16	11
2015	5	0.069±0.024	1.46±0.14	18	0.085±0.026	1.19±0.19	21			
2015	6	0.057±0.011	1.36±0.30	19	0.074±0.023	1.37±0.28	25			
2015	7	0.098±0.085	1.42±0.20	21	0.126±0.114	1.48±0.26	27			
2015	8	0.049±0.023	1.55±0.20	17	0.098±0.050	1.30±0.34	19	0.053±0.013	0.92±0.16	7
2015	9	0.047±0.010	1.12±0.43	8	0.053±0.023	1.33±0.30	12	0.035±0.011	1.02±0.19	16
2015	10				0.049±0.043	1.35±0.37	11	0.040±0.007	1.25±0.15	12
2015	11				0.042±0.026	0.82±0.39	10	0.033±0.007	1.22±0.29	11
2015	12				0.043±0.027	0.61±0.39	4	0.031±0.006	1.46±0.15	30
2016	1				0.022±0.003	1.29±0.17	5	0.036±0.007	1.51±0.10	21
2016	2				0.040±0.012	1.14±0.22	13	0.033±0.004	1.63±0.15	15
2016	3	0.090±0.047	1.33±0.27	11	0.055±0.075	1.20±0.20	11	0.026±0.004	1.43±0.08	14
2016	4	0.066±0.026	1.52±0.16	19	0.066±0.028	1.36±0.14	10	0.025±0.002	1.43±0.04	8
2016	5	0.076±0.032	1.57±0.08	11						
2016	6	0.064±0.018	1.52±0.19	11						
2016	7	0.038±0.011	1.48±0.28	17						
2016	8	0.050±0.037	1.44±0.27	16				0.039±0.009	1.35±0.22	7
2016	9	0.029±0.011	1.37±0.24	9				0.025±0.005	1.26±0.18	11
2016	10							0.023±0.004	1.34±0.23	16
2016	11							0.020±0.004	1.50±0.18	23
2016	12							0.019±0.002	1.52±0.09	23
2017	1							0.021±0.005	1.61±0.16	26
2017	2							0.021±0.003	1.69±0.11	16
2017	3							0.016±0.003	1.23±0.15	26

Year	Month	Ny Ålesund			Birkenes			Trollhaugen		
		AOD	AE	N	AOD	AE	N	AOD	AE	N
2017	4	0.073±0.025	1.44±0.18	19				0.016±0.001	1.18±0.09	9
2017	5	0.073±0.027	1.39±0.25	23	0.060±0.023	1.39±0.30	19			
2017	6	0.048±0.010	1.30±0.18	19	0.048±0.017	1.32±0.24	18			
2017	7	0.053±0.027	1.50±0.22	19	0.071±0.030	1.66±0.30	21			
2017	8	0.101±0.092	1.36±0.25	20	0.089±0.052	1.37±0.25	16	0.022±0.005	1.10±0.19	11
2017	9	0.072±0.041	1.36±0.21	6	0.100±0.022	0.97±0.18	6	0.021±0.005	1.19±0.22	12
2017	10				0.062±0.023	0.74±0.17	9	0.019±0.002	1.24±0.17	17
2017	11							0.020±0.004	1.29±0.20	13
2017	12							0.016±0.003	1.51±0.08	10
2018	1							0.017±0.003	1.52±0.10	25
2018	2							0.016±0.003	1.43±0.13	15
2018	3	0.051±0.008	1.35±0.14	4				0.014±0.002	1.33±0.12	15
2018	4	0.097±0.041	1.09±0.32	14	0.087±0.061	1.03±0.24	8	0.013±0.002	1.30±0.17	20
2018	5	0.097±0.058	0.90±0.44	16	0.123±0.055	1.29±0.22	29			
2018	6	0.061±0.064	1.40±0.37	15	0.085±0.062	1.24±0.28	24			
2018	7	0.038±0.011	1.33±0.22	13	0.102±0.056	1.55±0.26	27			
2018	8	0.075±0.048	1.25±0.30	20	0.106±0.080	1.32±0.23	18			
2018	9	0.056±0.033	1.17±0.26	12	0.069±0.044	1.05±0.29	12	0.028±0.006	1.41±0.17	14
2018	10							0.022±0.003	1.44±0.12	20
2018	11							0.019±0.002	1.57±0.11	19
2018	12							0.021±0.003	1.70±0.10	27
2019	1				0.032±0.013	0.82±0.24	6	0.028±0.007	1.57±0.17	14
2019	2				0.064±0.066	0.88±0.39	10	0.026±0.007	1.60±0.12	24
2019	3				0.041±0.023	0.93±0.36	14	0.021±0.003	1.54±0.09	23
2019	4	0.069±0.000	0.29±0.00	1	0.130±0.101	1.44±0.29	23	0.020±0.002	1.33±0.12	11
2019	5	0.068±0.020	1.22±0.26	11	0.066±0.044	1.27±0.19	24			
2019	6	0.074±0.020	1.43±0.27	20	0.151±0.113	1.42±0.17	15			
2019	7	0.052±0.012	1.30±0.23	21	0.210±0.062	1.59±0.18	5			
2019	8	0.209±0.110	1.41±0.17	13	0.168±0.041	1.35±0.11	11	0.031±0.004	0.87±0.11	4
2019	9	0.173±0.046	1.30±0.09	10				0.021±0.004	1.41±0.20	11
2019	10	0.100±0.011	1.22±0.11	13				0.023±0.002	1.43±0.12	18
2019	11				0.072±0.026	1.01±0.30	4	0.022±0.003	1.46±0.19	12
2019	12				0.052±0.002	1.10±0.16	3	0.026±0.002	1.60±0.10	21
2020	1				0.075±0.032	0.73±0.31	13	0.040±0.013	1.69±0.11	14
2020	2				0.080±0.025	0.73±0.29	12	0.056±0.013	1.56±0.13	25
2020	3				0.081±0.023	0.96±0.31	7	0.052±0.006	1.28±0.12	16
2020	4	0.064±0.009	1.43±0.06	6	0.079±0.009	1.22±0.12	3	0.048±0.005	1.24±0.03	9

Year	Month	Ny Ålesund			Birkenes			Trollhaugen		
		AOD	AE	N	AOD	AE	N	AOD	AE	N
2020	5	0.073±0.022	1.57±0.35	9	0.074±0.021	1.19±0.22	11			
2020	6				0.103±0.062	1.55±0.33	21			
2020	7				0.054±0.014	1.59±0.23	22			
2020	8				0.092±0.051	1.69±0.17	22	0.046±0.006	0.78±0.10	8
2020	9				0.117±0.078	1.30±0.42	17	0.042±0.007	0.89±0.12	18
2020	10				0.076±0.036	1.18±0.54	11	0.040±0.007	1.10±0.08	19
2020	11				0.042±0.021	1.24±0.24	9	0.031±0.003	1.17±0.10	13
2020	12				0.032±0.010	1.10±0.24	4	0.023±0.003	1.45±0.13	20
2021	1				0.040±0.020	1.36±0.37	10	0.024±0.004	1.50±0.17	25
2021	2				0.046±0.022	1.46±0.39	11	0.024±0.003	1.60±0.11	21
2021	3				0.046±0.031	1.19±0.65	9	0.020±0.002	1.34±0.13	13
2021	4				0.086±0.087	1.25±0.25	27	0.019±0.002	1.19±0.15	8
2021	5	0.090±0.000	1.32±0.00	1	0.091±0.087	1.54±0.20	15			
2021	6	0.090±0.016	1.51±0.16	21	0.081±0.038	1.40±0.26	26			
2021	7	0.046±0.008	1.51±0.21	19	0.166±0.090	1.65±0.26	23			
2021	8	0.056±0.016	1.50±0.24	20	0.111±0.046	1.53±0.19	27	0.040±0.014	0.92±0.21	10
2021	9	0.098±0.045	1.40±0.23	13	0.097±0.073	1.42±0.29	18	0.034±0.008	1.10±0.19	20
2021	10	0.065±0.014	1.39±0.17	10	0.039±0.008	1.18±0.35	9	0.027±0.004	1.31±0.16	23
2021	11				0.040±0.018	0.97±0.46	12	0.022±0.003	1.48±0.23	21
2021	12							0.027±0.005	1.58±0.14	20
2022	1							0.025±0.004	1.67±0.11	21
2022	2				0.030±0.003	1.49±0.12	3	0.022±0.004	1.61±0.10	20
2022	3	0.083±0.027	1.31±0.26	8	0.103±0.098	1.18±0.32	17	0.021±0.003	1.55±0.08	23
2022	4	0.077±0.013	1.37±0.19	24				0.021±0.006	1.41±0.18	13
2022	5	0.077±0.022	1.36±0.17	24	0.073±0.025	1.13±0.29	14	0.016±0.003	1.13±0.16	3
2022	6	0.063±0.024	1.30±0.31	15	0.059±0.026	1.28±0.32	22			
2022	7	0.043±0.011	1.27±0.14	13	0.082±0.085	1.44±0.24	19			
2022	8	0.037±0.015	1.53±0.17	12	0.083±0.046	1.40±0.38	17	0.029±0.004	1.10±0.12	11
2022	9	0.035±0.009	1.41±0.10	6	0.055±0.014	1.36±0.28	10	0.030±0.006	1.23±0.16	18
2022	10				0.036±0.016	1.03±0.34	7	0.031±0.009	1.25±0.19	15
2022	11							0.022±0.004	1.39±0.13	23
2022	12							0.026±0.007	1.29±0.18	20
2023	1				0.031±0.015	0.65±0.45	3	0.035±0.004	1.09±0.15	20
2023	2							0.035±0.003	0.99±0.06	19
2023	3				0.033±0.006	1.14±0.16	5	0.033±0.004	0.90±0.07	17
2023	4	0.102±0.017	1.54±0.13	6	0.062±0.031	1.03±0.40	7	0.029±0.005	0.84±0.08	15
2023	5	0.082±0.014	1.33±0.17	13	0.194±0.162	1.24±0.14	7	0.021±0.007	0.79±0.08	5

Year	Month	Ny Ålesund			Birkenes			Trollhaugen		
		AOD	AE	N	AOD	AE	N	AOD	AE	N
2023	6	0.085±0.019	1.47±0.09	19	0.149±0.062	1.50±0.21	24			
2023	7	0.085±0.028	1.52±0.08	22	0.086±0.021	1.34±0.18	21			
2023	8	0.063±0.019	1.46±0.14	13	0.121±0.091	1.25±0.23	17	0.031±0.009	0.71±0.19	11
2023	9	0.102±0.026	1.34±0.11	11	0.123±0.094	1.17±0.25	16	0.036±0.003	0.83±0.22	9
2023	10				0.085±0.067	0.77±0.28	11	0.031±0.002	0.87±0.11	13
2023	11							0.025±0.003	0.97±0.11	20
2023	12							0.025±0.003	0.92±0.11	16

Table A 6: Monthly means and standard deviation of AOD and Ångström coefficient measured in Ny-Ålesund, and Birkenes using lunar photometry. N gives the number of days with data in the respective months.

Year	Month	Ny Ålesund			Birkenes		
		AOD	AE	N	AOD	AE	N
2018	1	0.054±0.014	1.34±0.12	8			
2018	10	0.103±0.006	1.03±0.03	3			
2018	11	0.037±0.001	1.02±0.03	2			
2018	12	0.045±0.006	1.11±0.07	3			
2019	1	0.096±0.011	1.59±0.16	9	0.040±0.017	0.69±0.35	8
2019	2	0.075±0.024	1.35±0.23	3	0.032±0.010	0.67±0.17	2
2019	3				0.030±0.014	1.06±0.29	9
2019	4				0.073±0.024	1.37±0.37	12
2019	5				0.088±0.045	1.52±0.20	9
2019	6				0.101±0.036	1.53±0.17	3
2019	7				0.100±0.037	1.22±0.32	5
2019	8				0.170±0.031	1.31±0.16	6
2019	11				0.214±0.026	0.36±0.11	1
2019	12				0.076±0.007	1.11±0.06	3
2020	1				0.095±0.031	0.69±0.25	5
2020	2	0.081±0.021	1.10±0.39	11	0.092±0.044	0.84±0.30	11
2020	3	0.067±0.014	1.14±0.19	5	0.083±0.016	1.17±0.14	5
2020	4				0.112±0.048	0.88±0.28	10
2020	5				0.080±0.019	1.35±0.05	5
2021	3	0.081±0.071	0.65±0.17	8	0.094±0.037	0.49±0.11	5
2021	4	0.035±0.007	0.68±0.14	1	0.063±0.034	1.41±0.17	12
2021	5	0.056±0.014	1.15±0.10	1	0.055±0.018	1.52±0.62	3
2021	7				0.175±0.052	1.74±0.09	6
2021	8				0.109±0.054	1.56±0.17	9
2021	9				0.067±0.022	0.57±0.45	4
2021	10				0.039±0.015	0.96±0.36	8
2021	11				0.039±0.013	0.66±0.40	8
2021	12				0.046±0.041	1.22±0.56	7
2022	1	0.069±0.024	1.00±0.23	4			
2022	2	0.059±0.014	1.18±0.24	10			
2022	10				0.046±0.025	0.70±0.35	9
2022	11	0.006±0.007	0.63±0.46	3	0.089±0.013	0.31±0.10	2
2022	12	0.048±0.019	1.17±0.28	9	0.029±0.014	1.43±0.54	12
2023	1	0.058±0.016	0.92±0.32	9	0.031±0.006	0.50±0.09	1
2023	2	0.045±0.008	0.99±0.23	2	0.035±0.013	0.81±0.26	2
2023	3	0.053±0.029	0.71±0.37	4			
2023	4				0.037±0.016	1.09±0.24	6
2023	5				0.124±0.098	1.29±0.28	5
2023	6				0.130±0.033	1.15±0.16	1
2023	7				0.073±0.017	1.15±0.25	3
2023	8				0.098±0.059	1.35±0.31	7
2023	9				0.091±0.074	1.17±0.25	7
2023	10				0.353±0.333	0.70±0.14	3

Appendix B
Description of instruments and methodologies

METHODOLOGY, DATA QUALITY, AND UNCERTAINTIES

In this section of the appendix, a brief overview of the observatories and recent upgrades as well the current instrumental methods used in this report is presented. These methodologies, alongside prior instrumental methods, are summarized in Table B 1. Additionally the theoretical methods used in calculation of the trends and determination of equivalent black carbon from absorption measurements are explained.

THE OBSERVATORIES

The Zeppelin Observatory (78.90 N, 11.88 E) is located on Zeppelin Mountain at 472 m above sea level adjacent to Kongsfjorden and the settlement of Ny-Ålsesund (Figure B 1). The observatory is a cornerstone of the national monitoring programme and many research infrastructures including but not limited to those mentioned in this report: e.g., ICOS, AGAGE, ACTRIS. The location of the observatory on a mountain in the high Arctic ensures minimal local contamination or contamination from polluted regions making it a true atmospheric background observation site. Measurement of trace gases is via an inlet on a 15 m mast, with aerosol parameters measured via an inlet on the observatory roof (these require shorter lines to prevent sample losses to the inlet walls). For extensive details on instrumentation and the history of the Zeppelin Observatory see Platt et al. (2022).

Figure B 1: The Zeppelin Observatory with Kongsfjorden in the background. Photo credit: Ove Hermansen, NILU.

The Birkenes Observatory in Aust Agder, southern Norway (58.39° N, 8.25° E, 219 m a.s.l.) is an EMEP/GAW supersite surrounded by mixed forests, meadows, and agricultural areas. It experiences a maritime climate

due to its proximity to the Skagerrak coast and is in the boreo nemoral climatic zone (Yttri et al. 2021). The observatory is crucial for monitoring air pollution and carbonaceous aerosols, particularly from continental Europe, despite being a relatively clean rural background site, as it is influenced by both local biogenic sources and long-range transported pollutants. Birkenes is a class 2 site under ICOS. The prominent mast was constructed in 2020 to meet ICOS requirements.

Figure B 2: The Birkenes Observatory is located on top of a small hill with a prominent 75m mast. Photo credit: Kjetil Samuelsen, Fædrelandsvennen.

The Trollhaugen Observatory is located in Dronning Maud Land, Antarctica (72°00'42"S 02°32'06"E, 1533 m a.s.l.). The station is not part of national monitoring, but as one of the most remote and least disturbed areas of the planet, it is a useful reference for comparison.

Figure B 3: The Trollhaugen Observatory. Photo credit: Chris Lunder, NILU.

Intrumentation

Carbon dioxide at Birkenes, Trollhaugen and Zeppelin is monitored using a Cavity Ring-Down Spectrometer (CRDS, Picarro G2401) for continuous measurement. Data collection and curation is in accordance with integrated carbon observation system (ICOS) protocols (please see e.g., Yver-Kwok et al., 2021). For 1990 to 2012, measurements at Zeppelin were performed using a laser-based trace gas analyser (Li-Cor). At Trollhaugen, data CO_2 prior to 2021 were collected using a different CRDS model (Picarro G1301). All data were re-scaled in 2024 to the new WMO scale (WMO-CO_2-X2019). At Birkenes a 75 m mast was installed in 2020 to minimise the influence of local vegetation on greenhouse gas measureents. While data are available at 3 heights (15m, 45 m, and 75 m) only data from the top level at 75 m are used for reporting.

Methane is measured at both Birkenes and Zeppelin using the same CRDS system as for CO_2 and according to ICOS protocols. For 2001 to 2012 CH_4 was measured at Zeppelin using a gas chromatography with flame ionization detector (GC-FID) system. All data were re-scaled in 2024 to the new WMO scale (WMO-CH_4-X2019). Reported measurements at Birkenes are at the top of the 75 m mast at the site.

$\delta^{13}C_{CH4}$ air samples from Zeppelin are collected in 1 L steel or aluminium canisters at the same air inlet as CH_4. Two samples per week are sent to the Greenhouse Gas Laboratory at Royal Holloway University of London (RHUL). Methane mole fraction was measured using a Picarro 1301 cavity ring down spectrometer (CRDS). δ13C analysis is carried out using a modified gas chromatography isotope ratio mass spectrometry system for all samples (Trace Gas and Isoprime mass spectrometer, Isoprime Ltd.) with 0.05‰ repeatability. All measurements for the canisters are made in triplicate. See Fischer et al., 2017 and Myhre et al., 2016 for more details.

N_2O at Zeppelin is measured using a mid-IR Cavity Ring Down instrument (since December2017) which is calibrated against ICOS reference standards (NOAA scale). The instrument participates in ring tests and applies to the ICOS system for calibration and measurement control. The continuous data are also compared to weekly flask samples sent to NOAA CMDL, Boulder Colorado, which are also used in case of gaps in the continuous measurement time series.

Carbon Monoxide is measured at both Birkenes and Zeppelin using the same CRDS system as for CO_2 and according to ICOS protocols. Reported measurements at Birkenes are at the top of the 75 m mast at the site.

Halocarbons are measured using a Medusa-GCMS These include the CFCs, HCFCs, HFCs, halons, SF6 and other halogenated compounds in this report. The system fulfils the requirements of the Advanced Global Atmospheric Gases Experiment (AGAGE). Prior to 2010 an adsorption–desorption system gas chromatography with mass spectrometry (ADS-GCMS) system was used for the halons, with notable less precision for many compounds compared to the current system.

Aerosol Scattering is monitored at Birkenes and Trollhaugen using a Nephelometer (TSI 3563), providing hourly data with ACTRIS standards since 2010.

Aerosol Absorption is measured using the seven wavelength aethalometer (Magee AE33) at all sites. This instrument superseded a 3-wavelength particle soot absorption photometer (PSAP) at Birkenes and Trollhaugen and an older model aethalometer at Zeppelin (Magee AE31). The AE33 has an internal loading

compensation system, which reduces uncertainties related to filter loading effects that were common in previous models.

NUMBER AND SIZE at the observatories are measured using a combination of instruments. For fine-mode particles (0.01 µm to 0.8 µm), a custom-built Differential Mobility Particle Spectrometer (DMPS) is used. The DMPS charges particles and selects a size fraction by applying a voltage, which is then counted by a Condensation Particle Counter (CPC). For larger particles (up to 30 µm), an Optical Particle Spectrometer (OPS) or an Aerodynamic Particle Spectrometer (APS) is employed, using light scattering or aerodynamic acceleration to determine particle size and concentration. These measurements cover a broad range of particle sizes across all observatories.

To ensure data quality, aerosol in-situ instruments regularly participate in intercomparisons at the ACTRIS aerosol calibration center in Leipzig, Germany, minimizing uncertainties through routine calibration.

TOTAL COLUMN AEROSOL OBSERVATIONS – AOD and ÅNGSTRÖM COEFFICIENT

AERONET - Cimel C-318

- Sun (9 channels) and sky radiances
- Wavelength range: 340-1640 nm
- 15 min sampling
- No temperature stabilization
- AOD uncertainty: 0.01-0.02

PFR-GAW- Precision Filter Radiometer

- Direct sun measurements (4 channels)
- Wavelength range: 368 - 862 nm
- 1 min averages
- Temperature stabilized
- AOD uncertainty: 0.01

Figure B 4: Photos and typical features of the standard instrument of the AERONET, which is used at the Birkenes observatory (left panel) and the GAW PFR network instruments, which is utilized in Ny-Ålesund and the Trollhaugen Observatory (right panel).

In May 2002, Physical Meteorological Observatory in Davos / World Radiation Center (PMOD/WRC), in collaboration with NILU, started AOD observations in Ny-Ålesund as part of the global AOD network on

behalf of the WMO GAW program. A Precision Filter Radiometer (PFR) is used to measure the direct solar radiation in four narrow spectral bands centred at 862 nm, 501 nm, 411 nm, and 368 nm. These observations are used to calculate multi-wavelength aerosol optical depth (AOD), i.e. the aerosol extinction in the total column of the atmosphere, and its wavelength dependence, i.e. the Ångström coefficient. The instrument is located on the roof of the Sverdrup station, Ny-Ålesund, close to the EMEP station on the Zeppelin Mountain (78.9°N, 11.9°E, 474 m a.s.l.).

Data quality control includes instrumental control like detector temperature and solar pointing control as well as objective cloud screening. Measurements made at full minutes are averages of 10 samples for each channel made over a total duration of 1.25 seconds. To calculate a daily average, at least 50 single measurements are required. Calibration is performed annually at PMOD/WRC. Quality assured data are available at the World Data Centre of Aerosols (WDCA), hosted at NILU (see https://ebas.nilu.no).

In Ny-Ålesund, during summer months it is possible to measure day and night if the weather conditions are satisfactory. The sun is below 5° of elevation from 10th October to 4th March, limiting the period with sufficient sunlight to the spring-early autumn season. Lunar photometer can close the gap in obtaining a year-around aerosol climatology. As a collaborative initiative between NILU, PMOD/WRC and ISAC-CNR, seasonal deployments of a lunar photometer, which is owned by PMOD/WRC, were already made in the winters between 2014 and 2017. For further information see Mazzola at al., 2024. In the framework of the SIOS infrastructure project, multiple-season deployment started in autumn 2018.

At Birkenes Observatory, AOD measurements started in spring 2009, utilizing an automatic sun and sky radiometer (CIMEL type CE-318) of the global Aerosol Robotic Network (AERONET) at NASA-GSFC, with spectral interference filters centred at selected wavelengths: 340 nm, 380 nm, 440 nm, 500 nm, 675 nm, 870 nm, 1020 nm, and 1640 nm. The measurement frequency is approximately 15 minutes (this depends on the air-mass and time of day). Calibration is performed about once per year, at the Atmospheric Optics Group at the University of Valladolid (GOA-UVA), Spain. GOA manages the calibration for the AERONET sun photometers of the European sub-network of AERONET. Raw data are processed, and quality assured centrally by AERONET. Data reported for 2009 - 2017 are quality-assured AERONET level 2.0 data, which means they have been pre- and post-field-calibrated, automatically cloud cleared and have been manually inspected by AERONET. From 2017 onward, only the new analysis algorithm (version 3) is used at the central AERONET analysis unit at NASA GSFC. In this version, the data quality control, including cloud screening, has been improved and a temperature correction has been applied to all wavelength channels. For details, see Sinyuk A., et al., 2020.

Due to the large gaps in data acquisition caused by the obligatory annual calibrations at the University of Valladolid combined with technical problems and occasionally unfavourable weather conditions at Birkenes, NILU decided to purchase a second Cimel instrument which will be operated alternately with the current instrument. It was taken into operation in fall 2018. This model CE318-T performs not only sun and sky, but also lunar light measurements, which leads to a better data coverage, in particular during the winter months.

Table B 1: Instrumental details for the measurements in this report.

Component & Location	Instrument & Method	Time Res.	Calibration Procedures	Period	Data Coverage in 2024
Carbon dioxide (Birkenes)	CRDS (Picarro, G2401)	5 s	ICOS reference standards	2018 to present	96%
Carbon dioxide (Zeppelin)	CRDS (Picarro G2401)	5 s	ICOS reference standards	2012 to present	97%
Methane (Birkenes)	CRDS (Picarro, G2401)	5 s	ICOS reference standards	2018 to present	96%
Methane (Zeppelin)	CRDS (Picarro, G2401)	5 s	ICOS reference standards	2012 to present	97%
Carbon monoxide (Birkenes)	CRDS (Picarro, G2401) CO2/CH4/CO	5 s	ICOS reference standards	2018 to present	96%
Carbon monoxide (Zeppelin)	CRDS (Picarro)	5 s	ICOS reference standards	2012 to present	97%
Nitrous oxide (Zeppelin)	CRDS (Picarro)	5 s	ICOS reference standards	2018 to present	27%
CFCs, HFCs, HCFCs, Halons, and VOCs	Medusa-GCMS	2 h	Every 2 hours, working std. vs. AGAGE std	2010 to present	60%
Aerosol scattering coefficient (Birkenes)	Nephelometer (TSI, 3563)	1 h	ACTRIS reference standards	2010 to present	85 %
Aerosol scattering coefficient (Trollhaugen)	Nephelometer (TSI, 3563)	1 h	ACTRIS reference standards	2010 to present	99 %
Aerosol absorption coefficient (Birkenes)	PSAP (Radiance Research, 3W)	1 h	ACTRIS reference standards	2012 to 2022	
	Aethalometer (Magee, AE33)	1 h	ACTRIS reference standards	2023 to present	99 %
Aerosol absorption coefficient (Zeppelin)	Aethalometer (Magee, AE31)	1 h	ACTRIS reference standards	2015 to 2022	
	Aethalometer (Magee, AE33)	1 h	ACTRIS reference standards	2023 to present	99 %
Aerosol absorption coefficient (Trollhaugen)	PSAP (Radiance Research, 3W)	1 h	ACTRIS reference standards	2015 to 2022	
	Aethalometer (Magee, AE33)	1 h	ACTRIS reference standards	2023 to present	99%
Particle Number Size Distribution (Birkenes)	DMPS (NILU, Model 2)	1 h	ACTRIS reference standards	2010 to present	65 %
	OPS (Grimm, 190)	1h	ACTRIS reference standards	2010 to 2021	
Particle Number Size Distribution (Zeppelin)	DMPS (NILU, Model 2)	1 h	ACTRIS reference standards	2016 to present	99 %
Particle Number Size Distribution (Trollhaugen)	DMPS (NILU, Model 2)	1 h	ACTRIS reference standards	2016 to present	99 %
AOD (Birkenes)	Cimel CE318-T (sun/moon/sky)	15 m	RIMA-AERONET standards	2009 to present	

Component & Location	Instrument & Method	Time Res.	Calibration Procedures	Period	Data Coverage in 2024
AOD (Ny-Ålesund)	PFR (sun/moon)	1 m	GAW-PFR standards	2002 to present	
AOD ([Troll] &Trollhaugen)	PFR (sun)	1m	GAW-PFR standards	(2007-2014) 2014 to present	

Instrument Definitions:

CRDS Cavity Ring-Down Spectroscopy instrument; **CRDS**; **Li-Cor**: Infrared Gas Analyzer by Li-Cor Biosciences; **GC-FID**: Gas Chromatograph with Flame Ionization Detector; **GC-ECD**: Gas Chromatograph with Electron Capture Detector; **GC-HgO/UV**: Gas Chromatograph with Mercury Oxide/Ultraviolet Detector; **ADS-GCMS**: adsorption–desorption system gas chromatography with mass spectrometry; **Medusa-GCMS**: Automated Gas Chromatograph-Mass Spectrometry system for trace gas measurements; **PSAP**: Particle Soot Absorption Photometer; **DMPS**: Differential Mobility Particle Sizer; **PFR**: Precision Filter Radiometer

DATA ANALYSIS

DETERMINATION OF BACKGROUND DATA FOR TRACE GAS TRENDS

Based on the daily mean concentrations an algorithm is selected to find the values assumed as clean background air. If at least 75% of the trajectories within +/- 12 hours of the sampling day are arriving from a so-called clean sector, defined below, one can assume the air for that specific day to be non-polluted. The remaining 25% of the trajectories from European, Russian or North American sector are removed before calculating the background.

CALCULATION OF TRENDS FOR GREENHOUSE GASES AND VOCS

To calculate the annual trends the observations have been fitted as described in Simmonds et al. (2006) by an empirical equation of Legendre polynomials and harmonic functions with linear, quadratic, and annual and semi-annual harmonic terms:

$$f(t) = a + b\left(\frac{N}{12}\right)\cdot P_1\left(\frac{t}{N}-1\right) + \frac{1}{3}\cdot d\left(\frac{N}{12}\right)^2 \cdot P_2\left(\frac{t}{N}-1\right) + c_1\cdot\cos\left(\frac{2\pi t}{12}\right) + s_1\sin\left(\frac{2\pi t}{12}\right) + c_2\cos\left(\frac{4\pi t}{12}\right) + s_2\sin\left(\frac{4\pi t}{12}\right)$$

The observed *f* can be expressed as functions of time measures from the 2N-months interval of interest. The coefficient *a* defines the average mole fraction, *b* defines the trend in the mole fraction and *d* defines the acceleration in the trend. The *c* and *s* define the annual and inter-annual cycles in mole fraction. N is the mid-point of the period of investigation. P_i are the Legendre polynomials of order *i*.

This equation is used for all GHGs except for the halocarbons, where the fit between the empirical equation and observations improves if the semi-annual harmonic terms are replaced by an additional Legendre polynomial. Uncertainties in the trend estimates include the presence of autocorrelated errors in the fitted model residuals. The uncertainties also take possible presence of heteroscedasticity into account, which means that the variances of the residuals might vary with the level of the time series, which also affects the uncertainties of the estimated trend. The routine vcovHAC in the sandwich package in R (R Core Team, 2018) as described in Zeileis (2006; 2004), is used to estimate standard deviation of all

estimated parameters of the time series regression models. Here HAC is short for Heteroscedastic and Autocorrelation Consistent.

CALCULATION OF TRENDS FOR AEROSOL MICROPHYSICAL AND OPTICAL PROPERTIES

The calculation of the trends for aerosol microphysical and optical properties has been done by performing a Mann-Kendall trend detection and calculating the associated Sen's slope, which is the most widely applied non-parametric trend analysis method in atmospheric (and hydrologic) research (Gilbert, 1987; Sirois, 1998; and references therein).

The purpose of the Mann-Kendall test is to statistically assess if there is a monotonic upward or downward trend of the variable of interest over time, and whether the trend in either direction is statistically significant. The Sen's slope is calculated by computing all the slopes between pairs of points and choose the median as the estimate of the regression slope. The resulting slope estimate is unbiased and the process is resistant to outliers.

ON THE CONVERSION OF ABSORPTION TO EQUIVALENT BLACK CARBON

In multiwavelength aethalometers, the absorption coefficient ($BAbs$) is measured at seven wavelengths (λ= 370;470;520;590;660;880;950 nm), and at three wavelengths with the particle soot absorption photometer used previously at Birkenes and Trollhaugen (λ=470;522;660 nm). Equivalent black carbon (eBC) is an operational definition of black carbon referring to black carbon derived from such absorption measurements using a mass absorption cross section (MAC):

$$eBC(\lambda) = {BAbs(\lambda)}/{MAC(\lambda)} \quad .$$

In the monitoring programme MAC is derived at λ=520 nm using collocated filter measurements of elemental carbon (EC). The $BAbs$ must first be aggregated to the timestamp of the EC measurements before applying the following equation:

$$MAC_{(\lambda=522nm)} = {BAbs_{(\lambda=522nm)}}/{EC} \quad .$$

Appendix C
Abbreviations

Abbreviation	Full name
ACTRIS	Aerosols, Clouds, and Trace gases Research Infra Structure
ADS-GCMS	Adsorption-Desorption System – Gas Chromatograph Mass Spectrometer
AeroCom	Aerosol Comparisons between Observations and Models
AERONET	Aerosol Robotic Network
AGAGE	Advanced Global Atmospheric Gases Experiment
AIRS	Atmospheric Infrared Sounder
AMAP	Arctic Monitoring and Assessment
AOD	Aerosol optical depth
AWI	Alfred Wegener Institute
BC	Black carbon
CAMP	Comprehensive Atmospheric Monitoring Programme
CCN	Cloud Condensation Nuclei
CCNC	Cloud Condensation Nucleus Counter
CFC	Chlorofluorocarbons
CICERO	Center for International Climate and Environmental Research – Oslo
CIENS	Oslo Centre for Interdisciplinary Environmental and Social Research
CLTRAP	Convention on Long-range Transboundary Air Pollution
CO	Carbon monoxide
CPC	Condensation Particle Counter
DMPS	Differential Mobility Particle Sizer
eBC	Equivalent black carbon
EMEP	European Monitoring and Evaluation Programme
ENVRI^{plus}	Environmental Research Infrastructures Providing Shared Solutions for Science and Society
EOS	Earth Observing System
ERF	Effective radiative forcing ERF
ERFaci	ERF due to aerosol–cloud interaction
EU	European Union
EUSAAR	European Supersites for Atmospheric Aerosol Research
FLEXPART	FLEXible PARTicle dispersion model
GAW	Global Atmosphere Watch
GB	Ground based
GHG	Greenhouse gas
GOA-UVA	Atmospheric Optics Group of Valladolid University
GOSAT	Greenhouse Gases Observing Satellite
GWP	Global Warming Potential
HCFC	Hydrochlorofluorocarbons
HFC	Hydrofluorocarbons
ICOS	*Integrated Carbon Observation System*
IPCC	Intergovernmental Panel on Climate Change
ITM	Stockholm University - Department of Applied Environmental Science
JAXA	Japan Aerospace Exploration Agency
LLGHG	Well-mixed greenhouse gases
MAC	Mass absorption cross section
MOE	Ministry of the Environment
NARE	Norwegian Antarctic Research Expeditions
MP	Montreal Protocol

Abbreviation	Full name
NASA	National Aeronautics and Space Administration
NEOS-ACCM	Norwegian Earth Observation Support for Atmospheric Composition and Climate Monitoring
NIES	National Institute for Environmental Studies
NOAA	National Oceanic and Atmospheric Administration
NRS	Norsk Romsenter
OC	Organic Carbon
ODS	Ozone-depleting substances
OH	Hydroxyl radical
OPS	Optical Particle Spectrometer
PFC	Perflueorinated compounds
PFR	Precision filter radiometer
PMOD/WRC	Physikalisch-Meteorologisches Observatorium Davos/World Radiation Center
PNSD	Particle number size distribution
ppb	Parts per billion
ppm	Parts per million
ppt	Parts per trillion
PSAP	Particle Soot Absorption Photometers
RF	Radiative forcing
RHUL	Royal Holloway University of London
RI	Research Infrastructure
RIMA	Red Ibérica de Medida fotométrica de Aerosoles
SACC	Strategic Aerosol Observation and Modelling Capacities for Northern and Polar Climate and Pollution
SCIAMACHY	SCanning Imaging Absorption spectroMeter for Atmospheric CHartographY
SIS	Strategisk instituttsatsing
SMPS	Scanning Mobility Particle
TES	Tropospheric Emission Spectrometer
TOA	Top Of Atmosphere
TOMS OMI	Total Ozone Mapping Spectrometer Ozone Monitoring instrument
UN	United Nations
UNFCCC	United Nations Framework Convention on Climate Change
VOC	Volatile organic compounds
WDCA	World Data Centre for Aerosol
WDCS	World Data Centre of Aerosols
WMGHG	Well-mixed greenhouse gases
WMO	World Meteorological Organization

NILU is a Norwegian, non profit and independent climate and environmental research institute founded in 1969. We started as an institute for air research but have now expanded to research almost all aspects of how people, climate, and the environment affect each other.

Our goal is to attain a better quality of life for everyone! We contribute to this through our research into the composition of the atmosphere, climate change, air quality, environmental toxins, health effects, sustainable systems, circular economy, and digitalization. Together we enable sustainable solutions for current societal and business challenges.

www.nilu.no

nilu
science matters